

**REMOTE SENSING OF SOYBEAN CANOPY COVER, COLOR, AND  
VISIBLE INDICATORS OF MOISTURE STRESS USING IMAGERY  
FROM UNMANNED AIRCRAFT SYSTEMS**

by

**Anthony Ahau Hearst**

**A Thesis**

*Submitted to the Faculty of Purdue University*

*In Partial Fulfillment of the Requirements for the degree of*

**Doctor of Philosophy**



Department of Agricultural & Biological Engineering

West Lafayette, Indiana

May 2019

**THE PURDUE UNIVERSITY GRADUATE SCHOOL**  
**STATEMENT OF COMMITTEE APPROVAL**

Dr. Dharmendra Saraswat, Chair

Department of Agricultural and Biological Engineering

Dr. Bernard Engel

Department of Agricultural and Biological Engineering

Dr. Melba Crawford

Department of Agronomy

Dr. Katy Rainey

Department of Agronomy

**Approved by:**

Dr. Nathan Mosier

Head of the Graduate Program

*For my Father*

## **ACKNOWLEDGMENTS**

I would like to thank everyone on my committee for making me feel supported in my research and career goals. Special thanks to Dr. Saraswat, Dr. Engel, and Dr. Mosier for generously going out of their way to ensure I had all the support I needed to graduate successfully. This research was supported by the Purdue Doctoral Fellowship and the National Science Foundation Graduate Research Fellowship Program grant number 106469. Any opinion, findings, and conclusions or recommendations expressed in this material are those of the authors and do not necessarily reflect the views of the National Science Foundation. The soybean field operations were funded by multiple agencies, including the United Soybean Board, Dow AgroSciences, and the Indiana Soybean Alliance

## TABLE OF CONTENTS

LIST OF TABLES .....	8
LIST OF FIGURES .....	9
ABSTRACT .....	10
<b>CHAPTER 1. INTRODUCTION</b> .....	<b>11</b>
1.1 Background .....	11
1.2 Hypotheses and Objectives .....	13
1.3 Significance of Research .....	14
1.4 Dissertation Organization .....	15
1.5 Literature Review .....	15
1.5.1 Soybean Growth and Development .....	15
1.5.2 Moisture Stress .....	16
1.5.3 Visible Indicators of Moisture Stress .....	18
1.5.4 Indicators of Drought Stress .....	18
1.5.5 Indicators of Flood Stress .....	19
1.5.6 Remote Sensing of Visible Indicators of Moisture Stress .....	20
1.5.7 Crop Modeling .....	21
1.5.8 Model Calibration .....	25
1.5.9 Model Selection .....	26
1.5.10 The AquaCrop Model .....	27
<b>CHAPTER 2. MULTILAYER UAS IMAGE ORTHOMOSAICS FOR FIELD-BASED HIGH-THROUGHPUT PHENOTYPING</b> .....	<b>33</b>
2.1 Abstract .....	33
2.2 Introduction .....	34
2.3 Methods .....	36
2.3.1 Field Site .....	36
2.3.2 Image Acquisition .....	36
2.3.3 Single-Layer Mosaic Generation .....	36
2.3.4 Multilayer Mosaic Generation .....	37
2.3.5 Ground Reference Imagery .....	38

2.3.6	Row-Offset Errors .....	38
2.3.7	Phenotype Measurements .....	39
2.4	Results.....	40
2.4.1	Evaluation of Row-Offset Errors.....	40
2.4.2	Evaluation of Phenotype Measurements .....	40
2.5	Discussion.....	41
2.6	Conclusion .....	42
<b>CHAPTER 3. THE RELATIVE ACCURACY OF SOYBEAN CANOPY COVER AND COLOR FROM SINGLE AND MULTILAYER UAS IMAGE ORTHOMOSAICS .....</b>		<b>43</b>
3.1	Abstract.....	43
3.2	Introduction.....	44
3.3	Methods.....	46
3.3.1	Field Site.....	46
3.3.2	Image Acquisition.....	46
3.3.3	Single-Layer Mosaic Generation.....	47
3.3.4	Multilayer Mosaic Generation.....	47
3.3.5	Phenotype Measurements .....	47
3.3.6	Plot Rankings.....	47
3.3.7	Pairwise Plot Comparisons .....	48
3.4	Results.....	48
3.4.1	Evaluation of Plot Rankings .....	48
3.4.2	Evaluation of Pairwise Plot Comparisons .....	49
3.5	Discussion.....	50
3.6	Conclusion .....	50
<b>CHAPTER 4. CONSTRAINING THE ONSET OF MOISTURE STRESS IN AQUACROP USING CANOPY COVER TIME SERIES FROM UNMANNED AIRCRAFT SYSTEMS.....</b>		<b>52</b>
4.1	Abstract.....	52
4.2	Introduction.....	53
4.2.1	Background.....	53
4.2.2	The AquaCrop Model .....	55
4.2.3	Constraining the Onset of Moisture Stress in AquaCrop .....	57

4.3	Methods.....	59
4.3.1	Field Site.....	59
4.3.2	Climate.....	59
4.3.3	Ground Observations.....	59
4.3.4	UAS Observations.....	60
4.3.5	Ground-Based Model Calibration.....	61
4.3.6	UAS-Based Model Calibration.....	62
4.3.7	Model Validation.....	62
4.4	Results.....	62
4.4.1	Calibration.....	62
4.4.2	Validation.....	63
4.5	Discussion.....	63
4.6	Conclusion.....	64
<b>CHAPTER 5.</b>	<b>CONCLUSION.....</b>	<b>65</b>
5.1	Conclusion and Recommendations.....	65
<b>FIGURES.....</b>		<b>67</b>
<b>TABLES.....</b>		<b>88</b>
<b>REFERENCES.....</b>		<b>103</b>

## LIST OF TABLES

Table 1. Summary of the basic inputs needed to run AquaCrop. ....	88
Table 2. Summary of observations of outputs that may be used to calibrate AquaCrop.....	89
Table 3. Frequencies of row-offset errors (offset images/replicate images) for different plots on different flight dates based on visual .....	90
Table 4. Rankings of canopy cover for 21 test plots labelled ‘a’ through ‘u’ on 13 flight dates based on ground reference measurements .....	91
Table 5. Rankings of hue for 21 test plots labelled ‘a’ through ‘u’ on 13 flight dates based on ground reference measurements (REF), .....	92
Table 6. Rankings of green-to-red ratio (GR) for 21 test plots labelled ‘a’ through ‘u’ on 13 flight dates based on ground reference .....	93
Table 7. List of planting and flight dates during the 2014, 2015, 2016, and 2017 growing seasons. ....	94
Table 8. AquaCrop parameters for non-stressed growth and how they were constrained using ground-based observations from 2016.....	95
Table 9. AquaCrop model parameters for stressed growth and how they were constrained using ground-based observations from 2016.....	96
Table 10. AquaCrop parameters for non-stressed growth and how they were constrained using UAS-based observations from 2016. ....	97
Table 11. AquaCrop parameters for stressed growth and how they were constrained using UAS-based observations from 2016. ....	98
Table 12. Selected AquaCrop model parameter values from ground and UAS-based calibrations with default values for reference.....	99
Table 13. Calibration metrics of agreement between observed and simulated UAS and ground-based AquaCrop outputs in 2016.....	100
Table 14. Validation metrics of agreement between observed and simulated UAS and ground-based AquaCrop model canopy cover .....	101
Table 15. Observed and simulated soybean yields and yield prediction errors using ground and UAS-based AquaCrop models.....	102

## LIST OF FIGURES

Figure 1. Variation of AquaCrop’s stress coefficient for canopy expansion ( $K_s\_exp$ ) between .	67
Figure 2. Schematic diagram of the AquaCrop model (Raes et al., 2012). .....	68
Figure 3. An RGB image ortho-mosaic of the field site generated by Pix4Dmapper using.....	69
Figure 4. A single-layer (left) and 20-layer (right) UAS image ortho-mosaic of a portion of the 70	
Figure 5. Image time series of reference plot ‘a’ from single-layer layer mosaics (1.5 cm pixel 71	
Figure 6. Time series of canopy cover for reference plot ‘a’ based on measurements from single- .....	72
Figure 7. Time series of canopy pixel hue for reference plot ‘a’ based on measurements from..	73
Figure 8. Agreement of rankings of canopy cover for 21 test plots on 13 flight dates based on .	74
Figure 9. Agreement of rankings of hue for 21 test plots on 13 flight dates from Single Layer..	75
Figure 10. Agreement of rankings of green-to-red ratio (GR) for 21 test plots on 13 flight dates	76
Figure 11. Fraction of 2730 unique pairs of 21 soybean test plots on 13 flight dates for which..	77
Figure 12. Fraction of unique pairs of 21 soybean test plots on 13 flight dates that had .....	78
Figure 13. Fraction of 210 unique pairs of 21 test plots on each of 13 flight dates for which .....	79
Figure 14. Fraction of 210 unique pairs of 21 test plots on each of 13 flight dates for which hue .....	80
Figure 15. Fraction of 210 unique pairs of 21 test plots on each of 13 flight dates for which GR	81
Figure 16. Map of Purdue University Agronomy Center for Research and Education (ACRE)..	82
Figure 17. Cumulative precipitation in 2014, 2015, 2016, and 2017 measured at ACRE. ....	83
Figure 18. Timeline of planting and UAS flight dates in 2014, 2015, 2016, and 2017. Planting	84
Figure 19. Observed and simulated soybean canopy cover, biomass, and root length using .....	85
Figure 20. Rainfall and observed and simulated soil water content and moisture stress using .....	86
Figure 21. Observed and simulated soybean canopy cover in 2014, 2015, and 2017 at ACRE ..	87

## ABSTRACT

Author: Hearst, Anthony, A. PhD

Institution: Purdue University

Degree Received: May 2019

Title: Remote Sensing of Soybean Canopy Cover, Color, and Visible Indicators of Moisture Stress using Imagery from Unmanned Aircraft Systems.

Committee Chair: Dharmendra Saraswat

Crop improvement is necessary for food security as the global population is expected to exceed 9 billion by 2050. Limitations in water resources and more frequent droughts and floods will make it increasingly difficult to manage agricultural resources and increase yields. Therefore, we must improve our ability to monitor agronomic research plots and use the information they provide to predict impacts of moisture stress on crop growth and yield. Towards this end, agronomists have used reductions in leaf expansion rates as a visible ‘plant-based’ indicator of moisture stress. Also, modeling researchers have developed crop models such as AquaCrop to enable quantification of the severity of moisture stress and its impacts on crop growth and yield. Finally, breeders are using Unmanned Aircraft Systems (UAS) in field-based High-Throughput Phenotyping (HTP) to quickly screen large numbers of small agronomic research plots for traits indicative of drought and flood tolerance. Here we investigate whether soybean canopy cover and color time series from high-resolution UAS ortho-images can be collected with enough spatial and temporal resolution to accurately quantify and differentiate agronomic research plots, pinpoint the timing of the onset of moisture stress, and constrain crop models such as AquaCrop to more accurately simulate the timing and severity of moisture stress as well as its impacts on crop growth and yield. We find that canopy cover time series derived from multilayer UAS image ortho-mosaics can reliably differentiate agronomic research plots and pinpoint the timing of reductions in soybean canopy expansion rates to within a couple of days. This information can be used to constrain the timing of the onset of moisture stress in AquaCrop resulting in a more realistic simulation of moisture stress and a lower likelihood of underestimating moisture stress and overestimating yield. These capabilities will help agronomists, crop modelers, and breeders more quickly develop varieties tolerant to moisture stress and achieve food security.

## CHAPTER 1. INTRODUCTION

### 1.1 Background

Due to global population rise, yields of major food crops must be increased to ensure future food security. At the same time, limitations in water resources and climate change will make it increasingly difficult to manage agricultural resources and obtain higher yields (Bradshaw & Barry, 2014; Cohen, 2003; FAO, 2009; Sinha et al., 1989). This is particularly true for the US Midwest region, in which climate models predict more extreme weather, including droughts and floods, will reduce yields (Cherkauer & Sinha, 2010; Fan, 2014; Pryor, 2013; Rosenzweig, 2002). We therefore need to improve our understanding of how droughts and floods impact crop growth and yield.

Research in agronomy, crop modeling, and breeding have advanced our understanding of crop growth dynamics and water relations to yield by assimilating current knowledge and relying on meteorological and agronomic data to test our understanding (Boote et al., 1996). This has led to more accurate yield predictions, more effective breeding, better agricultural resource management, and higher yields. For example, agronomists have identified visible ‘plant-based’ indicators of moisture stress, such as reductions in leaf expansion rates, which help identify when crops are experiencing moisture stress (Widuri et al., 2017; Jones, 2004). Also, crop modeling researchers have developed models such as AquaCrop that allow quantification of impacts of moisture stress on crop growth and yield (Steduto et al., 2009a). And recently, breeders have begun studies on field-based High-Throughput Phenotyping (HTP) (Xing et al., 2017; Araus and Cairns, 2014; Cabrera-Bosquet et al., 2012). This involves planting many varieties of a crop in thousands of small agronomic research plots and precisely measuring standard physical traits, or ‘phenotypes’, for every plot. These phenotypes serve as indicators of crop performance. This allows many varieties to be quickly screened for desired characteristics, enabling rapid progress towards varieties that are high-yielding and tolerant to moisture stress.

The main challenges of field-based HTP are that phenotypes must be measured precisely enough to distinguish the often-subtle differences between plots, and, when fields are large enough, additional field observations may be needed to prevent within-field variation from confounding observed differences between plots. The need for high measurement precision and the high cost of

manual labor traditionally required to collect these data are significant obstacles that must be addressed for these types of studies to progress (Araus & Cairns, 2014).

To overcome these obstacles, it will be critical for researchers to exploit new technologies as they become available. For example, with minimal manual labor, Unmanned Aircraft Systems (UAS) equipped with imaging sensors can acquire imagery at the field scale with the spatial resolution required to resolve individual plots and the temporal resolution required to capture differences in plot behavior over time. With appropriate remote sensing and image analysis techniques, these data may enable frequent, rapid, and precise observations of crop status at the plot scale, leading to more rapid research progress at the field scale (Araus & Cairns, 2014).

For example, a promising phenotype for UAS observation is plot-scale observations of canopy cover. Canopy cover is defined as the fraction of a fixed ground area covered by the canopy or delimited by the vertical projection of the outermost perimeter of the canopy (Eysn et al., 2012). With regards to plant breeding, canopy cover has proven useful for field-based HTP because it may be measured precisely and is related to light interception and yield (Xavier et al., 2017). With regards to crop modeling, the Food and Agriculture Organization (FAO) developed the AquaCrop model to rely on observations of canopy cover instead of Leaf Area Index (LAI) (the surface area of leaves per area of ground surface) with the expectation that canopy cover is a reliable indicator of crop status that is easier to measure remotely (Steduto et al., 2009b).

UAS observations of canopy cover may also be detailed enough to provide new avenues for calibrating crop models such as AquaCrop to simulate impacts of moisture stress on crop growth and yield. For example, if canopy cover is measured frequently and precisely enough, then perhaps an analyses of canopy cover, combined with meteorological and agronomic data, could pinpoint the timing of reductions in leaf expansion rates in field-grown soybean to within a few days. This could be used to constrain AquaCrop to more accurately simulate the timing of moisture stress as well as the severity of its impacts on crop growth and yield.

These challenges, knowledge gaps, and possibilities bring up specific topics for investigation. First, it is necessary to confirm whether canopy cover and color can be measured at the plot scale with UAS imagery. Next, it is critical to quantify how accurate and precise these observations can be and how frequently they can be collected. Once potentially valuable data in the UAS imagery are

identified, the next step is to apply these data to see if they lead to more accurate simulations of moisture stress or better selections of high-yielding varieties that are resistant to moisture stress.

The goal of this study is to evaluate UAS observations of canopy cover and color and combine these data with meteorological and agronomic data to see if UAS observations enable detection of visible indicators of moisture stress that can be used to constrain AquaCrop to more realistically and accurately simulate impacts of moisture stress on crop growth and yield. This would not only demonstrate the utility of UAS imagery for providing precise and useful data for research in agronomy, crop modeling, and breeding at minimal labor cost, but it would also demonstrate that UAS observations can lead to a better understanding of crop growth dynamics and water relations to yield. This is critical in a world where water resources are increasingly scarce and food security is at risk.

## 1.2 Hypotheses and Objectives

### **Hypothesis 1**

In the context of field-based research in agronomy, crop modeling, and breeding, plot scale observations of canopy cover and color can be obtained from visual UAS imagery with enough accuracy, precision, and frequency to detect changes within plots and differences between plots during a growing season.

### **Hypothesis 2**

When combined with meteorological and agronomic data, visual UAS imagery enables detection of visible indicators of moisture stress such as reductions in canopy expansion rates.

### **Hypothesis 3**

Plot scale observations of canopy cover and reductions in canopy expansion rates derived from visual UAS imagery provide additional constraints for calibrating AquaCrop to more realistically simulate the timing and severity of moisture stress as well as its impacts on crop growth and yield.

**Objective 1. Experimental Design and Data Acquisition**

Identify appropriate experimental crop fields for this study and obtain visual UAS imagery, meteorological data, and agronomic data for these experiments for multiple growing seasons that represent moisture-stressed and non-stressed conditions.

**Objective 2. Image Analysis at the Plot Scale**

Evaluate whether the UAS imagery allows canopy cover and color to be measured at the plot scale with enough accuracy, precision, and frequency to detect differences between plots and changes within plots during a growing season.

**Objective 3. Analysis of Stress Indicators**

Perform a joint analysis of the UAS imagery, meteorological data, and agronomic data to determine whether visible indicators of moisture stress can be detected.

**Objective 4. Crop Modeling and Yield Prediction**

Use the AquaCrop model to evaluate whether plot scale observations of canopy cover, color, and visible indicators of moisture stress from visual UAS imagery provide additional constraints for calibrating AquaCrop to more realistically simulate the timing and severity of moisture stress as well as its impacts on crop growth and yield.

### 1.3 Significance of Research

This study will demonstrate new ways of obtaining plot scale observations of canopy cover, color, and visible indicators of moisture stress in experimental crop fields using visual UAS imagery. This could lead to drastic reductions in manual labor for field-based research in agronomy, crop modeling, and breeding. This will be one of the first studies that attempts to quantify both the precision and accuracy of UAS observations of canopy cover and color. This will also be one of the first studies that attempts to use UAS imagery to constrain both the timing and severity of moisture stress in a crop model. This study will also contribute to the discovery and characterization of new phenotypes related to moisture stress that may most effectively be observed by a UAS. Such phenotypes could be applied in field-based HTP to discover new varieties that are high-yielding and resistant to moisture stress.

## 1.4 Dissertation Organization

First, a review of literature on impacts of moisture stress on soybean growth and yield is provided. Then, chapters 2 through 4 present three case studies - the first two addressing hypothesis 1 and objectives 1 and 2 and the third addressing hypotheses 2 and 3 and objectives 3 and 4. Finally, chapter 5 concludes with a summary of findings and recommendations for future work.

## 1.5 Literature Review

### 1.5.1 Soybean Growth and Development

Field-grown soybean begin as seeds planted in soil which germinate and form roots. A few days later, the first leaves emerge from the soil and the plant becomes autotrophic (it attains enough leaf area to synthesize its own food and sustain growth via photosynthesis). From this point, stress free soybean exhibit exponential canopy growth until they approach full size (Oikawa et al., 2013; Board, 1996). During this period, soybean progress through various vegetative and reproductive growth stages. These stages may overlap for indeterminate cultivars (Purcell et al., 2014).

The entire growth cycle, from emergence to maturity, takes approximately four months. During this period, the plant relies on pressure gradients within its shoots and roots to take up water and nutrients from the soil to use for gas exchange and photosynthesis. Soybean maintain the required temperature and pressure (turgor) for these physiological processes to occur via transpiration (Ahuja, 2008). Denmead & Shaw (1962) describe this as a dynamic process, in which water moves from the soil to the roots and finally to transpiring leaves along pressure gradients in the soil and within the plant. At any time during this process, there is a certain pressure gradient between the soil and roots that is required to maintain a given rate of water uptake by the roots and a given transpiration rate. The required pressure gradient is proportional to the potential transpiration rate and inversely proportional to the capillary conductivity of the soil. The potential transpiration rate corresponds to the transpiration rate that a non-stressed plant would maintain under a given set of environmental conditions. It varies dynamically depending on air temperature, humidity, and other variables. The capillary conductivity represents the tendency of the soil to allow water to flow out of it and into the plant. Capillary conductivity decreases rapidly as the soil dries out. Therefore, to maintain a given transpiration rate in drying soil, the pressure gradient within the plant must

continually rise. Under non-stressed conditions, the plant adjusts its pressure gradients as needed to maintain the potential transpiration rate.

### 1.5.2 Moisture Stress

There may come a point when there is not enough moisture in the soil to maintain the potential transpiration rate. As the soil dries beyond this point, the pressure gradient in the plant is forced to rise to a level that causes a decrease in turgor in the plant tissue (Denmead & Shaw, 1962). As a result, the stomata close and the leaves become dehydrated. Once this occurs, the permeability of the plant to water flow decreases and the transpiration rate is forced to drop below the potential rate. The onset of drought stress is defined as the moment when the transpiration rate drops below that of a well-watered crop in the same locality (Meyer & Green, 1981).

From the dynamics described by Denmead & Shaw (1962) we gain a better understanding of the conditions under which drought stress may occur. For example, we expect drought stress to occur when the soil moisture drops below a certain threshold, and we expect it to occur at higher soil moistures when environmental conditions demand higher potential transpiration rates. Additionally, we understand that the soil moisture threshold at which drought stress occurs depends on local soil properties such as capillary conductivity, which may vary throughout a crop field depending on soil type, compaction, and possibly other factors. For example, in soils in which most of the water is loosely held at low pressure (high capillary conductivity), drought stress should not occur until most of the available soil water has been depleted.

This brings up the concept of Plant Available Water (PAW) (Sadras & Milroy, 1996). PAW represents the fractional amount of total soil water capacity that is available for extraction by the plant (Ritchie, 1981). It is defined according to the following expression:

$$PAW = \frac{(\theta - \theta_{PWP})}{(\theta_{FC} - \theta_{PWP})}$$

Where  $\theta$  is the volumetric water content of the soil within the root zone,  $\theta_{PWP}$  is the volumetric water content at the plant wilting point, and  $\theta_{FC}$  is the volumetric water content at field capacity. At any given moment, there is a specific PAW threshold below which a plant begins to experience drought stress (Sadras & Milroy, 1996).

Excessive soil moisture can also cause stress in plants. Terminology for this type of stress varies in the literature, so for the purposes of this discussion, we refer to this type of stress as ‘flood stress’. Flood stress occurs when excessively high soil moisture causes the root zone of the crop to lose access to oxygen which is needed for proper root functioning and nutrient uptake (Rhine et al., 2010). Such conditions have been classified as saturated, waterlogged, and flooded, and soybean respond differently to each type of condition (Pezeshki & Delaune, 2012; Troedson et al., 1989). Saturated conditions are when the soil moisture is maintained above field capacity ( $PAW > 1$ ) (Troedson et al., 1989). Waterlogged conditions are when the water level is a few millimeters to a few centimeters above the soil surface (Rhine et al., 2010). Flooded conditions are when the water level is high enough to submerge all or part of the plant (Sullivan et al., 2001). With regards to the onset of flood stress, a comprehensive review of soybean waterlogging and flooding studies reported that most cultivars can endure waterlogged or flooded conditions for 48-96 hours without injury depending on the cultivar (Rhine et al., 2010).

Both drought and flood stress negatively impact crop growth and yield (Rhine et al., 2010; Steduto et al., 2009a). The magnitude of this impact depends on the timing, duration, and severity of the stress (Ahuja, 2008; Steduto et al., 2009a). For example, it has been shown that soybean yields are most vulnerable to drought and flood stress during the reproductive growth stages, particularly flowering and seed filling (De Souza, 1997; Rhine et al., 2010). Quantifying how sensitive soybean is to moisture stress during each of its growth stages is a subject of ongoing research. Here we briefly summarize findings on these topics.

With regards to drought stress, studies have typically withheld irrigation from stressed treatments for a period ranging from a few days to a few weeks. They then resumed irrigation, allowed the soybean to recover, and recorded yields. These types of studies have shown that drought stress may decrease yields by 30-70% (Ahuja, 2008; De Souza, 1997; Pathan, 2014; Sloane et al., 1990). In a similar manner, studies focused on assessing the impacts of flood stress on soybean yields have typically imposed saturated, waterlogged, or flooded conditions for a few days to a couple of weeks. The plots were then drained, allowed to recover, and yields were recorded. In general, saturated soil conditions have been found to decrease yields by up to 40% (Troedson et al., 1989). But, in hot, arid climates they have also been found to increase yields by as much as 50% (Purcell et al., 1997). Waterlogging has been found to decrease yields by 20-80% (Linkemer, 1998; Reyna

et al., 2003; Rhine et al., 2010). Flooding has been found to reduce yields by 40-100% (all plants dead) (Henshaw, 2007; Rhine et al., 2010; Sullivan et al., 2001).

Clearly, it is important to simulate impacts of moisture stress on crop growth and yield. A great deal of progress has been made with regards to understanding conditions that lead to drought and flood stress and quantifying their impacts on yield. But many challenges remain in terms of understanding how to simulate these scenarios. It is particularly difficult to simulate the timing of the onset of moisture stress within a crop. Traditionally, this has been accomplished using sensors installed in individual plots that continuously monitor transpiration, turgor, soil moisture, and other stress-related properties. However, this is impractical for experimental crop fields containing thousands of small agronomic research plots that require separate analysis (Jones, 2004).

### 1.5.3 Visible Indicators of Moisture Stress

One goal of this study is to determine whether UAS observations of canopy cover could enable detection of visible indicators of moisture stress that can pinpoint the timing of the onset of moisture stress in large numbers of small agronomic research plots. This goal is shared by research on ‘plant-based’ irrigation scheduling (Widuri et al., 2017; Jones, 2004). These studies advocate plant-based indicators of moisture stress since they provide a more direct indication of stress than soil moisture observations alone (Widuri et al., 2017; Jones, 2004; Sivakumar & Shaw, 1978). Here we review research on plant-based indicators of moisture stress to identify indicators that may be detected by a UAS.

### 1.5.4 Indicators of Drought Stress

There are multiple visible indicators of drought stress in soybean. The earliest is a reduction in leaf expansion rate (Ahuja, 2008; Denmead & Shaw, 1962). In general, researchers agree that a reduction in leaf expansion rate precisely indicates the timing of the onset of drought stress. This is because of the strong coupling between leaf expansion and the turgor of plant tissue (Ahuja, 2008; Boyer, 1970; Sadras & Milroy, 1996). Greenhouse experiments have demonstrated that this indicator can be detected at the leaf and plant scale within 24 hours of the onset of drought stress (Ahuja, 2008; Boyer, 1970; Jones, 2004; Liu et al., 2003). Field-based studies have found that weekly measurements of leaf area in selected plots can allow moisture stress to be detected early enough to avoid significant crop damage or yield reductions (Sivakumar & Shaw, 1978).

Another visible indicator of drought stress in soybean is increases in leaf angle (Ahuja, 2008; Boyer, 1970; King, 2009; Oosterhuis et al., 1985; Sivakumar & Shaw, 1978; Wright & Berliner, 1986). Studies have shown that leaf angles begin increasing immediately upon the onset of drought stress, but they increase slowly and progressively over a period of a few days. On top of this, leaf angles vary diurnally, which makes early or precise detection of this indicator difficult (Oosterhuis et al., 1985; Wright & Berliner, 1986).

After changes in leaf angle, the next visible indicator of drought stress in soybean is leaf wilting (King, 2009; Pathan, 2014; Sloane et al., 1990). The PAW threshold known as the 'Permanent Wilting Point' (PWP) was named after this stress indicator (Denmead & Shaw, 1962). However, leaf wilting begins before the PWP is reached. The precise timing of this indicator relative to the onset of drought stress remains unclear. In field experiments with multiple varieties of soybean, King (2009) and Pathan (2014) observed signs of leaf wilting approximately two to three weeks after withholding irrigation from stress treatments. In these experiments, the timing of the onset of drought stress was unclear, so it is difficult to draw conclusions about the timing of leaf wilting relative to the onset of drought stress.

Finally, leaf yellowing is a late indicator of drought stress in soybean that it is induced by severe, prolonged drought (Ahuja, 2008; Carter & Miller, 1994; Marquez-Garcia, 2015). Based on the reviewed studies, it appears that yellowing becomes visible approximately two weeks after the onset of drought stress and begins in the oldest leaves in the understory of the canopy before progressing to the leaves at the top of the canopy (Ahuja, 2008; De Souza, 1997; Marquez-Garcia, 2015). When leaf yellowing is induced by drought stress near the end of the growth cycle, this phenomenon is referred to as 'accelerated leaf senescence' and it may lead to a reduction in the duration of the seed-filling period and losses in yield (De Souza, 1997).

#### 1.5.5 Indicators of Flood Stress

As with drought stress, there are multiple visible indicators of flood stress in soybean. Again, the earliest indicator is a decrease in leaf expansion rate (Henshaw, 2007; Kramer, 1951; Linkemer, 1998; Rhine et al., 2010). Observations collected by Linkemer (1998) and Henshaw (2007) indicate that leaf expansion rates decrease immediately upon initiating a flooding treatment. Linkemer (1998) report that leaf expansion rates in a well-drained site increased in a pattern

indicative of normal exponential growth while a flooded treatment exhibited constant or slowly increasing leaf expansion rates, which they interpret as a sign of ongoing flood stress.

Kramer (1951) and Henshaw (2007) report that leaf wilting is the next visible indicator of flood stress in soybean. But they do not precisely quantify leaf wilting due to flood stress or relate the timing of leaf wilting to the timing of the onset of flood stress.

The last visible indicator of flood stress in soybean is chlorosis, in which leaf color transitions from a healthy dark green to pale green and finally to yellow (Kramer, 1951; Mozafar et al., 1992; Reyna et al., 2003; Rhine et al., 2010). Mozafar et al. (1992) report that soybean leaves show visible signs of chlorosis three to five days after flooding begins and recover from chlorosis (re-green) as soon as four to five days after the soil dries out. Rhine et al. (2010) reported chlorosis one week after flooding was initiated. Troedson et al. (1989) reported chlorosis starting within one week of the start of a saturated soil treatment. The chlorosis persisted for approximately seven to ten days and then the leaves recovered. Nathanson et al. (1984) reported chlorosis within several days of applying flooding treatments. The chlorosis persisted for seven to fourteen days. Reyna et al. (2003) found that ten to fourteen days of flooding were required for soybean to exhibit moderate to severe yellowing due to chlorosis. In general, these studies suggest that chlorosis sets in approximately three to fourteen days after a flooding event.

In summary, visible indicators of drought stress in soybean are: 1) reduced leaf expansion rates, 2) increases in leaf angle, 3) leaf wilting, and, 4) yellowing, while visible indicators of flood stress in soybean are: 1) reduced leaf expansion rates, 2) leaf wilting, and 3) chlorosis. Next, we review research on remote sensing of these visible indicators of moisture stress.

#### 1.5.6 Remote Sensing of Visible Indicators of Moisture Stress

There has been a great deal of research on remote sensing of moisture stress using thermal imagery (Govender et al., 2009; Jones, 2004). A review of thermal remote sensing could help provide a broader historical context for this study. However, we are interested primarily in using visible UAS imagery to detect these visible indicators of moisture stress. Therefore, we consider studies on thermal imagery to be beyond the scope of this review.

When focusing on the visible spectrum, we find that few researchers have attempted to remotely measure these specific visible indicators of moisture stress. Gradual changes in leaf angle and leaf wilting have been observed visually, but not remotely. Changes in leaf color have been observed remotely but based on our review this is not an early or precise indicator of the onset of moisture stress in soybean. Zhou et al. (2016) are one of the only research groups that have attempted to use a UAS to remotely measure canopy cover in outdoor environments for the purpose of detecting moisture stress – most other researchers have only monitored individual leaves using ground-based methods (*e.g.* Jones, 2004). However, Zhou et al (2016) limited their analysis to distinguishing stressed treatments from non-stressed treatments using imagery from a single sampling date rather than looking at time series. Therefore, we focus on measuring canopy expansion rates, as it seems reasonable to expect that this can be done with a UAS with enough spatial and temporal resolution to pinpoint the timing of reductions in canopy expansion rates and the onset of moisture stress.

Although reductions in canopy expansion rates have been strongly linked to moisture stress, it is important to recognize that this indicator could be elicited by other sources of stress, such as adverse air temperatures or soil nutrient deficiencies (Ahuja, 2008; Steduto et al., 2009a). Therefore, it is best to think of such indicators as indicative of stress in general. The type of stress that is occurring can be determined using meteorological and agronomic data. For example, one may analyze rainfall, soil moisture, and air temperature around the time the indicator of stress was observed to identify whether it was elicited by adverse soil moisture, temperature, or other factors. This highlights the need for meteorological and agronomic data for such indicators to be useful. Therefore, it makes sense to apply them in a crop modeling study.

### 1.5.7 Crop Modeling

The goal of this study is to demonstrate that UAS observations of canopy cover and visible indicators of moisture stress can provide additional constraints for calibrating AquaCrop to more realistically simulate the timing and severity of moisture stress and its impacts on crop growth and yield. To clarify our modeling objectives, we provide a brief overview of crop modeling, including an explanation of what crop models are, what they are used for, and basic techniques for simulating crop growth and yield. We then discuss model calibration, with a focus on calibrating models to simulate impacts of moisture stress on crop growth and yield. Finally, we explain why we selected the AquaCrop model for this study, how it works, and how we used it to test hypothesis 3.

A crop model is a conceptual and mathematical model used to make quantitative predictions about the behavior of a crop within a limited range of scenarios (van Ittersum et al., 2003). Crop models are inherently a simplification of the complexities of the physical systems that they are trying to represent (Boote et al., 1996). The amount of simplification that is allowable depends on the processes that are being simulated and the intended purpose of the model (van Ittersum et al., 2003). Crop models typically require input data, which represent the scenario of interest, and rely on a set of equations and parameters that, when properly calibrated, allow them to calculate output variables that represent how the crop would behave in similar scenarios.

One of the most important uses of crop models is to combine data from multiple sources and utilize our current understanding of crop growth to enable research applications that would otherwise be impossible (Boote et al., 1996). Modeling objectives vary widely, as they can range from investigating detailed crop growth mechanisms to predicting farm yields or assessing impacts of pollution or soil erosion. Crop models have also been developed for a variety of spatial and temporal scales, such as the leaf, plant, plot, field, and regional scale, and for time periods spanning hours to years (Hammer et al., 2002).

Many state-of-the-art crop models such as CropSyst (Stöckle et al., 2003), CROPGRO (Wang et al., 2003), APSIM (Keating, 2003), SWAT (Gassman et al., 2007), and AquaCrop (Steduto et al., 2009a) have been designed to simulate crop growth and yield on a daily time step at the plot and field scale. To accurately simulate crop growth, many models start by simulating the progression of the crop through its basic vegetative and reproductive growth stages (Hammer et al., 2002). This is typically accomplished using a concept referred to as Growing Degree Days (GDD) (McMaster & Wilhelm, 1997). GDD are accumulated daily according to the following equation:

$$GDD = \frac{(T_{max} + T_{min})}{2} - T_{base}$$

Where  $T_{max}$  and  $T_{min}$  are the daily minimum and maximum air temperatures and  $T_{base}$  is a crop-specific parameter that represents a median air temperature below which no crop growth occurs (if  $(T_{max} + T_{min})/2 < T_{base}$ , then  $GDD = 0$ ). Basically, the rate of progression of the crop through its basic growth stages is assumed to be largely determined by daily air temperatures represented by an accumulation of  $GDD$  over time (McMaster & Wilhelm, 1997).

As the crop proceeds through its various growth stages, crop growth is simulated concurrently as the production of biomass over time. At the end of the simulation, yield is estimated as a fraction of the total biomass. This fraction is typically expressed in terms of a parameter known as the Harvest Index (*HI*), which represents the fraction of the total biomass that is partitioned into the yield component of the crop at harvest (Bindi et al., 1999).

Crop growth is driven primarily by leaf area, water use, and photosynthesis. Therefore, some measure of leaf area available for photosynthesis and transpiration is necessary for accurate simulation of crop growth (Ahuja, 2008; Hammer et al., 2002; van Ittersum et al., 2003). For this purpose, models typically rely on observations of LAI over time. There are also a few models that have been developed to rely on canopy cover instead of LAI (Steduto et al., 2009b). Based on this review, there is no evidence suggesting that one approach is necessarily better than the other, and both approaches have been shown to produce accurate simulations in a variety of scenarios (Gassman et al., 2007; Keating, 2003; Steduto et al., 2009a; Stöckle et al., 2003; Wang et al., 2003).

Different models use different equations to describe crop growth. We will not present specific equations here. Instead, we will discuss their basic characteristics. Many of the first crop models and most currently existing models estimate biomass production by assuming that it is proportional to the amount of leaf area, the solar radiation intercepted by the canopy, and a Radiation Use Efficiency (RUE) parameter. The decision to estimate crop growth by relying on RUE has been largely motivated by the fact that the RUE of a crop is a relatively stable parameter that is straightforward to estimate (Hammer et al., 2002; Steduto et al., 2007; Warmink, 2010).

To better simulate moisture stress, researchers have also developed ‘water-driven’ models that assume that biomass production is proportional to the amount of leaf area, the amount of water transpired by the crop, and a Water Use Efficiency (WUE) parameter (Steduto et al., 2007). Estimating WUE is more difficult than estimating RUE, mainly because it requires the measurement of crop transpiration separate from soil evaporation. But recent advances have made it easier to estimate WUE and there have been several studies suggesting that WUE is a more stable and conservative parameter than RUE that enables better model performance (Hammer et al., 2002; Steduto et al., 2007; Warmink, 2010). For this reason, researchers advocate further testing and evaluation of water-driven models, especially when the objective of the study is to improve our understanding of water relations to yield (Hammer et al., 2002; Steduto et al., 2007).

In addition to using water-driven growth equations, some models simulate the soil-water balance over the course of the growing season (Ahuja, 2008; Gassman et al., 2007; Hammer et al., 2002; Keating, 2003; Steduto et al., 2009a; Stöckle et al., 2003; Wang et al., 2003). This is typically accomplished by treating the root zone of the crop as a compartment of porous soil of fixed volume. This compartment is assumed to have fixed soil properties that determine its ability to absorb water from precipitation or irrigation, provide water to the plant, or drain water to deeper soil layers (Saxton & Rawls, 2006). These soil properties are typically determined experimentally or estimated based on soil type and texture (Saxton & Rawls, 2006).

Typically, a soil-water balance equation is used to compute the Plant Available Water (PAW) in the root zone over time. Precipitation data are the main input for this equation. Different models use different soil-water balance equations. We will not present specific equations here. Instead, we will discuss their basic applications. Models typically assume that certain PAW thresholds correspond to drought or flood stress (Sadras & Milroy, 1996). Proper specification of these thresholds is critical for accurately simulating impacts of moisture stress on crop growth and yield, since they determine both the timing and severity of simulated stress (Sadras & Milroy, 1996; Steduto et al., 2009a). Currently, many models simulate drought stress, but few simulate both drought and flood stress (Steduto et al., 2009a; Wang et al., 2016).

In addition to precipitation data, meteorological data such as air temperature and humidity are used as inputs for estimating crop transpiration. Sometimes, air temperature is also used to simulate heat stress (Ahuja, 2008; Hammer et al., 2002; Steduto et al., 2009a). Some models even attempt to simulate impacts of soil salinity, fertility, and differences between cultivars (Boote et al., 1996; Hammer et al., 2002; Steduto et al., 2009a).

When the objective of the model is to estimate crop growth and yield, impacts of stress are typically modeled as penalties to biomass production or the harvest index administered via stress coefficients (Bindi et al., 1999; Gassman et al., 2007; Keating, 2003; Steduto et al., 2009a; Stöckle et al., 2003; Wang et al., 2003). Different models assign penalties differently and the best ways of doing so remains an active area of research (Boote et al., 1996; Hammer et al., 2002).

### 1.5.8 Model Calibration

Crop models typically require a significant amount of input data and direct observations of model outputs to calibrate various model parameters. Calibration is typically a manual and iterative process involving the following three steps: 1) Obtain model inputs and direct observations of model outputs (observed data), 2) Run the model to obtain simulated outputs (simulated data), and, 3) Evaluate the agreement between simulated and observed data using appropriate metrics (Hammer et al., 2002). For example, Willmott's index of agreement ( $d$ ) is often used to evaluate the agreement between simulated and observed data (Willmott, 1982):

$$d = 1 - \frac{\sum(S_i - O_i)^2}{\sum(|S_i - \bar{O}| + |O_i - \bar{O}|)^2}$$

Here,  $S_i$  are the simulated values for a given variable,  $O_i$  are the corresponding observed values, and  $\bar{O}$  is the mean of the observed values. The value of  $d$  ranges from 0 to 1, with 0 indicating no agreement and 1 indicating perfect agreement between simulated and observed data. Unlike simpler metrics such as the coefficient of determination ( $r^2$ ) or the Root-Mean-Squared-Error (RMSE), this metric is sensitive to systematic overestimation or underestimation (Gaile & Willmott, 1984; Legates & McCabe, 1999). These three steps are repeated until one gets the best overall agreement between simulated and observed data.

Every direct observation of a simulated output variable provides an additional constraint on the model parameters during calibration, so the more output variables that are observed, the more likely a calibration will be successful. For example, if a model is designed to simulate the soil-water balance, canopy expansion, and biomass production, then observations of soil moisture, canopy cover, and biomass will help constrain parameters related to these processes. However, such processes are often simulated as being interdependent. For example, canopy cover may impact the amount of water transpired by the canopy, which may impact the amount of biomass produced (Steduto et al., 2009a). As a result, it is usually not possible to calibrate parameters independently using different sets of observations. Instead, parameters must be jointly optimized to maximize the overall agreement between observed and simulated data.

This brings up a major issue in model calibration - equifinality - in which multiple sets of parameter values lead to the same simulation results for a given set of input data (Beven, 2006; Rajib et al., 2016). The possibility of equifinality increases as the model becomes more complex. In such cases,

there is an increased risk of obtaining erroneous parameters that appear to reproduce observed results but lead to errors in other scenarios. The likelihood of encountering problems related to equifinality may be reduced by using a model that is as simple as possible and by using as many different types of observations as possible to constrain the model (Hammer et al., 2002; Beven, 2006; Rajib et al., 2016). This includes dynamic constraints such as ensuring that the timing of simulated moisture stress is consistent with the timing of observed indicators of moisture stress.

#### 1.5.9 Model Selection

Considering the challenges of model calibration, it is best to use the simplest model that is appropriate for the study objectives and best utilizes the available observations for calibration. It is also critical that the intended purpose of the model supports the study objectives (Boote et al., 1996). In this study, we are focused on using ground and UAS-based observations of canopy cover and visible indicators of moisture stress to constrain calibration of PAW thresholds and stress coefficients to simulate moisture stress and yield for a single soybean cultivar. This objective is simple and applicable to almost any plot or field scale model that implements a soil-water balance with PAW thresholds and stress coefficients. Therefore, in this case, it is acceptable to use a model that is relatively simple, in which the specification of PAW thresholds and stress coefficients for moisture stress have significant, easily measurable impacts on simulation results.

Various crop models that roughly satisfy these criteria were considered for this study, including CropSyst (Stöckle et al., 2003), Crop-Gro-Soybean (Bhatia, 2008; Wang et al., 2003), APSIM (Holzworth, 2014; Keating, 2003), SWAT (Gassman et al., 2007), and AquaCrop (Steduto et al., 2009a). We selected AquaCrop for this study because it is the only plot and field scale model that uses canopy cover, rather than Leaf Area Index (LAI), as the primary metric of leaf area available for crop growth (Steduto et al., 2009a). Also, AquaCrop was designed specifically to address the problem of increasing yields with finite water resources by improving our ability to model water relations to yield (Steduto et al., 2007). For example, it has been successfully applied to modeling drought stress for irrigation scheduling (Geerts et al., 2010). Also, among the considered models, it is the simplest and easiest to calibrate (while still representing the characteristics of crop growth that are most important to this study), requiring the smallest number of input parameters and providing resources and tools to facilitate iterative model calibration and evaluation (Lorite, 2013; Raes et al., 2009; Steduto et al., 2009a; Vanuytrecht, 2014). Various sensitivity analyses of

AquaCrop have shown that it would be well suited to a study focused on PAW thresholds and stress coefficients, since variations in these parameters have been shown to significantly impact yield predictions (Vanuytrecht, 2014).

With regards to yield prediction errors, error tolerance depends on the study objectives (Refsgaard, 2007). For this study, we do not require maximal accuracy, only that AquaCrop simulates crop growth and yield realistically enough to compare the relative accuracy of two different calibration methods. Yield prediction error may be defined as follows:

$$\text{Yield Prediction Error} = \frac{\text{Predicted Yield} - \text{Observed Yield}}{\text{Observed Yield}}$$

Researchers have reported field-scale yield prediction errors with AquaCrop ranging from 1% to 31% for sixteen experiments with irrigated soybean in Brazil (Da Silva et al., 2018), 1% to 20% for four experiments in Nigeria (Abeboye et al., 2017), 4% to 33% for six experiments with rain-fed soybean in India (Steduto et al., 2009b), 2% to 12% for five experiments with irrigated soybean in China (Paredes, 2015), and 10% for one experiment with irrigated soybean in Lebanon (Saab et al., 2014). AquaCrop has also been applied to other crops with similar success, including corn (Heng et al., 2009; Hsiao et al., 2009; Mebane et al., 2013; Steduto et al., 2009b), sorghum (Steduto et al., 2009b), wheat (Jin et al., 2014), sunflower (Saab et al., 2014), quinoa (Steduto et al., 2009b), and cotton (Steduto et al., 2009b). Based on these results, it seems reasonable to assume that AquaCrop simulates crop growth and yield accurately enough for the purposes of this study.

#### 1.5.10 The AquaCrop Model

Here we provide a brief description of AquaCrop's basic algorithms and parameters. Like most crop models, AquaCrop uses Growing Degree Days (*GDD*) to model the progression of the crop through its basic reproductive growth stages: 1) flowering, 2) yield formation, and, 3) maturity. Calculations run on a daily time step. Here we present the basic form of the most important equations in AquaCrop to illustrate AquaCrop's basic concepts. For further detail, the reader is referred to various papers describing the model (Raes et al., 2009; Steduto et al., 2009a) and the user manual (Raes et al., 2012). AquaCrop calculates yield (*Y*) by multiplying the biomass of the crop (*B*) by a harvest index (*HI*):

$$Y = B \times HI$$

AquaCrop estimates biomass production using a water-driven growth equation:

$$B = WP \times \sum Tr$$

Where  $\sum Tr$  is the cumulative crop transpiration and  $WP$  is the biomass water productivity (biomass per unit of cumulative crop transpiration).  $WP$  is a constant and conservative parameter for a given crop type and climate (Steduto et al., 2009a).  $Tr$  is calculated as follows:

$$Tr = Kcb \times ET_0$$

Where  $Kcb$  is the crop coefficient for transpiration and  $ET_0$  is the reference evapotranspiration according to the Penman-Monteith Equation (Monteith, 1965).  $Kcb$  is calculated as the product of the crop coefficient at 100% canopy cover ( $Kcb_x$ ) and the current canopy cover ( $CC$ ):

$$Kcb = CC \times Kcb_x$$

Canopy cover increases exponentially for non-stressed soybean until full size is approached (Board, 1996). Accordingly, AquaCrop simulates canopy expansion using exponential growth and decay equations. The form of the equation depends on how close the crop is to maximum canopy cover and maturity. Exponential growth is assumed during the first half of canopy expansion. During the second half, canopy cover increases according to an exponential decay equation until maximum canopy cover is reached. Later, a different form of exponential decay is used to simulate the expected decline in canopy cover approaching maturity:

$$1^{\text{st}} \text{ half of canopy expansion } \left( CC < \frac{CC_x}{2} \right): CC = CC_0 e^{(CGC)t}$$

$$2^{\text{nd}} \text{ half of canopy expansion } \left( CC \geq \frac{CC_x}{2} \right): CC = CC_x - (CC_x - CC_0) e^{-(CGC)t}$$

$$\text{Decline of } CC \text{ towards maturity: } CC = CC_x \left[ 1 - 0.05 \left( e^{\left( \frac{CDC}{CC_x} \right) t} - 1 \right) \right]$$

Here,  $CC_0$  is the canopy cover at which the canopy first becomes autotrophic and starts to grow exponentially,  $CC_x$  is the maximum canopy cover,  $CGC$  is a canopy growth coefficient,  $CDC$  is a canopy decline coefficient, and  $t$  is the time passed. Together, these equations allow AquaCrop to simulate non-stressed canopy expansion, transpiration, biomass production, and yield.

Evaluating the detailed mechanics of AquaCrop's simulation of the soil-water balance or comparing this aspect of AquaCrop to other models is beyond the scope of this study. Therefore, we describe AquaCrop's soil-water balance with enough detail to show that this aspect of the model is reasonable, similar to other models, and appropriate for this study.

AquaCrop simulates the soil-water balance by estimating surface run-off, soil evaporation, infiltration, drainage, and root uptake for different soil compartments within the root zone. Surface-runoff is estimated based on the Curve Number method (Hjelmfelt, 1991). The Curve Number method was originally developed for large scale hydrologic modeling of storm runoff in agricultural areas. It is a simple and computationally efficient method which makes it desirable for many modeling applications. However, there has been a great deal of debate as to whether the Curve Number method is appropriate for different environments or smaller spatial scales such as the plot scale (Hawkins, 2014). Fortunately, AquaCrop allows the user to avoid relying on the Curve Number method by assuming that surface runoff is negligible. This assumption is reasonable for flat, well-drained crop fields where little to no runoff occurs.

Soil evaporation is modeled in two stages; 1) an energy limiting stage where there is readily available water on the soil surface for evaporation and, 2) a falling-rate stage where water transport to the surface from layers below is limiting (Philip, 1957; Ritchie, 1972). Soil evaporation ( $E$ ) is calculated as follows:

$$E = Kr \times (1 - CC^*) \times Kc_{e,wet} \times ET_0$$

Where  $ET_0$  is the reference evapotranspiration,  $Kc_{e,wet}$  is the evaporation coefficient for fully wet and unshaded soil surface (Allen et al., 1998),  $CC^*$  is the canopy cover slightly adjusted for micro-advective effects, and  $Kr$  is an evaporation reduction coefficient ( $Kr = 1$  for stage I evaporation). Details on the adjustment of  $CC^*$  are available in Adams et al. (1976) and Villalobos (1990). Details on the adjustment of  $Kr$  are available in Raes et al. (2009).

Rainfall that is not lost as runoff or soil evaporation is assumed to infiltrate the soil and drain through the root zone. The depth of the root zone is simulated using the following equation:

$$Z = Z_{ini} + (Z_x - Z_{ini}) \sqrt[n]{\frac{(t - \frac{t_0}{2})}{(t_x - \frac{t_0}{2})}}$$

Where  $Z$  is the effective rooting depth,  $Z_{ini}$  is the planting depth,  $Z_x$  is the maximum effective rooting depth,  $t$  is the time after planting,  $t_0$  is the time when the canopy becomes autotrophic,  $t_x$  is the time when  $Z_x$  is reached, and  $n$  is a shape factor. This equation results in a slow and steady increase in root length over the course of the growing season. The root zone is divided into compartments of different depths (12 by default). AquaCrop adjusts the thickness of each compartment to best simulate the soil-water balance. For example, for deep root zones, the thickness is not constant but increases exponentially with depth so that infiltration, evaporation, and transpiration from the top layers are simulated with enough detail.

Drainage of water through soil compartments in the root zone is simulated by a set of equations where the volumetric water content ( $\theta$ ) of the soil is the dependent variable. A drainage coefficient ( $\tau$ ) is calculated based on the saturated hydraulic conductivity of the soil ( $K_{sat}$ ) and it is used to simulate downward movement of water through the soil profile. Drainage occurs when the volumetric water content of a soil compartment is above field capacity. The amount of water that drains out of soil compartment  $i$  at time step  $\Delta t$  is described by an exponential drainage function:

$$\frac{\Delta\theta_i}{\Delta t} = \tau(\theta_{sat} - \theta_{FC}) \left( \frac{e^{\theta_i - \theta_{FC}} - 1}{e^{\theta_{sat} - \theta_{FC}} - 1} \right)$$

Where  $\Delta\theta_i$  is the volumetric water content of soil compartment  $i$ ,  $\theta_{sat}$  and  $\theta_{FC}$  are the volumetric water contents of the soil at saturation and field capacity, and  $\frac{\Delta\theta_i}{\Delta t}$  is the decrease in the volumetric water content of soil compartment  $i$  during time step  $\Delta t$ . When  $\tau$  is close to 1, a thoroughly wetted soil profile will drain to field capacity in approximately 1 day. Lower values of  $\tau$  result in slower drainage (Raes et al., 2009). This function has been shown to closely mimic drainage observed in the field (Geerts, 2008; Raes et al., 2009).

Finally, extraction of water by the roots within each soil compartment is estimated based on the simulated transpiration rate ( $Tr$ ), the depth of the root zone ( $Z$ ), and a sink term ( $S$ ) that denotes a maximum rate of water extraction per unit of soil depth (Belmans et al., 1983; Feddes, 1978):

$$S = \frac{Tr}{Z}$$

The total extraction of water from the root zone is calculated by integrating water extraction over the soil compartments until it equates to the simulated transpiration rate.

AquaCrop simulates various types of stress due to drought, flood, heat, cold, soil fertility, and soil salinity. Stress caused by diseases or pests are not considered. Here we focus on illustrating how moisture stress is simulated in AquaCrop and how this relates to the specification of PAW thresholds and stress coefficients. AquaCrop simulates moisture stress by applying stress coefficients to its equations governing canopy expansion, transpiration, and yield formation. These stress coefficients are functions of simulated PAW values and thresholds for moisture stress. For example, the onset of drought stress is simulated by assuming that there are upper and lower PAW thresholds between which canopy expansion rates are reduced. When the simulated PAW drops below the upper PAW threshold, a stress coefficient for expansive growth ( $Ks_{exp}$ ) is reduced from 1 to some number between 1 and 0 according to a convex curved mapped between the upper and lower PAW thresholds (Figure 1). The shape of this curve is typically convex to account for plant acclimation to mild stress and decreased soil capillary conductivity at low PAW values, but it may be adjusted using a shape factor ( $f_{exp}$ ). This stress coefficient slows canopy expansion by reducing the  $CGC$  parameter according to the following equation:

$$CGC_{adjusted} = Ks_{exp} \times CGC$$

AquaCrop uses four different stress coefficients to simulate impacts of moisture stress on crop growth, stomatal conductance, canopy senescence, transpiration, and yield formation. Three of these coefficients affect drought stress and one affects flood stress. The coefficients for drought stress are referred to as coefficients for expansive growth ( $Ks_{exp}$ ), stomatal closure ( $Ks_{sto}$ ), and accelerated senescence ( $Ks_{sen}$ ). The coefficient for flood stress is referred to as an aeration stress coefficient ( $Ks_{aer}$ ). All of AquaCrop's moisture stress coefficients are defined in the same manner as  $Ks_{exp}$  (using upper and lower PAW thresholds and a shape factor).

Overall, there are eight independent parameters that must be correctly specified for moisture stress to be triggered and simulated properly in AquaCrop. Five of these are PAW thresholds: upper and lower thresholds for reductions in canopy expansion ( $a_{exp}$  and  $b_{exp}$ ), an upper threshold for accelerated senescence ( $a_{sen}$ ), an upper threshold for stomatal closure ( $a_{sto}$ ), and an upper threshold for aeration stress ( $a_{aer}$ ). Three are shape factors for: expansive growth ( $f_{exp}$ ), stomatal closure ( $f_{sto}$ ), and accelerated leaf senescence ( $f_{sen}$ ). The remaining PAW thresholds and shape parameters are fixed. For example, the lower PAW threshold for flood stress is set to  $PAW = 1$  so flood stress only occurs when the soil moisture exceeds field capacity.

AquaCrop's parameters for stressed and non-stressed growth may be calibrated separately (Raes et al, 2012). Specifically, parameters such as the canopy growth coefficient ( $CGC$ ) and maximum canopy cover ( $CC_x$ ) may be calibrated using observations of non-stressed plants, while parameters related to stressed growth such as PAW thresholds and shape parameters for stress coefficients may be calibrated using observations of stressed plants. In summary, AquaCrop is a water-driven model that dynamically simulates canopy cover, root length, the soil-water balance, and their combined impacts on transpiration, biomass production, and yield via stress coefficients (Figure 2). The basic inputs required to run AquaCrop include daily air temperature, reference evapotranspiration, rainfall, initial soil moisture conditions, soil drainage properties, flowering, seed-filling, and maturity (Table 1). Observations of model outputs required for calibration include periodic observations of canopy cover and biomass (Table 2). Additional constraints such as periodic observations of soil moisture, root length, and yield are considered optional but can enhance the quality of the calibration (Raes et al., 2012).

Here we present three case studies addressing our primary hypotheses and objectives. The first two address hypothesis 1 and objectives 1 and 2, while the third addresses hypotheses 2 and 3 and objectives 3 and 4. We conclude with a summary of findings and recommendations for future work.

## CHAPTER 2. MULTILAYER UAS IMAGE ORTHOMOSAICS FOR FIELD-BASED HIGH-THROUGHPUT PHENOTYPING

### 2.1 Abstract

High-Throughput Phenotyping (HTP) of agronomic research plots using imagery from Unmanned Aircraft Systems (UAS) is a promising area of research for increasing crop yields to ensure food security. Currently, researchers are extracting phenotypes from single-layer image ortho-mosaics (SLMs) generated by stitching overlapping frame photos into a single composite image using commercial software such as Pix4Dmapper™. SLMs are prone to geometric and radiometric distortion and row-offset errors caused by image stitching errors and variations in lighting, bi-directional reflectance, and image quality. In addition, they provide only one observation per plot per flight date, which makes it impossible to quantify measurement precision or apply statistical quality control. To reduce geometric and radiometric distortion and allow better quality control, we propose separately ortho-rectifying replicate images of plots from overlapping frame photos using collinearity and nearest-neighbor resampling. We tile these images to form ‘multilayer mosaics’ (MLMs), in which replicate images of plots are contained in different layers of the mosaic. We demonstrate advantages of MLMs by evaluating row-offset errors, canopy cover, and color for twenty-one soybean research plots on thirteen flight dates spanning canopy emergence to closure. We find row-offset errors in 24 out of 3790 replicate plot images. Canopy cover measurements from SLMs and MLMs were significantly different for 198 out of 273 sampling points (21 plots x 13 flight dates), with median values from MLMs being closer to ground reference values by an average of 2.4% cover. Canopy hues were also significantly different for 153 out of 273 sampling points.

#### *Keywords*

(1) High-throughput phenotyping, (2) unmanned aircraft systems, (3) single-layer image ortho-mosaics (SLMs), (4) multilayer image ortho-mosaics (MLMs), (5) geometric distortion, (6) radiometric distortion, (7) row-offset errors, (8) canopy color, (9) canopy cover.

## 2.2 Introduction

Field-based High-Throughput Phenotyping (HTP) of agronomic research plots is a promising area of research for increasing crop yields to ensure food security (Araus & Cairns, 2014). HTP involves measuring physical characteristics of hundreds to thousands of small research plots in experimental crop fields. In this case, the field scale corresponds to a few hectares and the plot scale corresponds to a few square meters ( $1 \text{ ha} = 10,000 \text{ m}^2$ ). Plots may be used to identify best performing varieties, or for other purposes, such as optimizing management practices. Measuring phenotypes can require excessive manual labor. In addition, phenotypic differences between plots are often subtle, so measurements must be precise. Labor costs and the need for high precision and accuracy are major obstacles to research progress (Araus & Cairns, 2014).

Unmanned Aircraft Systems (UAS) are a promising low-cost platform for collecting plot-scale observations for field-based HTP. They can automatically and rapidly collect hundreds of overlapping frame photos of a crop field from a low altitude. These photos can be stitched into a single large composite image ortho-mosaic (hence referred to as a ‘single-layer mosaic’ or SLM) using techniques from photogrammetry and computer vision implemented in commercial software such as Pix4Dmapper (Pix4D, Lausanne, Switzerland). Phenotypes for each plot can then be extracted from the SLM or the frame photos.

So far, researchers have focused on extracting phenotypes from SLMs. They have reported high measurement accuracies for various phenotypes including canopy cover and color (Haghighatablab et al., 2016; Shi et al., 2016). However, they have also found that SLMs are prone to geometric and radiometric distortion caused by image stitching errors and variations in lighting, bi-directional reflectance, and image quality (Tao et al., 2017). This is especially true in agricultural terrain that lacks distinct features needed for image stitching.

Image stitching errors often show up in SLMs as spatial discontinuities. If these occur within plots, they can obstruct phenotype measurements related to crop structure. They can also cause row-offset errors, in which a row of plants is incorrectly aligned with imagery of a neighboring row. This problem is exacerbated when blending algorithms combine overlapping photos into a single composite image that appears to be spatially continuous and representative of the scene, as done by default in Pix4Dmapper. In this case, an image of a plot in an SLM may appear reliable, but it may actually be composed of some images of the correct plot and some images of neighboring

plots. This can lead to costly mistakes in small plot research, such as selecting wrong varieties for advancement through breeding pipelines when their neighboring plots should have been selected.

Image stitching errors and variations in lighting, bi-directional reflectance, and image quality also show up in SLMs as discontinuities in brightness, color, and sharpness. If these occur within plots, they can obstruct phenotype measurements related to color. This too is exacerbated by image blending algorithms which can radiometrically and geometrically distort objects in areas of image misalignment.

Few researchers (*e.g.* Tao et al., 2017) have been able to quantify impacts of these types of distortion on the precision and accuracy of UAS observations because SLMs only offer one observation per plot per sampling date. A better understanding of these problems is needed to ensure effective usage of UAS imagery for making important research decisions.

Instead of using SLMs, we propose separately ortho-rectifying replicate images of plots from overlapping frame photos using collinearity and nearest-neighbor resampling. These images can be tiled to form a new type of ortho-mosaic – a ‘multilayer mosaic’ or MLM – in which replicate images of plots are contained in different mosaic layers. This will allow researchers to: 1) improve mosaic fidelity to the raw frame photos, 2) avoid undesired color modification by commercial image stitching software, 3) minimize geometric and radiometric distortion caused by image stitching errors, 4) visualize and correct row-offset errors, 5) visualize variations from photo to photo caused by changes in lighting, bi-directional reflectance, and image quality, and, 6) quantify and enhance the precision and accuracy of UAS observations.

Here we present a case study to illustrate a methodology for generating MLMs from overlapping frame photos of two hectares of experimental soybean. The imagery was collected on thirteen flight dates spanning emergence to canopy closure and processed with Pix4Dmapper and Matlab. We evaluate whether our methodology achieves the capabilities listed above by comparing plot-scale measurements of two phenotypes – canopy cover and color – from SLMs and MLMs. Ground reference measurements from ground-based imagery and replicate measurements from MLMs and allow us to quantify both the precision and accuracy of our UAS observations. We also measure the frequency of row-offset errors and explain how to correct them. This will help researchers understand how to maximize the precision and accuracy of UAS observations for field-based HTP and other research applications.

## 2.3 Methods

### 2.3.1 Field Site

The case study was a collaborative research project involving soybean breeders in the Agronomy Department and remote sensing researchers in the Agricultural and Biological Engineering Department at Purdue University. The field site was located at the Agronomy Center for Research and Education at Purdue University. It consisted of two hectares of experimental soybean planted with a precision plot planter on May 23<sup>rd</sup>, 2016 as arrays of plots classified by row and range numbers. The row orientation was south to north and the row spacing was 76 cm. Each two-row plot was approximately 4 m<sup>2</sup> in size. Twenty-one test plots were used for this study (Figure 3).

### 2.3.2 Image Acquisition

The UAS was a small, fixed-wing Precision Hawk Lancaster Mark-III (3 kg total weight, 1.5 m wingspan) equipped with a 14-megapixel Nikon 1-J3 digital camera collecting imagery in the visible spectrum with manually adjusted aperture, shutter speed, ISO sensitivity, and focus. The UAS stored GPS coordinates for each photo with a horizontal and vertical accuracy of approximately 2 m and 5 m, respectively.

We conducted flights twice a week from June 3<sup>rd</sup> to July 19<sup>th</sup>, 2016 resulting in thirteen sampling dates spanning canopy emergence to closure. We flew the UAS 50 m above ground level resulting in a spatial resolution of 1.5 cm per pixel. We captured 70-90% forward and lateral image overlap to allow accurate image stitching and at least four images of each plot on every sampling date.

### 2.3.3 Single-Layer Mosaic Generation

We stitched the imagery using Pix4Dmapper with default settings for mosaic generation. This produced SLMs, digital elevation models, and estimates of camera positions and orientations for every photo and flight date. Pix4Dmapper also provided estimates of internal camera parameters for modeling geometric lens distortion. These outputs were horizontally co-registered to UTM eastings and northings of twenty-five Ground Control Points (GCPs) that were set up in the field before flights and imported into Pix4Dmapper before image stitching.

#### 2.3.4 Multilayer Mosaic Generation

Our methodology differs from previous studies in the way we ortho-rectified the imagery. Researchers in photogrammetry have known for many years that it is possible to remove geometric lens distortion from frame photos and apply a collinearity relationship to trace rays of light from 3D coordinates in the scene to their corresponding 2D coordinates in the frame photos (*e.g.* Mikhail, 1974). In this case, if we obtain map coordinates of individual research plots (UTM eastings, northings, and altitudes) from the SLMs and digital elevation models, then we can apply collinearity to the camera positions and orientations and internal camera parameters to locate the plots in the frame photos and separately ortho-rectify multiple replicate images of plots.

We obtained the map coordinates of the plots as follows: First, we segmented an SLM into green vegetation and background using the Excess Green Index (ExG) and Otsu thresholding (Otsu, 1979; Woebbecke et al., 1995). Then, we gridded the segmented mosaic into individual plots using a custom algorithm implemented in Matlab. This gave us image coordinates for every plot in the SLMs. We used the appropriate affine transformations to convert these image coordinates into UTM eastings and northings (Hearst & Cherkauer, 2015). We obtained altitudes from corresponding coordinates in the digital elevation models. These coordinates were consistent across flight dates due to image co-registration.

Once we had map coordinates for every plot, we applied collinearity to the camera positions and orientations and internal camera parameters to locate the plots in the frame photos and separately ortho-rectify replicate images of every plot. Ortho-rectification calculations were performed in Matlab using nearest-neighbor resampling to preserve pixel colors from the raw frame photos.

Small errors in image stitching led to small spatial offsets from correct plot locations when collinearity was used to extract plots from the frame photos. When these offsets were large enough, they led to row-offset errors. These could be visualized by inspecting replicate images of each plot and determining whether they were centered on the correct plot. To ensure that every plot was extracted in its entirety from every frame photo, we ortho-rectified an additional spatial buffer around the edges of each plot. Finally, we corrected row-offset errors by manually cropping each image to the correct plot.

We saved the plot images in uncompressed Tiff format using a file-naming convention that documented the flight date, field experiment, row and range number, and replicate image number for each plot. We grouped the plot images by flight date and field experiment. Then we tiled the images in positions corresponding to their rows and ranges in the field and layered them according to their replicate image numbers to form MLMs. There was one MLM per field experiment per flight date (Figure 4). Each MLM had  $N$  layers, where  $N$  was the maximum number of replicate images in that experiment on that flight date.

Ortho-rectifying images of plots of fixed pixel dimensions and tiling them in this manner allowed us to; 1) preserve pixel colors from the raw frame photos, 2) avoid color modifications by Pix4Dmapper, and, 3) avoid geometric and radiometric distortion from image stitching errors. It guaranteed spatial continuity within plot images in the mosaic. However, it did not guarantee spatial continuity between plots since the spacing between the plots in the field was not perfectly constant. As a result, small portions of the field near the borders of the plots were either replicated or omitted at the borders between plots in the MLMs.

### 2.3.5 Ground Reference Imagery

Ground photos of the twenty-one test plots were also collected on every flight date. These were captured from 4 m above the canopy at nadir perspective using a 13-megapixel smartphone camera fixed to a pole. Real-time digital video feed from the smartphone camera to a smartwatch facilitated manual adjustment of the pole to ensure nadir camera perspective. The ground photos were manually cropped to the same plot areas that were analyzed in the SLMs and MLMs. Thus, we obtained detailed time series of twenty-one plots from ground photos, SLMs, and MLMs (Figure 5).

### 2.3.6 Row-Offset Errors

We evaluated row-offset errors by visually inspecting replicate images of plots and determining whether they were centered on the correct plot. We measured the frequency of row-offset errors on each date as the number of offset images divided by the total number of replicate images.

### 2.3.7 Phenotype Measurements

For phenotype measurements, we chose to focus on canopy cover and color because recent studies indicate that they are critical for field-based HTP and can be measured accurately via remote sensing techniques (Normanly, 2012; Xavier et al., 2017). Canopy cover is defined as the fraction of a fixed ground area covered by the canopy (Eysn et al., 2012). It is a useful phenotype because it is closely related to light interception and yield (Hall, 2015). For example, the Food and Agriculture Organization (FAO) developed the AquaCrop model to predict yield based on periodic observations of canopy cover instead of Leaf Area Index (LAI – the surface area of leaves per area of ground surface), with the expectation that canopy cover is a reliable indicator of crop status that can be more easily and accurately measured via remote sensing techniques (Steduto et al., 2009a). We measured canopy cover as the fraction of canopy pixels in each plot image based on maximum-likelihood classification.

Canopy color is also a useful indicator of crop status that has been applied in HTP (Normanly, 2012). Researchers speculate that it can be used to model crop stress, senescence, and maturity (Hatfield et al., 2010; Viña, 2004). Canopy color is determined by its spectral reflectance. It has been characterized using a variety of absolute and relative image-based metrics including spectral vegetation indices and pixel hues. When imagery is not calibrated to absolute units of color such as reflectance, relative color metrics such as pixel hues allow comparison of imagery collected with the same sensor under similar lighting conditions (Hatfield et al., 2010; Normanly, 2012; Xue et al., 2017). It was not possible to calibrate our imagery to reflectance due to a lack of documentation of sensor characteristics. Therefore, we measured canopy color as the average hue of all canopy pixels in each plot image and we limited color analyses to relative differences between images from the SLMs and MLMs.

Our analysis focuses on assessing row-offset errors, visualizing variations in canopy cover and color from photo to photo, and quantifying measurement precision and accuracy. We used the frequency of row-offset errors to evaluate how often row-offset errors occur and how significant of a problem they might be. We evaluated variations from photo to photo using medians and standard deviations from MLM images. We plotted measurements from SLM and MLMs to visualize variations from photo to photo and impacts of geometric and radiometric distortion. We evaluated whether these distortions significantly influenced canopy cover and color measurements

by using t-tests to determine whether measurements from SLMs and MLMs were significantly different. Finally, we compared canopy cover measurements from SLMs and MLMs to ground reference measurements to evaluate their accuracy. Our results shed light on the quality of UAS data and methods of enhancing its precision and accuracy.

## 2.4 Results

### 2.4.1 Evaluation of Row-Offset Errors

Row-offset errors occurred on four out of thirteen sampling dates with frequencies ranging from 1/22 to 6/27 offset images per replicate plot image (Table 3). Over the entire study period, they occurred in 24 out of 3790 replicate plot images.

### 2.4.2 Evaluation of Phenotype Measurements

UAS and ground-based time series of canopy cover exhibited sigmoidal curves typical of plant growth (Figure 6). T-tests indicate that measurements from SLMs and MLMs were significantly different ( $P < 0.01$ ) for 198 (73%) out of 273 sampling points (21 plots x 13 sampling dates). Median values from MLMs were closer to ground reference values by an average of 2.4% cover for 173 of those 198 sampling dates. Measurements from SLMs were higher than MLMs by an average of 3.4% cover for 153 of those sampling dates. These differences were caused by geometric and radiometric distortion in the SLMs.

Canopy cover measurements from MLMs had standard deviations ranging from 0.3% cover to 7.2% cover with an overall average standard deviation of 1.7% cover. Measurement errors (median – reference value) ranged from -12.2% cover to 9.8% cover with an overall average of 0.4% cover. Standard deviations and errors were twice as large on the last four flight dates compared to the first nine. This is due to a low sun angle causing small portions of the canopies to be shadowed which prevented them from being classified accurately.

Canopy pixel hues exhibited slow and primarily upward shifts in value (Figure 7). T-tests indicate that hues from the SLMs and MLMs were significantly different ( $P < 0.01$ ) for 153 (56%) out of 273 sampling points. These differences are also caused by geometric and radiometric distortion in the SLMs.

## 2.5 Discussion

Our results confirm that row-offset errors can occur, although they are probably rare. A simple remedy would be to use median values from MLMs. Further research on row-offset errors, their frequency, and methods of detection and avoidance is recommended.

Our results also confirm that measurements from SLMs and MLMs are significantly different with SLMs over-estimating canopy cover. These results are consistent with Tao et al. (2017) who also found that SLMs over-estimate canopy cover. However, they compared measurements from ortho-mosaics to measurements from nadir-perspective ‘undistorted’ frame photos generated by Pix4Dmapper. Our method is not limited to nadir-perspective imagery since it removes perspective distortion via ortho-rectification.

Small standard deviations of canopy cover and color from MLMs reflect the small changes from photo to photo that are expected due to changes in wind, lighting, shadowing, viewing angle, and camera focus. Some researchers have suggested that using weighted average pixel colors or other methods of color blending in SLMs might help account for variations in lighting, bi-directional reflectance, and image quality from photo to photo (*e.g.* Haghigattalab et al., 2016). By allowing us to quantify these variations, MLMs can play an important role in investigating this possibility.

Researchers have also attempted to minimize geometric and radiometric distortion in SLMs by only using pixel colors from the closest frame photo to every point in the scene (*e.g.* Haghigattalab et al., 2016). Although this preserves raw pixel colors in the mosaic, it does not prevent the possibility of introducing spatial discontinuities within plots and it needlessly discards replicate observations. MLMs avoid these problems by retaining replicate observations and constraining spatial discontinuities to the borders between plots.

MLMs create new opportunities for evaluating and enhancing the quality of UAS observations. They can help standardize UAS observations by ensuring that all measurements are extracted directly from raw frame photos without unintended modifications. This will make it easier to replicate studies. In addition, knowledge of the precision of UAS measurements will facilitate outlier detection and other methods of quality control. For example, in this study, the unusually low and highly variable canopy cover measurements on the last four flight dates caused by variable shadowing might have been improved by using maximum values on these dates. As additional examples, one could investigate whether applying an image-sharpening filter could improve

measurement precision and one could compare the precision of different methods of pixel classification. MLMs could also be used to evaluate different metrics of color or temperature derived from multispectral or thermal imagery.

The ability to quantify the precision of UAS observations has great practical value. For example, it allows us to calculate how often we need to fly to track canopy expansion, since we know how much growth we can reliably detect from day to day. Most importantly, we can now determine whether observed differences between experimental plots are statistically significant.

## 2.6 Conclusion

MLMs are more appropriate than SLMs for field-based HTP and other areas of research in which we wish to observe large numbers of small spatial plots with as much precision and accuracy as possible. This is because they preserve replicate observations of plots in their raw format and avoid much of the geometric and radiometric distortion present in SLMs. They also make it possible to evaluate and enhance the precision and accuracy of UAS observations by correcting row-offset errors and applying outlier detection and other statistical analyses to the results. MLMs do not preserve spatial continuity from plot to plot, so SLMs may still be needed in mapping and other applications where positioning is critical. Hopefully new software or other resources will become available that will make MLMs available to more researchers.

The primary objective of this study was to introduce MLMs and demonstrate their advantages over SLMs. Weaknesses of this study include the inability to calibrate our imagery to reflectance and only testing one method of quantifying canopy cover and color. Follow up studies could focus on comparing different methods of measuring canopy cover and color and assessing impacts of image distortion on other types of downstream analyses.

## **CHAPTER 3. THE RELATIVE ACCURACY OF SOYBEAN CANOPY COVER AND COLOR FROM SINGLE AND MULTILAYER UAS IMAGE ORTHOMOSAICS**

### 3.1 Abstract

Crop improvement is necessary for food security as the global population is expected to rise to 9.1 billion by 2050. Imagery from Unmanned Aircraft Systems (UAS) will facilitate crop improvement by providing breeders more precise plant phenotypes that enable discrimination of higher-performing varieties in agronomic research plots with higher throughput and less manual labor. To help breeders avoid basing selections on phenotype values that are statistically indistinguishable, it will be critical to maximize the relative accuracy of UAS observations of plant phenotypes and enable statistical comparison of agronomic research plots. Towards these aims, we evaluate the relative accuracy of three plant phenotypes (canopy cover, hue, and green-to-red ratio or GR) for twenty-one soybean plots on thirteen sampling dates spanning canopy emergence to closure, extracted from two types of UAS ortho-image products: 1) single composite stitched image ortho-mosaics, or Single Layer Mosaics (SLMs), and, 2) separately ortho-rectified and tiled replicate ortho-images of individual research plots, or Multilayer Mosaics (MLMs). We measure relative accuracy by 1) ranking plots from lowest to highest phenotype values, and, 2) estimating relative phenotype values for all 210 unique pairs of 21 plots on each sampling date and evaluating the agreement with ground reference data. We find that MLMs and SLMs perform equally well at ranking plots, but MLMs enable higher relative accuracy by restricting analyses to significantly different plots using two-sided hypothesis testing. We also find that GR is more sensitive, accurate, and computationally efficient than hue at characterizing the relative greenness of soybean plots.

#### *Keywords*

(1) High-Throughput Phenotyping (HTP), (2) Unmanned Aircraft Systems (UAS), (3) Single-layer UAS image ortho-mosaic (SLM), (4) Multilayer UAS image ortho-mosaic (MLM), (5) Canopy cover, (6) Hue, (7) Green-to-red ratio (GR).

### 3.2 Introduction

Crop improvement is necessary for food security as the global population is expected to rise to 9.1 billion by 2050 (FAO, 2009). This requires both lab and field-based research in High-Throughput Phenotyping (HTP), since studies in controlled environments cannot ensure specific varieties will achieve desired performance in outdoor environments. Unfortunately, field-based HTP is costly and logistically challenging as it requires regularly and precisely measuring physical traits or plant phenotypes for large numbers of small agronomic research plots scattered across multiple environments. Traditionally, breeders have accomplished this by relying heavily on subjective visual ratings of plant phenotypes, as this has been the fastest and most economical way of collecting the data needed to make selections. However, as crop varieties have improved, it has become increasingly difficult to discriminate higher-performing varieties solely by eye. Therefore, breeders are looking to Unmanned Aircraft Systems (UAS) with imaging sensors as a low-cost platform for digitally measuring plant phenotypes more quickly and precisely than previously possible (Araus & Cairns, 2014; Cabrera-Bosquet et al., 2012).

Successful application of UAS imagery in field-based HTP depends on our ability to quickly and accurately convert raw UAS imagery into ortho-images and plant phenotypes for individual research plots. This process is not trivial – proper application of various techniques from remote sensing, photogrammetry, and computer vision are necessary to extract individual research plots from raw UAS imagery and measure plant phenotypes in a manner that is robust to image distortion. Unfortunately, no standard methodology currently exists for this process. Identifying a standard requires testing different methods on multiple phenotypes, crops, growth stages, environments, and seasons. Such a standard should optimize sensitivity to phenotypic differences between plots, or relative accuracy, since the goal is usually to discriminate varieties based on their relative phenotype values rather than accurately measure the phenotypes themselves (*e.g.* does plot A have a lower or higher phenotype value than plot B?). It would be particularly helpful if this methodology could help breeders avoid basing selections on phenotype values that are statistically indistinguishable.

Currently, the most common method of converting raw UAS imagery into ortho-images and plant phenotypes for agronomic research plots is to stitch raw UAS imagery into a large composite image ortho-mosaic of an entire field site and extract images and plant phenotypes for individual

plots from the ortho-mosaic (Tao et al., 2017; Shi et al., 2016; Haghghattalab et al., 2016). We refer to this approach as the ‘Single-Layer Mosaic’ (SLM) approach, as it relies on a single composite stitched image of the field site. Alternatively, it is possible to extract plant phenotypes from separately ortho-rectified and tiled replicate ortho-images of individual research plots from overlapping UAS images. We refer to this approach as the ‘Multilayer Mosaic’ (MLM) approach, as it relies on multiple layers of replicate imagery of the field site.

MLMs could enable higher relative accuracy by allowing breeders to restrict analyses to plots with significantly different phenotype values based on two-sided hypothesis testing. This is not possible with SLMs since they only offer one observation per plot. It seems that both SLMs and MLMs warrant consideration as standard methodologies for applying UAS imagery in field-based HTP, but to our knowledge, no studies have compared the relative accuracy of phenotypes from these two different types of UAS ortho-image products.

To address these knowledge gaps, we evaluate the relative accuracy of three plant phenotypes (canopy cover, hue, and green-to-red ratio or GR) for twenty-one soybean plots on thirteen sampling dates spanning canopy emergence to closure using SLM and MLM ortho-imagery. We measure relative accuracy in two ways: 1) ranking plots from lowest to highest phenotype values, and, 2) estimating the relative phenotype values of all 210 unique pairs of 21 plots on each sampling date and evaluating the agreement with ground reference data. We also investigate whether relative accuracy can be improved by restricting analyses to plots with significantly different phenotype values using two-sided hypothesis testing.

We consider canopy cover (the fraction of a fixed ground area covered by the canopy) to be a good target for analysis because it is closely related to light interception and yield (Hall, 2015). For example, the Food and Agriculture Organization (FAO) developed the AquaCrop model to predict yield based on periodic observations of canopy cover instead of Leaf Area Index (LAI – the surface area of leaves per area of ground surface), with the expectation that canopy cover is a reliable indicator of crop status that can be more easily and accurately measured via remote sensing techniques (Steduto et al., 2009b).

We also consider hue and GR to be good targets for analysis because both are designed to measure relative color differences in uncalibrated digital imagery and both have been used extensively in previous phenotyping research as metrics of plant greenness (*e.g.* Normanly, 2012; Majer, 2010;

Adamsen et al., 1999; Marchant, 2004). However, the GR ratio is less computationally intensive than hue, which may be a significant advantage when breeders must extract greenness from large numbers of high-resolution ortho-images of agronomic research plots. Therefore, if GR and hue offer similar relative accuracy, it may make sense for breeders to favor GR as a more efficient metric of plant greenness for field-based HTP. Our results lead to practical recommendations for applying UAS imagery in field-based HTP and outdoor small plot research in general.

### 3.3 Methods

#### 3.3.1 Field Site

The field site is located at the Agronomy Center for Research and Education (ACRE) at Purdue University. It consists of two hectares of experimental soybean used for plant breeding research. The field was planted with a precision plot planter on May 23<sup>rd</sup>, 2016 as rectangular arrays of plots classified by row and range number. The row orientation was south to north and the row spacing was 76 cm. Twenty-one test plots scattered across the field were used for this study. Each two-row plot was approximately 4 m<sup>2</sup> in size (Figure 3).

#### 3.3.2 Image Acquisition

The UAS was a small, fixed-wing Precision Hawk Lancaster Mark-III (3 kg total weight, 1.5 m wingspan) equipped with a 14-megapixel Nikon 1-J3 digital camera. It collected imagery from nadir-view in the visible spectrum with manually adjusted aperture, shutter speed, ISO sensitivity, and focus. It recorded GPS coordinates for each photo with a horizontal and vertical positional accuracy of approximately 2 m and 5 m, respectively.

Flights were conducted approximately twice a week from June 3<sup>rd</sup> to July 19<sup>th</sup>, 2016 between 9:00AM and 11:00AM local time resulting in thirteen sampling dates spanning canopy emergence to closure. We flew the UAS at an altitude of 50 m above ground level resulting in a nominal spatial resolution of 1.5 cm per pixel. We captured 70-90% forward and lateral image overlap to allow accurate image stitching and at least four replicate images of each plot on every sampling date. Concurrent with flights, we also collected ground reference (REF) images of the twenty-one test plots between 2:00PM and 4:00PM local time from 4 m above the canopy at nadir-view using a 13-megapixel digital camera mounted on a pole.

### 3.3.3 Single-Layer Mosaic Generation

We stitched the raw UAS imagery into single-layer ortho-mosaics (SLMs) using Pix4Dmapper™ with default settings for image stitching and mosaic generation (Pix4D, Lausanne, Switzerland). This produced SLMs, digital elevation models, and estimates of internal and external camera parameters. Outputs were horizontally co-registered to the UTM eastings and northings of twenty-five ground control points that were surveyed with 1 cm horizontal and vertical positional accuracy to ensure accurate image stitching and co-registration. We gridded the SLMs to obtain ortho-images and GPS coordinates for every plot.

### 3.3.4 Multilayer Mosaic Generation

We applied the collinearity equation with nearest-neighbor resampling to the camera internals, externals, and plot GPS coordinates to separately ortho-rectify multiple replicate ortho-images of every plot (Mikhail, 1974). Then, we manually centered every replicate image of every plot on the correct plot to ensure no row-offset errors were present. Finally, we tiled the plot ortho-images according to their row and range numbers in the field and stacked replicate images on top of each other to form multilayer mosaics (MLMs).

### 3.3.5 Phenotype Measurements

We used supervised maximum-likelihood classification to accurately segment the REF, SLM, and MLM images of each plot into canopy and background pixels (Campbell & Wynne, 2011). Then, we calculated canopy cover for each plot as the fraction of canopy pixels in each plot image. Finally, we calculated canopy greenness in terms of the average hue and average green-to-red ratio (GR) of the raw digital number values of canopy pixels in each plot image.

### 3.3.6 Plot Rankings

To evaluate the relative accuracy of canopy cover, hue, and GR observations from SLMs and MLMs, we ranked the twenty-one test plots from lowest to highest phenotype values on each flight date (Tables 4-6). We obtained REF and SLM rankings by comparing single phenotype observations for the plants in each plot. We obtained MLM rankings by comparing median phenotype observations for the plants in each plot. We used median observations because these are robust to outliers caused by the occasional blurry or poorly-stitched UAS image. We measured

the accuracy of SLM and MLM rankings based on their agreement with REF rankings according to Cohen's Kappa statistic with linear weighting. Cohen's Kappa ranges from 1 if metrics are in complete agreement, 0 if there is no more agreement than would be expected by chance, and negative if the agreement is worse than by chance (Watson & Petrie, 2010).

### 3.3.7 Pairwise Plot Comparisons

As another means of evaluating the relative accuracy of canopy cover, hue, and GR observations from SLMs and MLMs, we compared plant phenotypes for all unique pairs of the twenty-one test plots on every flight date. This resulted in 210 (21-choose-2) pairs of plots on each flight date, for a total of 2730 ( $13 \times 210$ ) pairwise plot comparisons over the study period. First, we obtained relative phenotype values (*e.g.* plot A has a lower or higher phenotype value than plot B) from the REF and SLM images by comparing single phenotype observations for each pair of plots. Then, we obtained relative phenotype values from the MLM images by comparing median phenotype observations for each pair of plots. We also restricted MLM analyses to pairs of plots with significantly different phenotype values using Wilcoxon Rank-Sum tests with a range of significance levels to show its effect on the sensitivity and accuracy of the test. Finally, we measured the relative accuracy of canopy cover, hue, and GR for pairs of plots by calculating the fraction of pairwise plot comparisons that indicated the same relative values as the REF images.

## 3.4 Results

### 3.4.1 Evaluation of Plot Rankings

In general, the relative accuracy of plot rankings based on median phenotype values from MLM images and single phenotype values from SLM images were very similar (Figures 8-10). One exception was the first flight date in which the canopies were too small to be detected in the SLM images. The minimum, maximum, and overall average Cohen's Kappa ( $\kappa$ ) with REF canopy cover rankings were 0.29, 0.77, and 0.53 for the SLMs and 0.28, 0.81, and 0.53 for the MLMs, respectively. For hue, the minimum, maximum, and overall average  $\kappa$  with REF rankings were 0.13, 0.62, and 0.28 for the SLMs and 0.07, 0.71, and 0.28 for the MLMs, respectively. For GR, the minimum, maximum, and overall average  $\kappa$  with REF rankings were 0.07, 0.52, and 0.31 for the SLMs and 0.13, 0.52, and 0.30 for the MLMs, respectively. For both the MLMs and SLMs, the overall average  $\kappa$  with REF rankings was slightly higher for GR (0.30) than hue (0.28).

### 3.4.2 Evaluation of Pairwise Plot Comparisons

The fraction of 2730 pairs of plots in this study that were found to have significantly different phenotype values based on Wilcoxon Rank-Sum tests increased as the significance level of the test was increased (Figure 11). At a standard significance level of 0.05, 68%, 48%, and 51% of all pairs of plots were found to have significantly different canopy cover, hue, and GR, respectively. For all significance levels, GR was slightly more sensitive than hue to relative differences in greenness between pairs of plots.

The downside of increasing the significance level of the two-sided hypothesis test was that the fraction of pairs of plots that had significantly different and correct relative phenotype values decreased (Figure 12). This reflects that there is a tradeoff in the sensitivity and accuracy of the test with respect to detecting phenotypic differences between pairs of agronomic research plots. At a standard significance level of 0.05, 87%, 74%, and 76% of pairs of plots with significantly different canopy cover, hue, and GR had correct relative values, respectively. For all significance levels, GR measured greenness with slightly higher relative accuracy than hue.

The relative accuracy of pairwise plot comparisons based on median phenotype values from MLMs and single phenotype values from SLMs were similar (Figures 13-15). For canopy cover, the minimum, maximum, and overall fraction of pairs of plots with correct relative values were 62%, 90%, and 78% for the SLMs and 67%, 93%, and 79% for the MLMs, respectively. For hue, the minimum, maximum, and overall fraction of pairs of plots with correct relative values were 58%, 82%, and 66% for the SLMs and 54%, 89%, and 65% for the MLMs, respectively. For GR, the minimum, maximum, and overall fraction of pairs of plots with correct relative values were 53%, 78%, and 67% for the SLMs and 53%, 80%, and 66% for the MLMs, respectively.

When Wilcoxon Rank-Sum tests with a standard significance level of 0.05 were used to restrict analyses to significantly different pairs of plots, the relative accuracy of the MLM observations was higher than that of the SLM observations for all phenotypes and almost all flight dates. For canopy cover, the minimum, maximum, and overall increases in relative accuracy for a given flight date were 4%, 14%, and 9%, respectively. For hue, the minimum, maximum, and overall increases in relative accuracy were -4%, 27%, and 8%, respectively. For GR, the minimum, maximum, and overall increase in relative accuracy were -3%, 19%, and 9%, respectively. The tradeoff of these

increases in accuracy were that 32%, 52%, and 49% of pairs of plots were found to have statistically indistinguishable canopy cover, hue, and GR, respectively.

### 3.5 Discussion

There have been many studies on the absolute accuracy of observations of canopy cover and color from SLMs (*e.g.* Tao et al., 2017; Shi et al., 2016; Haghghattalab et al., 2016). However, to our knowledge, this is the first study focused on evaluating the relative accuracy of phenotypes from SLMs and MLMs. Our results indicate that SLMs and MLMs measure canopy cover, hue, and GR for small soybean research plots with similar relative accuracy, particularly with regards to ranking plots from lowest to highest phenotype values. However, when Wilcoxon Rank-Sum tests with a standard significance level of 0.05 are used to restrict analyses to pairs of plots with significantly different phenotype values, the relative accuracy of MLM observations can become up to 27% higher than that of SLM observations. This increase in relative accuracy comes at the expense of designating up to 50% of pairs of plots as statistically indistinguishable.

However, relative accuracy can also be increased by other means, such as decreasing the flying height of the UAS or using higher quality imaging sensors to improve measurement precision. Whether such measures can render differences between SLMs and MLMs negligible remains an important topic for future research. Ultimately, breeders will need to determine what tradeoffs in sensitivity and accuracy are appropriate for their research purposes.

These results also indicate that GR measures the greenness of soybean plots with a relative accuracy and sensitivity at least equivalent to hue, both in terms of ranking plots and detecting significant differences between pairs of plots. Therefore, breeders may want to consider using GR rather than hue as a more efficient metric of plant greenness for field-based HTP.

### 3.6 Conclusion

MLMs and SLMs perform similarly well at ranking canopy cover, hue, and GR for small soybean research plots, but MLMs enable higher relative accuracy by restricting analyses to pairs of plots with significantly different phenotype values. This can help breeders avoid making selections based on phenotype values that are statistically indistinguishable. We also find that GR discriminates soybean plot greenness at least as well as hue both when ranking and comparing

pairs of plots. Therefore, breeders may want to consider using GR rather than hue as a more efficient metric of greenness for field-based HTP.

It would be interesting to investigate whether two-sided hypothesis testing could be used to produce more accurate rankings of plots. Perhaps this would involve ranking plots based on the number of plots that have significantly smaller phenotype values and assigning equal ranks to plots that are statistically indistinguishable. It would also be interesting to compare the absolute accuracy of SLMs and MLMs and see how this relates to their relative accuracy. Further research covering other phenotypes, crop types, growth stages, environments, and seasons is needed before more general recommendations can be made. Ultimately, breeders must decide what levels of sensitivity and accuracy are appropriate for their research purposes.

## **CHAPTER 4.     CONSTRAINING THE ONSET OF MOISTURE STRESS IN AQUACROP USING CANOPY COVER TIME SERIES FROM UNMANNED AIRCRAFT SYSTEMS**

### 4.1 Abstract

Crop improvement is necessary for food security as the global population is expected to exceed 9 billion by 2050. Limitations in water resources and more frequent droughts and floods will make it increasingly difficult to manage agricultural resources and increase yields. Therefore, we must improve our ability to predict impacts of moisture stress on crop growth and yield. Towards this end, agronomists have identified visible ‘plant-based’ indicators of moisture stress, such as reductions in leaf expansion rates, which identify when crops are experiencing moisture stress. Also, modeling researchers have developed crop models such as AquaCrop that enable quantification of the severity of moisture stress and its impacts crop growth and yield. Finally, breeders are applying Unmanned Aircraft Systems (UAS) in field-based High-Throughput Phenotyping (HTP) to quickly screen many crop varieties for traits indicative of drought and flood tolerance. Here we investigate whether canopy cover time series from high-resolution UAS imagery could pinpoint the timing of reductions in leaf expansion rates in field-grown soybean and whether this information can be used to constrain AquaCrop to more accurately simulate the timing and severity of moisture stress as well as its impacts on crop growth and yield. We find that UAS observations of canopy cover can pinpoint the timing of reductions in canopy expansion rates to within a couple of days and that this can be used to help AquaCrop avoid underestimating moisture stress and overestimating yield. This approach to model calibration will help agronomists and breeders more quickly identify varieties tolerant to moisture stress and achieve food security.

#### *Keywords*

(1) High-Throughput Phenotyping, (2) Unmanned Aircraft Systems (UAS), (3) Canopy Cover, (4) Crop Modeling, (5) Moisture Stress, (6) Drought Stress, (7) Flood Stress, (8) AquaCrop

## 4.2 Introduction

### 4.2.1 Background

Due to global population rise, yields of major food crops must be increased to ensure future food security. Limitations in water resources and climate change will make it increasingly difficult to manage agricultural resources and obtain higher yields (Bradshaw & Barry, 2014; Cohen, 2003; FAO, 2009; Sinha et al., 1989). This is particularly true for the US Midwest region, in which climate models predict more extreme weather, including droughts and floods, will reduce yields (Cherkauer & Sinha, 2010; Fan, 2014; Pryor, 2013; Rosenzweig, 2002). We therefore need to improve our understanding of how droughts and floods impact crop growth and yield.

Research in agronomy, crop modeling, and breeding advance our understanding of crop growth dynamics and water relations to yield by assimilating current knowledge and relying on meteorological and agronomic data to test our understanding (Boote et al., 1996). This leads to more accurate yield predictions, more effective breeding, better agricultural resource management, and higher yields. For example, agronomists have identified visible ‘plant-based’ indicators of moisture stress, such as reductions in leaf expansion rates, which help identify when crops are experiencing moisture stress (Jones, 2004). Also, crop modeling researchers have developed models such as AquaCrop that allow quantification of impacts of moisture stress on crop growth and yield (Steduto et al., 2009a). And recently, breeders have begun studies on field-based High-Throughput Phenotyping (HTP) (Araus and Cairns, 2014; Cabrera-Bosquet et al., 2012). This involves planting many varieties of a crop in thousands of small agronomic research plots and precisely measuring standard physical traits, or ‘phenotypes’, for every plot. These phenotypes serve as indicators of crop performance. This allows many varieties to be quickly screened for desired characteristics, enabling rapid progress towards varieties that are high-yielding and tolerant to moisture stress.

The main challenges of field-based HTP are that phenotypes must be measured precisely enough to distinguish the often-subtle differences between plots, and, when fields are large enough, additional field observations may be needed to prevent within-field variation from confounding observed differences between plots. The need for high measurement precision and the high cost of manual labor traditionally required to collect these data are significant obstacles that must be addressed for these types of studies to progress (Araus & Cairns, 2014).

To overcome these obstacles, it will be critical for researchers to exploit new technologies as they become available. For example, with minimal manual labor, Unmanned Aircraft Systems (UAS) equipped with imaging sensors can acquire imagery at the field scale with the spatial resolution required to resolve individual plots and the temporal resolution required to capture differences in plot behavior over time. With appropriate remote sensing and image analysis techniques, these data may enable frequent, rapid, and precise observations of crop status at the plot scale, leading to more rapid research progress at the field scale (Araus & Cairns, 2014).

For example, a promising phenotype for UAS observation is plot-scale observations of canopy cover. Canopy cover is defined as the fraction of a fixed ground area covered by the canopy or delimited by the vertical projection of the outermost perimeter of the canopy (Eysn et al., 2012). With regards to plant breeding, canopy cover has proven useful for field-based HTP because it may be measured precisely and is related to light interception and yield (Xavier et al., 2017). With regards to crop modeling, the Food and Agriculture Organization (FAO) developed the AquaCrop model to rely on observations of canopy cover instead of Leaf Area Index (LAI) (the surface area of leaves per area of ground surface) with the expectation that canopy cover is a reliable indicator of crop status that is easier to measure remotely (Steduto et al., 2009b).

UAS observations of canopy cover may also be detailed enough to provide new constraints for calibrating crop models such as AquaCrop to simulate impacts of moisture stress on crop growth and yield. For example, if canopy cover is measured frequently and precisely enough, then perhaps analyses of these data, combined with meteorological and agronomic data, could pinpoint the timing of reductions in leaf expansion rates in field-grown soybean to within a few days. This could be used to constrain AquaCrop to more accurately simulate the timing of the onset of moisture stress as well as the severity of its impacts on crop growth and yield.

This study focuses on exploring these possibilities by comparing the performance of AquaCrop calibrated in the traditional manner with ground-based observations and in an alternative manner using UAS observations of soybean canopy cover and dates corresponding to reductions in canopy expansion rates. Our hypothesis is that UAS observations of canopy cover can be collected with enough precision and temporal resolution to pinpoint the timing of reductions in canopy expansion rates in field-grown soybean to within a few days and that these observations can be used to constrain AquaCrop to more accurately simulate the timing of the onset of moisture stress and the

severity of its impacts on soybean growth and yield. This type of analysis may reveal new phenotypes related to moisture stress that could be applied in field-based HTP. For example, possible phenotypes may include 1) the number of times crops exhibit reduced canopy expansion rates during a growing season, and, 2) how long crops endure adverse soil moisture conditions before exhibiting reduced canopy expansion rates. Such phenotypes could help quickly identify varieties that are resistant to moisture stress. This would not only demonstrate that UAS imagery can provide precise and useful data for research in agronomy, crop modeling, and breeding at minimal labor cost, but it would also demonstrate that UAS observations can lead to a better understanding of crop growth dynamics and water relations to yield. This is critical in a world where water resources are increasingly difficult to manage and food security is at risk.

To clarify our modeling objectives, we provide a brief description of the AquaCrop model and aspects of the model relevant to our study. For further detail, the reader is referred to various papers describing the model (Raes et al., 2009; Steduto et al., 2009a) and the user manual (Raes et al., 2012). Then we present a case study in which we test our hypothesis by comparing the performance of AquaCrop calibrated with ground vs. UAS observations of canopy cover.

#### 4.2.2 The AquaCrop Model

AquaCrop dynamically simulates canopy expansion, root growth, Plant Available Water (PAW), and their combined impacts on transpiration, biomass production, and yield via the application of a harvest index and stress coefficients (Figure 2). The basic inputs required to run AquaCrop include daily air temperature, reference evapotranspiration, rainfall, initial soil moisture conditions, soil drainage properties, flowering, seed-filling, and maturity (Table 1). Observations of model outputs required for calibration include periodic observations of canopy cover and biomass (Table 2). Periodic observations of soil moisture, root length, and yield are considered optional but can enhance the quality of the calibration (Raes et al., 2012).

AquaCrop uses growing degree days to simulate a crop's progression through its basic reproductive growth stages: 1) flowering, 2) yield formation, and, 3) maturity (Purcell et al., 2014). Concurrently, AquaCrop simulates root growth, canopy expansion, transpiration, and biomass production. Finally, AquaCrop estimates yield ( $Y$ ) by multiplying biomass ( $B$ ) by a harvest index ( $HI$ ) (Steduto et al., 2009a; McMaster & Wilhelm, 1997):

$$Y = B \times HI$$

AquaCrop estimates biomass production over time using a water-driven growth equation:

$$B = WP \times \sum Tr$$

Where  $\sum Tr$  is the cumulative crop transpiration and  $WP$  is the biomass water productivity (biomass per unit of cumulative crop transpiration).  $WP$  is constant for a given crop and climate (Steduto et al., 2009a; Steduto et al., 2007).  $Tr$  is calculated as follows:

$$Tr = Kcb \times ET_0$$

Where  $Kcb$  is the crop coefficient for transpiration and  $ET_0$  is the reference evapotranspiration according to the Penman-Monteith Equation (Monteith, 1965).  $Kcb$  is calculated as the product of the crop coefficient at 100% canopy cover ( $Kcb_x$ ) and the canopy cover of the crop ( $CC$ ):

$$Kcb = CC \times Kcb_x$$

Canopy cover increases exponentially for non-stressed soybean until full size is approached (Board, 1996). Accordingly, AquaCrop simulates canopy expansion using exponential equations. The form of the equation depends on how close the crop is to maximum canopy cover and maturity:

$$1^{\text{st}} \text{ half of canopy expansion } \left( CC < \frac{CC_x}{2} \right): CC = CC_0 e^{(CGC)t}$$

$$2^{\text{nd}} \text{ half of canopy expansion } \left( CC \geq \frac{CC_x}{2} \right): CC = CC_x - (CC_x - CC_0) e^{-(CGC)t}$$

$$\text{Decline of } CC \text{ towards maturity: } CC = CC_x \left[ 1 - 0.05 \left( e^{\left( \frac{CDC}{CC_x} \right) t} - 1 \right) \right]$$

Here,  $CC_0$  is the canopy cover at which the canopy first becomes autotrophic (attains enough leaf area to synthesize its own food and sustain growth via photosynthesis) and starts to grow exponentially,  $CC_x$  is the maximum canopy cover,  $CGC$  is a canopy growth coefficient,  $CDC$  is a canopy decline coefficient, and  $t$  is the time after planting. Together, these equations allow AquaCrop to simulate non-stressed crop growth and yield.

AquaCrop simulates various types of stress due to drought, flood, heat, cold, soil fertility, and soil salinity. Stress caused by diseases or pests are not considered. Parameters for stressed and non-stressed growth may be calibrated separately (Raes et al, 2012). Specifically, parameters such as

the canopy growth coefficient ( $CGC$ ) and maximum canopy cover ( $CC_x$ ) may be calibrated using observations of non-stressed plants, while parameters related to stressed growth may be calibrated using observations of stressed plants. Here we focus on illustrating how moisture stress is simulated in AquaCrop.

AquaCrop simulates moisture stress by applying stress coefficients to its equations governing canopy expansion, transpiration, and yield formation. These stress coefficients are functions of simulated Plant Available Water (PAW) values, PAW thresholds for moisture stress, and the growth stage of the crop. For example, the onset of drought stress is simulated by assuming that there are upper and lower PAW thresholds between which canopy expansion rates are reduced. When the simulated PAW drops below the upper PAW threshold, a stress coefficient for expansive growth ( $K_{s_{exp}}$ ) is reduced from 1 to some number between 1 and 0 according to a convex curve mapped between the upper and lower PAW thresholds (Figure 1). The shape of this curve is usually convex to account for plant acclimation to mild stress and decreased soil capillary conductivity at low PAW, but it may be adjusted using a shape factor ( $f_{exp}$ ) (Denmead & Shaw, 1962). This coefficient slows simulated canopy expansion by reducing AquaCrop's  $CGC$  parameter as follows:

$$CGC_{adjusted} = K_{s_{exp}} \times CGC$$

Overall, AquaCrop uses four stress coefficients to simulate impacts of moisture stress on four processes: 1) canopy expansion, 2) stomatal conductance, 3) canopy senescence, and, 4) root aeration. The first three coefficients represent drought stress and are referred to as coefficients for: 1) expansive growth ( $K_{s_{exp}}$ ), 2) stomatal closure ( $K_{s_{sto}}$ ), and, 3) accelerated leaf senescence ( $K_{s_{sen}}$ ). The fourth represents flood stress and is referred to as an aeration stress coefficient ( $K_{s_{aer}}$ ). All four are defined by upper and lower PAW thresholds and a shape factor. Some of these parameters are predetermined. For example, the lower PAW threshold for flood stress ( $b_{aer}$ ) is set to 1 so flood stress can only occur when the soil moisture exceeds field capacity.

#### 4.2.3 Constraining the Onset of Moisture Stress in AquaCrop

During the first half of canopy expansion, a linear equation in which the  $CGC$  is given by the slope may be obtained by taking the logarithm of the canopy expansion equation:

$$\ln(CC) = \ln(CC_0) + (CGC)t$$

Accordingly, one may detect the timing of the onset of moisture stress during the first half of canopy expansion by testing for decreases in slope or *CGC* between canopy cover values from successive pairs of sampling dates. Dates when adverse soil moisture conditions and reductions in slope are observed correspond to onsets of moisture stress. This approach (linearization, followed by detection of reductions in slope) is also applicable during the second half of canopy expansion. Decreases in *CGC* detected in this manner will have limited temporal precision, as the actual decrease in *CGC* may have occurred at any time between the successive pairs of sampling dates. For example, if the sampling interval is 4 days, then a decrease in *CGC* detected between three successive sampling dates will have a temporal precision of approximately  $\pm 4$  days about the middle date. The shorter the sampling interval, the more precisely the timing of the decrease in *CGC* (and onset of moisture stress) may be pinpointed. Additionally, the canopy cover observations will have limited precision. Therefore, only statistically significant reductions in *CGC* should be considered indicative of stress. This may be enforced by applying classical linear regression to replicate observations of canopy cover on successive pairs of sampling dates and checking if confidence intervals for the *CGC* overlap.

Decreases in *CGC* are also more likely to be detected at the plot scale than field scale. This is because within-field variation of terrain and soil conditions will lead to variation in the timing of the onset of moisture stress from plot to plot. For example, ponding may cause plots at low spots in a field to exhibit drought stress later than plots at higher elevations. Therefore, if plot-scale canopy cover times series are aggregated to the field scale, reductions in *CGC* may become smoothed out and harder to pinpoint. To overcome this issue, one may detect reductions in canopy expansion rates at the plot scale and then calculate the overall fraction of plots in the field that exhibit reduced canopy expansion rates on each sampling date. One may then calibrate AquaCrop such that it simulates moisture stress on dates when any field plots exhibit significant reductions in canopy expansion rates. This equates to imposing a temporal constraint on simulated moisture stress during model calibration in a way that is currently only feasible with UAS imagery. Here we present a case study in which we calibrate AquaCrop in this manner and evaluate whether this produces more realistic and accurate simulations of moisture stress, crop growth, and yield compared to the traditional ground-based method of calibration.

## 4.3 Methods

### 4.3.1 Field Site

The field site was located at the Agronomy Center for Research and Education at Purdue University in West Lafayette, Indiana (Figure 16). It consists of flat fields of silty-clay loam soil with sub-surface tile-drainage. It was planted with 151, 47, 147, and 11 plots of IA-3023 soybean in late May 2014, 2015, 2016, and 2017, respectively, at a density of 35 plants per square meter using a precision plot planter. The rows were oriented north-to-south with a spacing of 0.76 m. Each two-row plot was approximately 4 square meters in area.

### 4.3.2 Climate

Daily air temperature, rainfall, and reference evapotranspiration were obtained from a weather station located a few hundred yards from the field site. The total amount of rainfall from planting to harvest for all four seasons was 455 mm, 446 mm, 492 mm, and 524 mm in 2014, 2015, 2016, and 2017, respectively (Figure 17). However, during the first five weeks of the growing season (May 23<sup>rd</sup> to July 1<sup>st</sup>), which is when most of the canopy expansion occurred, there was relatively little rain in 2014 (81 mm) compared to 2015 (228 mm), 2016 (127 mm), and 2017 (169 mm). Therefore, if any early season drought stress occurred, it was expected to be most pronounced in 2014. In contrast, there was heavy rain in the beginning of the 2015 season (228 mm). Visual observations of early season flooding, delayed canopy expansion, and chlorosis indicated that flood stress was most pronounced in 2015. In 2016, rain was infrequent but heavy. Visual observations of slightly delayed canopy expansion in the early season and mild chlorosis during the late season supported the expectation that 2016 might exhibit mild drought and flood stress.

### 4.3.3 Ground Observations

During the 2016 growing season, we measured flowering, seed-filling, maturity, soil moisture, above-ground biomass, yield, root length, and canopy cover at twenty-one selected plots uniformly dispersed across the field site. Soil moisture was measured in the center of each plot at 20 cm depth using a Campbell Scientific HydroSense II probe with nine replicate measurements per plot. Based on the size of the field and the spatial distribution of sampling locations, we expected this sampling scheme to allow us to accurately estimate the average soil moisture of the field near the soil surface (Brocca, 2010; De Lannoy, 2006; Reynolds, 1974; Vereecken et al., 2014; Wang, 2008) and we

assumed this would enable accurate simulation of the soil water balance. We regularly monitored the growth stage of the plots via visual inspection. We measured above-ground biomass by destructively sampling randomly selected plots. Each sample was dried in a controlled temperature oven at 65°C until constant weight was reached and weighed using a scale sensitive to the nearest 0.1 gram (Paredes, 2015). We measured root length by digging up the roots of five randomly selected plants within each sampled plot and measuring their length with a ruler.

We obtained ground-based observations of canopy cover from ground-based digital imagery of the twenty-one selected plots taken between 2:00PM and 4:00PM local time from 4 m above the soil surface at nadir-view with a 13-megapixel digital camera mounted on a pole. These images were manually cropped to the plot area and accurately segmented into canopy and non-canopy pixels using the Excess Green index and Otsu's Method (Meyer, 2008; Otsu, 1979). Canopy cover was then calculated as the fraction of canopy pixels in each plot image. Yield data (and flowering, seed-filling, and maturity notes when available), were provided by researchers from the Department of Agronomy at Purdue University who managed the field site.

#### 4.3.4 UAS Observations

The UAS was a small, fixed-wing Precision Hawk Lancaster Mark-III (3 kg total weight, 1.5 m wingspan) equipped with a 14-megapixel Nikon 1-J3 digital camera and a GPS sensor accurate to 2 m and 5 m in the horizontal and vertical, respectively. The camera collected imagery from nadir-view in the visible spectrum with manually adjusted aperture, shutter speed, ISO sensitivity, and focus. We conducted flights in June, July, and August 2014, 2015, 2016, and 2017 between 9:00AM and 1:00PM local time resulting in multiple sampling dates spanning canopy emergence to closure (Table 7 and Figure 18). We flew the UAS at an altitude of 50 m above ground level resulting in a spatial resolution of 1.5 cm per pixel. We captured 70-90% forward and lateral image overlap and used a minimum of four Ground Control Points (GCPs) along the perimeter of the field to ensure accurate image stitching and geo-referencing (Hearst & Cherkauer, 2015).

We obtained UAS observations of canopy cover for all plots using Pix4Dmapper™, MATLAB™, and ENVI-IDL™ (Pix4D, Lausanne, Switzerland). First, we marked GCPs in the images using MATLAB. Next, we stitched the imagery into geo-referenced ortho-mosaics using Pix4Dmapper. Then, we used MATLAB to grid the ortho-mosaics into individual plots and extract replicate ortho-images of every plot. This was done by applying collinearity (Mikhail, 1974) to the internal

and external camera parameters and plot coordinates from Pix4Dmapper. We captured four to twenty-five replicate ortho-images of every plot on every sampling date depending on the image overlap. We manually centered these ortho-images on their respective plots and accurately segmented canopy and non-canopy pixels using maximum likelihood classification implemented in ENVI-IDL. Finally, we detected dates corresponding to significant reductions in canopy expansion rates by taking the natural logarithm of the canopy cover time series and applying classical linear regression with a significance level of 0.05 to test for significant decreases in slope or *CGC* between successive pairs of sampling dates.

#### 4.3.5 Ground-Based Model Calibration

In general, we assumed there was no heat stress, cold stress, salinity stress, or fertility stress. We believe these were reasonable assumptions because air temperatures remained well above freezing, the fields were fertilized, soybean is a nitrogen-fixing species, and no problems related to heat or salinity were reported by the field managers during the study period. We also assumed there was no surface runoff, since the fields were flat, well-drained through sub-surface tile drainage, and almost never received enough rainfall to produce visible runoff.

Generally, it is best to use multiple years of ground reference data to calibrate a model if the objective is to produce a model capable of accurate predictions in a wide range of scenarios. However, due to limited field personnel and the extensive amount of time required for UAS flight planning, image acquisition, and processing, we were only able to obtain enough ground and UAS observations for model calibration in 2016. Nevertheless, a single year of calibration data is enough at least for an insightful comparison of our two calibration methods. First, in accordance with traditional methods, we calibrated AquaCrop using ground-based observations of soil moisture, flowering, seed-filling, maturity, above-ground biomass, yield, root length, and canopy cover aggregated to the field scale (Tables 8 and 9). Initially, we fixed parameters related to stressed conditions such that they had no impact on the simulation results. Then, we manually adjusted parameters related to non-stressed conditions until the agreement between simulated and observed canopy cover, above-ground biomass, and soil moisture was maximized according to Willmott's index of agreement (with other metrics such as RMSE used as a secondary means of evaluation) (Willmott, 1982). Finally, we manually optimized all parameters, including those related to stressed conditions, resulting in our 'ground-based' model.

#### 4.3.6 UAS-Based Model Calibration

Alternatively, we calibrated AquaCrop using UAS observations of canopy cover and dates corresponding to reductions in canopy expansion rates detected at the plot scale and aggregated to the field scale (Tables 10 and 11). First, we categorized plots as ‘stressed’ and ‘non-stressed’ based on whether they exhibited any statistically significant reductions in canopy expansion rates during the 2016 season. Then, using canopy cover observations from non-stressed plots, we manually adjusted parameters related to non-stressed conditions until the agreement between simulated and observed canopy cover, above-ground biomass, and soil moisture was maximized for non-stressed plots according to Wilmott’s index of agreement (with other metrics such as RMSE used as a secondary means of evaluation). Finally, using canopy cover observations from stressed plots and dates corresponding to significantly reduced canopy expansion rates, we manually optimized parameters related to stressed conditions until the agreement between simulated and observed canopy cover, above-ground biomass, soil moisture, and dates of moisture stress was maximized for stressed plots to obtain our ‘UAS-based’ model (Table 12).

#### 4.3.7 Model Validation

We validated the ground and UAS-based models using plot scale observations of canopy cover and yield from 2014, 2015, and 2017 aggregated to the field scale. The primary metric of agreement between observed and simulated canopy cover was Wilmott’s index of agreement (with other metrics such as the RMSE used as a secondary means of evaluation). The primary metric of agreement between observed and simulated yields was the percent error of simulated yields. We also evaluated the correspondence between dates of simulated moisture stress and dates when visible indicators of moisture stress were observed in the field.

### 4.4 Results

#### 4.4.1 Calibration

In 2016, Wilmott’s index of agreement for canopy cover was 1.00 for the ground-based model and 0.99 for the UAS-based model. Similarly, Wilmott’s index of agreement for biomass was 1.00 for the ground-based model and 0.99 for the UAS-based model. For soil water content, Wilmott’s index of agreement was 0.58 for both the ground and UAS-based models (Figures 19 and 20, Table

13). During the first five weeks of the 2016 season, the timing of simulated moisture stress corresponded closely to the timing of reductions in canopy expansion rates for the UAS-based model, but the ground-based model indicated no moisture stress during this period (Figure 20).

#### 4.4.2 Validation

In 2014, 2015, and 2017, Wilmott's index of agreement for canopy cover was 0.98, 0.64, and 0.97 for the ground-based model and 0.99, 0.65, and 0.98 for the UAS-based model, respectively (Figure 21, Table 14). Corresponding yield prediction errors were 44%, 30%, and 12% for the ground-based model and 42%, 23%, and 8% for the UAS-based model (Table 15).

#### 4.5 Discussion

In general, calibrated values for the conservative crop parameters were consistent with those reported in the literature. For example, our biomass water productivity (*WP*) and harvest index (*HI*) were 20 g m<sup>-2</sup> and 32%, respectively, while Paredes et al. (2015) reported 17 g m<sup>-2</sup> and 38% and Adeboye et al. (2018) reported 17.6 g m<sup>-2</sup> and 40% for soybean grown under similar conditions. However, our soil drainage coefficient ( $\tau = 1.0$ ) was considerably higher than those reported in the literature ( $\tau \leq 0.5$ ), indicating that we over-estimated soil drainage. This may have been due to our lack of soil moisture observations at multiple depths in the soil profile and our assumption that surface runoff was negligible.

The least accurate canopy cover simulations occurred in 2015 (Wilmott's index of agreement below 0.66). As expected, this corresponded with relatively poor yield predictions (errors greater than 23% for both models). However, in 2014, the most accurate canopy cover simulations (Wilmott's index of agreement above 0.97) corresponded with the least accurate yield predictions (errors above 41% for both models). This inconsistency between canopy cover and yield simulation accuracies during the seasons when drought and flood stress were expected to be most pronounced, along with the fact that the ground-based model failed to detect any stress in early 2016, further suggest that parameters related to soil drainage were not well calibrated for either model. This demonstrates a need for additional constraints on the soil water balance to improve the sensitivity of the model to drought and flood stress.

In general, both the ground and UAS-based models systematically over-estimated yield but errors were consistently lower for the UAS-based model by 2-7%. However, these differences in accuracy are small and could be attributed to the fact that the UAS observations were simply more numerous and covered more plots than the ground-based observations. Although these results may be inconclusive, they illustrate the potential benefit of using indicators of moisture stress (*e.g.* reductions in canopy expansion rates) as an additional constraint during model calibration – they can improve the sensitivity of the model to moisture stress and thereby help prevent overestimation of yield.

#### 4.6 Conclusion

Overall, the UAS-based model was more sensitive to moisture stress than the ground-based model and produced slightly more accurate simulations of canopy cover and yield. Although these results may not be conclusive, they warrant further investigation of this approach to model calibration and the possibility of using reductions in canopy expansion rates as a phenotype for field-based HTP to help identify new varieties tolerant to moisture stress. Future work could also investigate whether larger improvements in accuracy could be achieved with additional calibration years, more detailed observations of soil moisture profile, or new ways of imposing constraints with the available data.

## CHAPTER 5. CONCLUSION

### 5.1 Conclusion and Recommendations

Multilayer UAS image ortho-mosaics (MLMs) are more appropriate than single-layer UAS image ortho-mosaics (SLMs) for field-based HTP and other areas of research in which researchers wish to observe large numbers of small plots with as much precision and accuracy as possible. This is because they preserve replicate observations of plots in their raw format and avoid much of the geometric and radiometric distortion present in SLMs. They also make it possible to evaluate and enhance the precision and accuracy of UAS observations by correcting row-offset errors and applying outlier detection and other statistical analyses to the results. MLMs and SLMs perform similarly well when ranking the canopy cover and greenness of soybean plots, but MLMs enable higher relative accuracy by restricting analyses to pairs of plots with significantly different phenotype values. This capability will help breeders avoid making selections based on phenotype values that are statistically indistinguishable. Additionally, GR differentiates soybean plot greenness at least as well as hue, both when ranking and comparing pairs of plots. Therefore, breeders may want to consider using GR rather than hue as a more efficient metric of greenness for field-based HTP. This constitutes strong evidence in favor of hypotheses 1 of this thesis – that plot scale observations of canopy cover and color can be obtained from visual UAS imagery with enough accuracy, precision, and frequency to detect changes within plots and differences between plots during a growing season.

There were several limitations of the experimental design and data acquisition for testing hypothesis 1. First, these results may have been dependent on the flying altitude, as this is known to impact both the precision and accuracy of UAS-based observations of canopy cover and color (Torrez et al., 2014). Second, these results may have also been dependent on the image segmentation algorithm used to calculate canopy cover. Maximum likelihood classification was chosen because it was sure to be highly accurate and straightforward to implement but testing alternative algorithms may have allowed for a more detailed assessment.

Overall, the AquaCrop model was more sensitive to moisture stress when it was calibrated with UAS observations of canopy cover and reductions in canopy expansion rates than ground-based observations and this led to slightly more accurate simulations of canopy cover and yield. Although

these results may not be conclusive, they warrant further investigation as to whether UAS observations of reductions in canopy expansion rates can pinpoint the timing of the onset of moisture stress in field-grown crops and help crop models more realistically simulate the timing and severity of moisture stress as well as its impacts on crop growth and yield. This constitutes weak evidence in favor of hypotheses 2 and 3 – that visual UAS imagery enables detection of reductions in canopy expansion rates and that this can provide additional constraints for calibrating AquaCrop to more realistically simulate the timing and severity of moisture stress as well as its impacts on crop growth and yield.

There were also several limitations of the experimental design and data acquisition with regards to testing hypotheses 2 and 3. First, it would have been better to have ground reference observations of plant stress based on evapotranspiration or water potential measurements, rather than solely relying on reductions in canopy expansion rates and visual observations of stunted growth and leaf yellowing as stress indicators. Ideally, these ground-reference measurements would have focused on quantifying the fraction of field plots that were stressed on each sampling date, as this was the specific quantity that was ultimately used to constrain the AquaCrop model. Additionally, the differences between the ground and UAS-based models may have been due, in part, to the fact that the UAS-based model was calibrated with more numerous observations than the ground based model. Although more numerous observations may be considered an inherent advantage of UAS over ground-based approaches, it would have been interesting to test whether correcting for this imbalance could have influenced the outcome of the study.

Future work could investigate whether larger improvements in yield prediction accuracy can be achieved with additional calibration years, more soil moisture observations throughout the soil profile, or new ways of constraining the model using the available data. Future work could also investigate whether two-sided hypothesis testing can be used to produce more accurate rankings of plots that may be more applicable to plant breeding than pairwise comparisons of plots. Perhaps this would involve ranking plots based on the number of plots that have significantly lower phenotype values and assigning equal ranks to plots that are statistically indistinguishable. It would also be interesting to explore relationships between the relative and absolute accuracy of SLMs and MLMs. Additional research covering other phenotypes, crops, growth stages, environments, and seasons is also needed before more general recommendations can be made.

## FIGURES

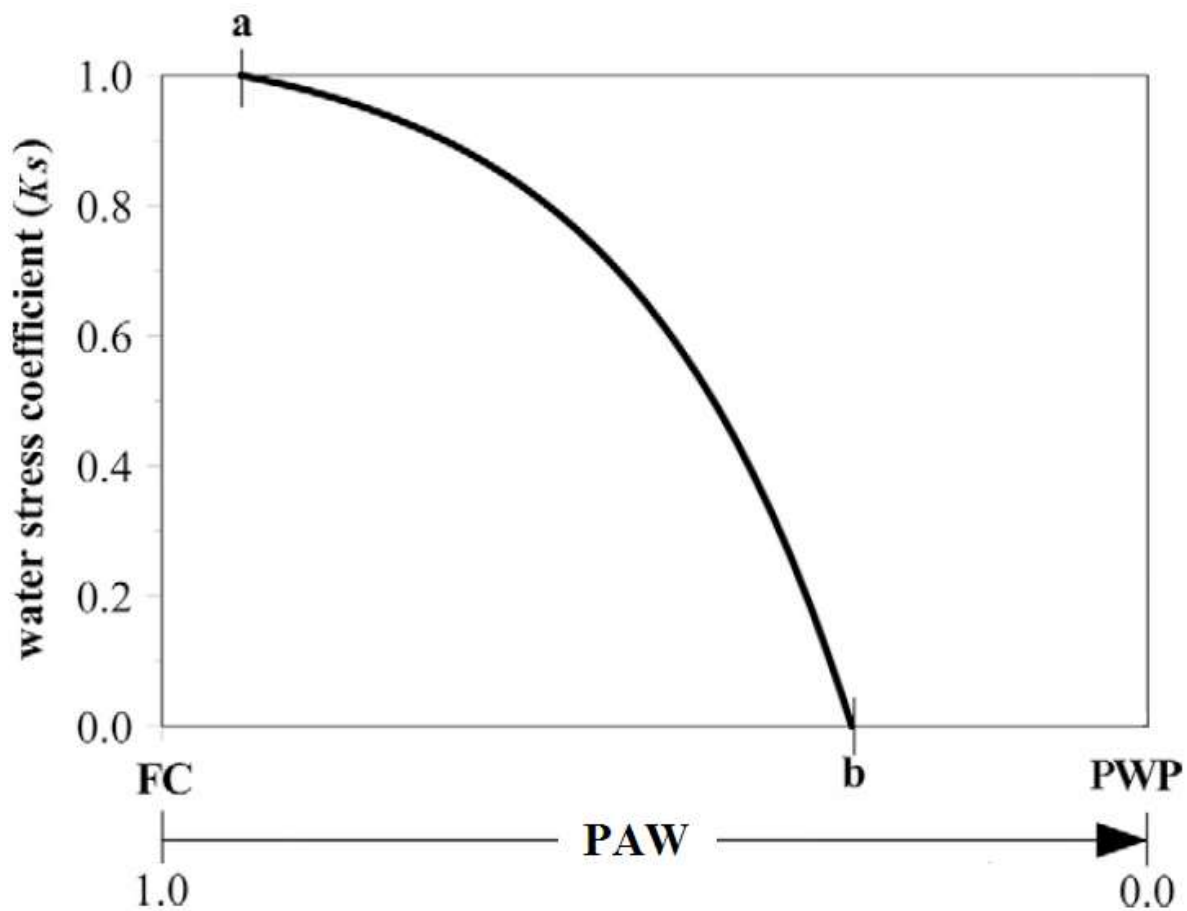


Figure 1. Variation of AquaCrop's stress coefficient for canopy expansion ( $K_{s\_exp}$ ) between upper (a) and lower (b) PAW thresholds. FC and PWP correspond to the field capacity and plant wilting point (Raes et al., 2012).

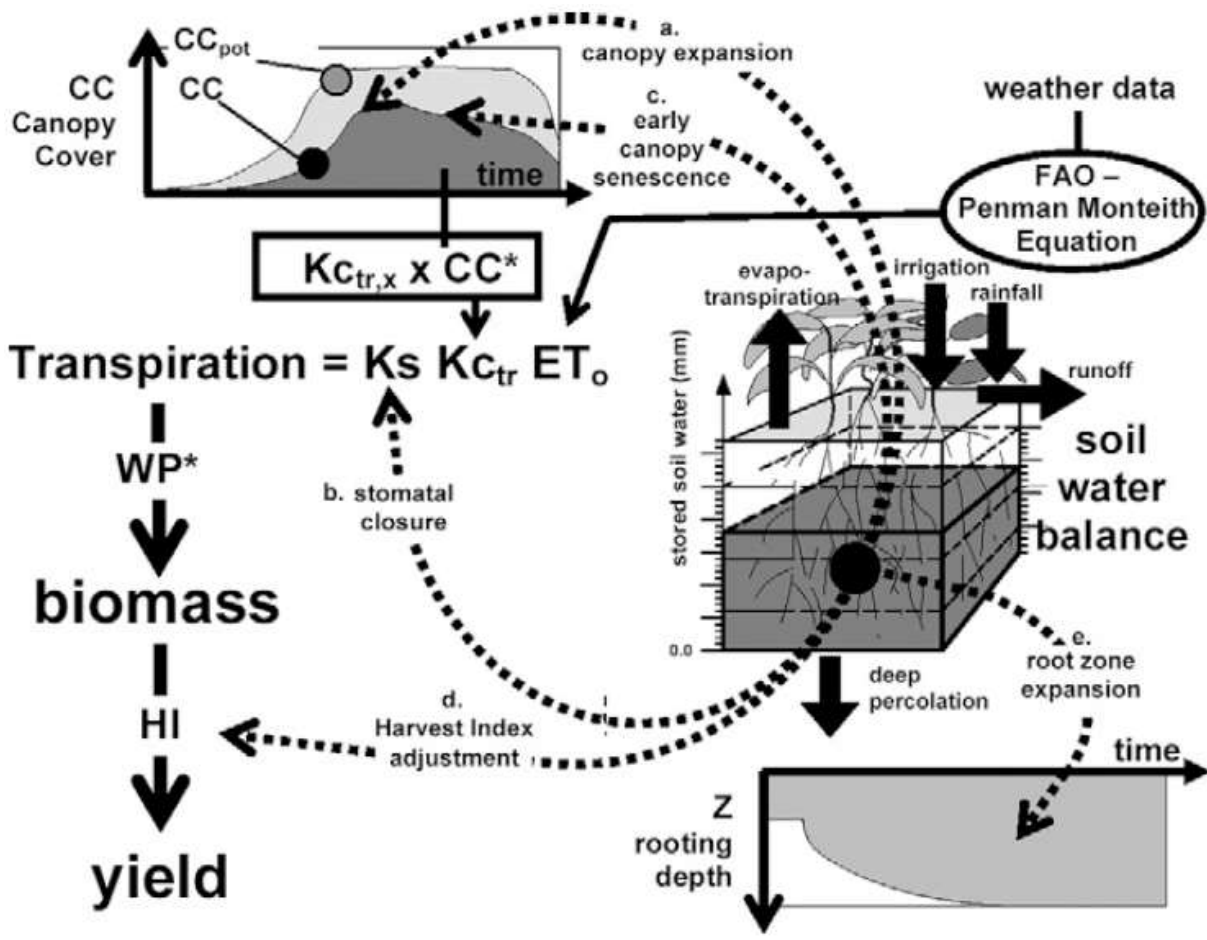


Figure 2. Schematic diagram of the AquaCrop model (Raes et al., 2012).

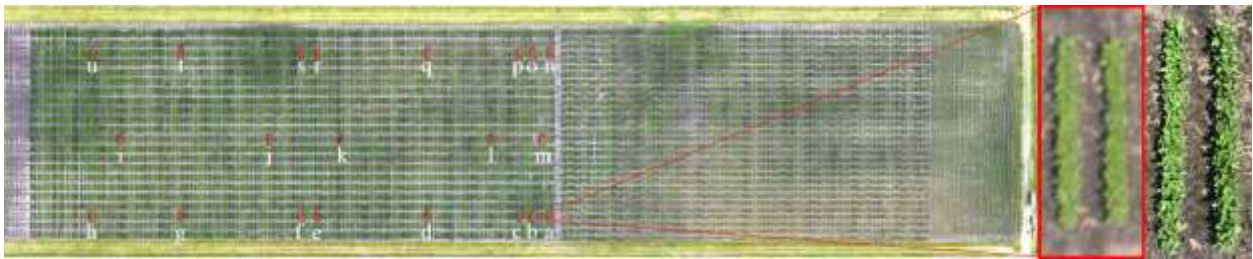


Figure 3. An RGB image ortho-mosaic of the field site generated by Pix4Dmapper using imagery from one of thirteen flight dates. Analysis focuses on the twenty-one soybean field plots outlined in red and labelled alphabetically from a to u. Plot a is magnified in aerial and ground images on the right.

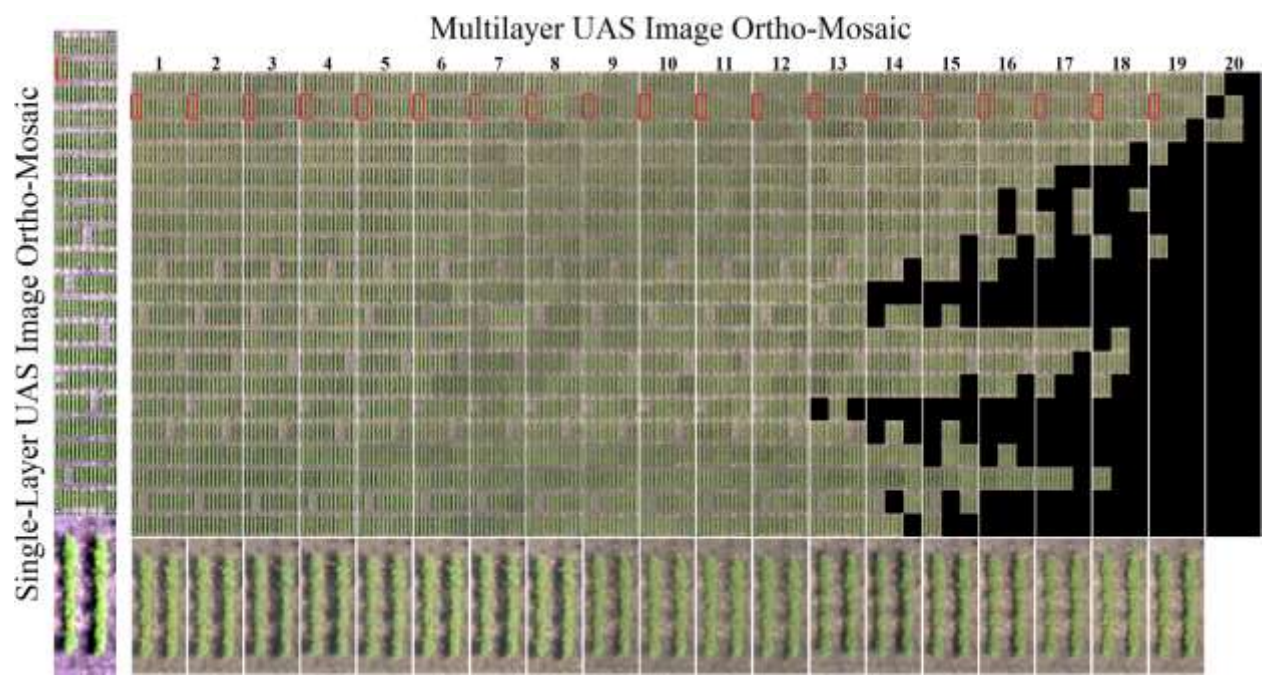


Figure 4. A single-layer (left) and 20-layer (right) UAS image ortho-mosaic of a portion of the field in Figure 2 made from RGB imagery from a single-layer flight date. At the bottom are magnified images of the plot outlined in red. The single-layer mosaic yields one image of the plot, while the multilayer mosaic yields nineteen replicate images from each frame photo that captured the plot.

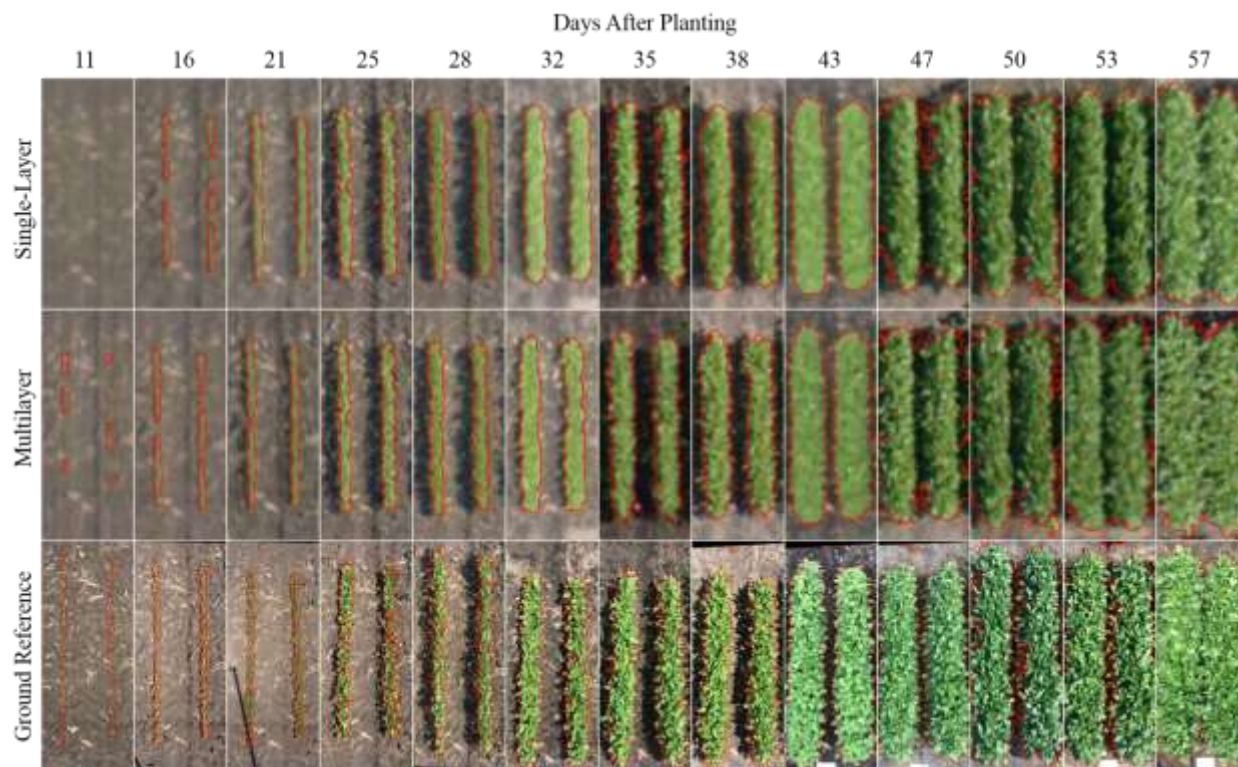


Figure 5. Image time series of reference plot ‘a’ from single-layer layer mosaics (1.5 cm pixel width), representative images from multilayer mosaics (1.5 cm pixel width), and ground-based nadir-perspective photos (sub-millimeter pixel width). The accuracy of canopy cover measurements based on maximum-likelihood classification is illustrated by the canopy edges outlined in red.

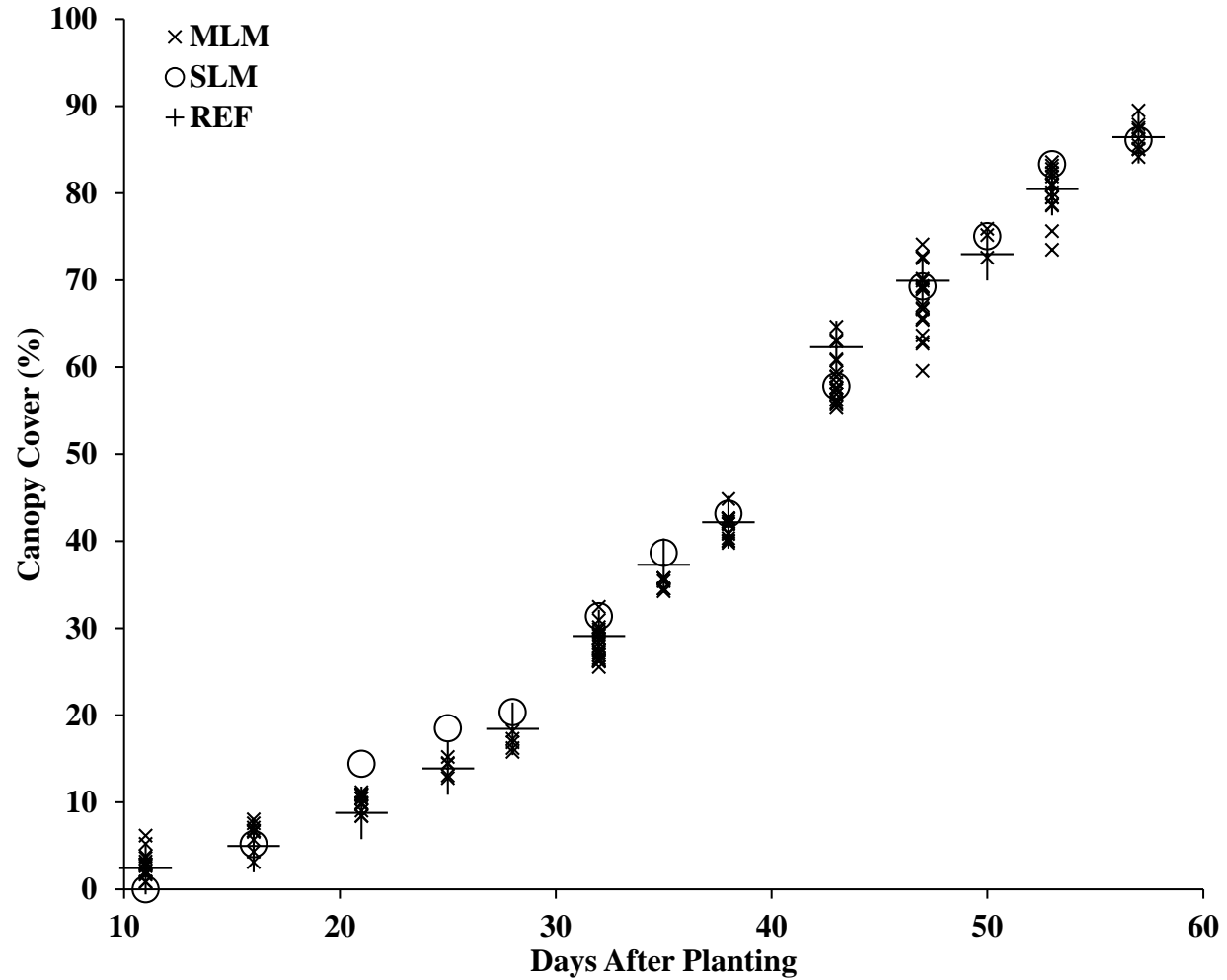


Figure 6. Time series of canopy cover for reference plot 'a' based on measurements from single-layer UAS image ortho-mosaics (SLM), multilayer UAS image ortho-mosaics (MLM), and ground reference photos (REF).

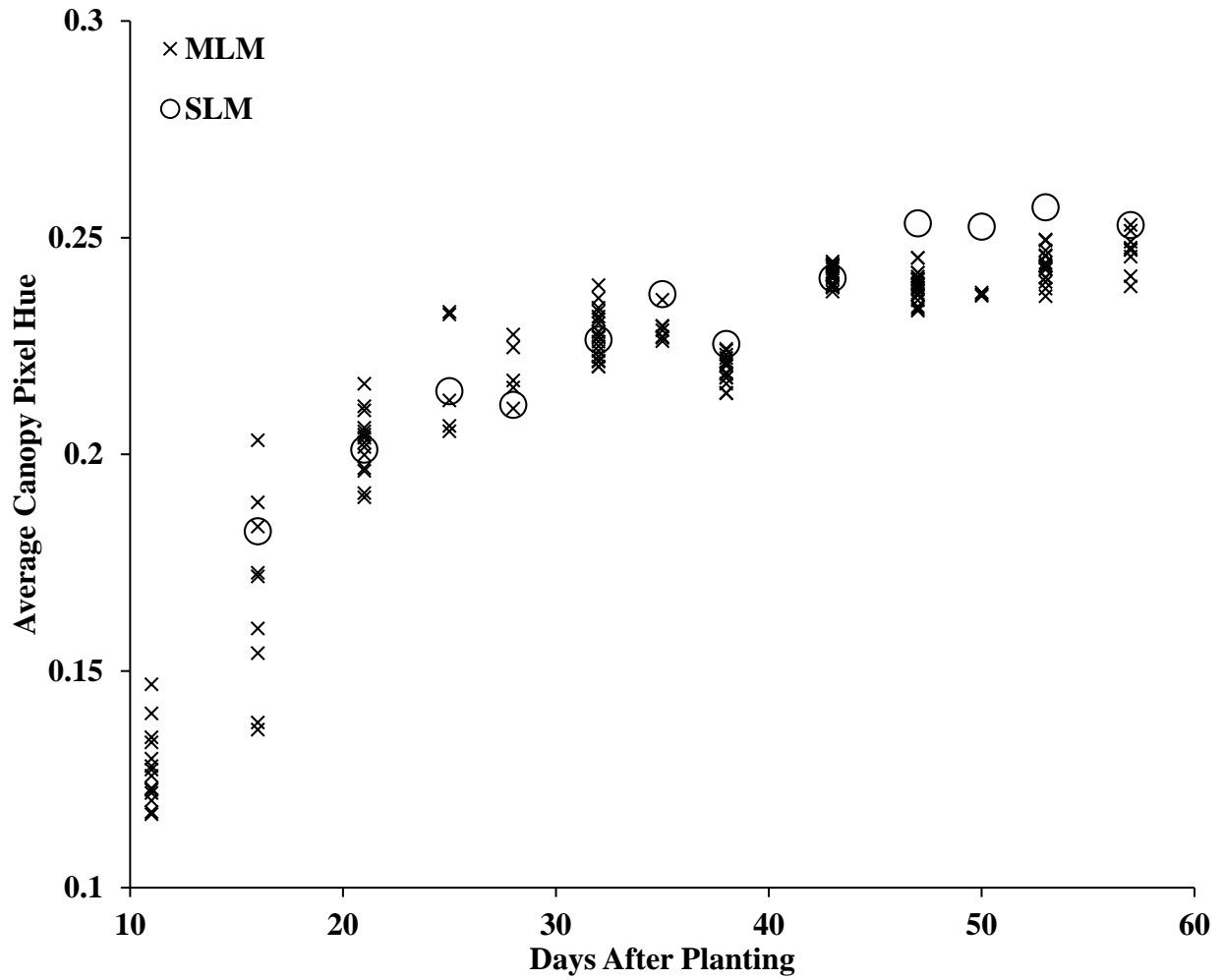


Figure 7. Time series of canopy pixel hue for reference plot ‘a’ based on measurements from single-layer UAS image ortho-mosaics (SLM) and multilayer UAS image ortho-mosaics (MLM).

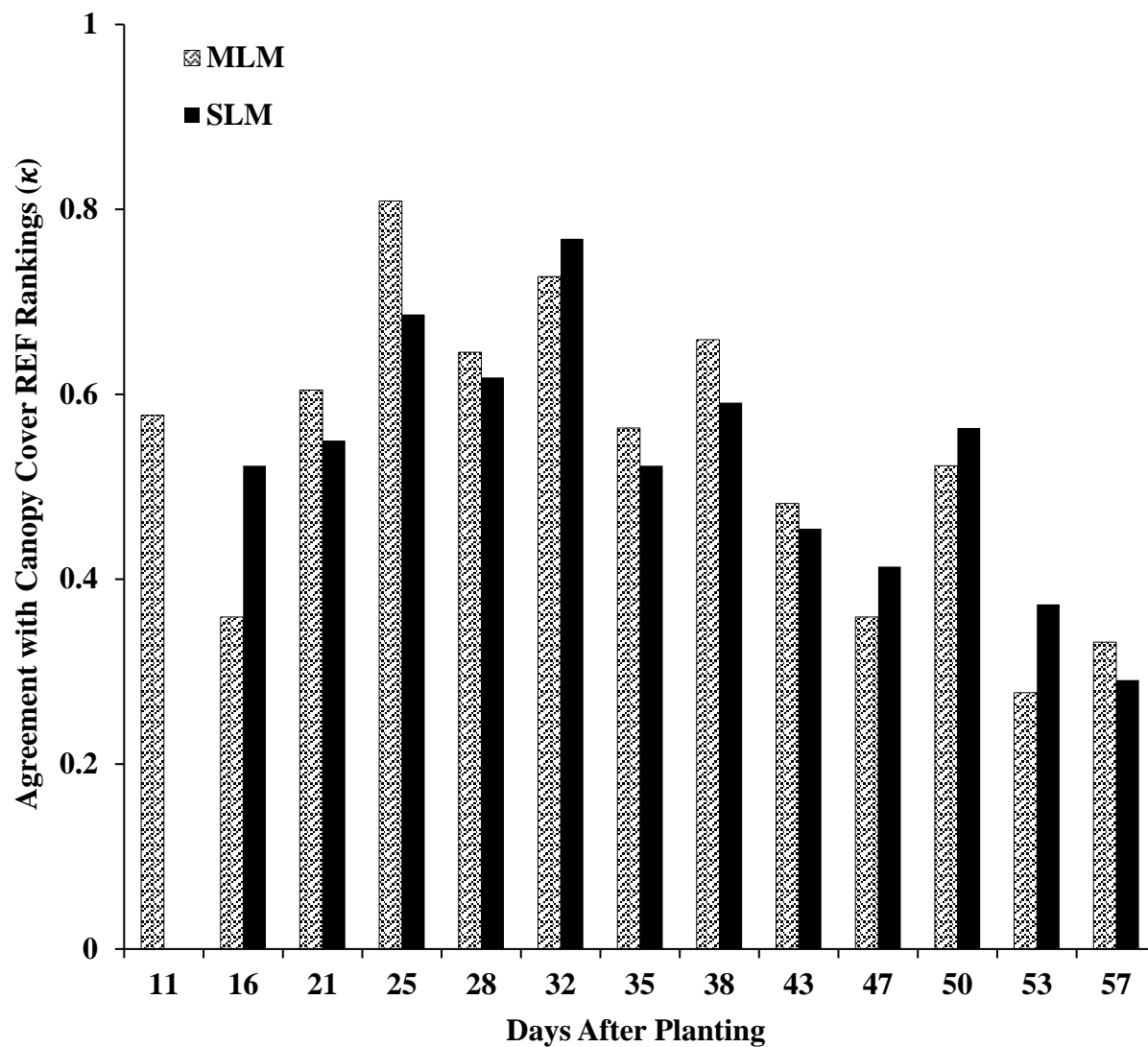


Figure 8. Agreement of rankings of canopy cover for 21 test plots on 13 flight dates based on Single Layer Mosaics (SLMs), Multilayer Mosaics (MLMs), and nadir-view ground reference images (REF) according to Cohen's Kappa statistic ( $\kappa$ ) with linear weighting (Watson & Petrie, 2010).

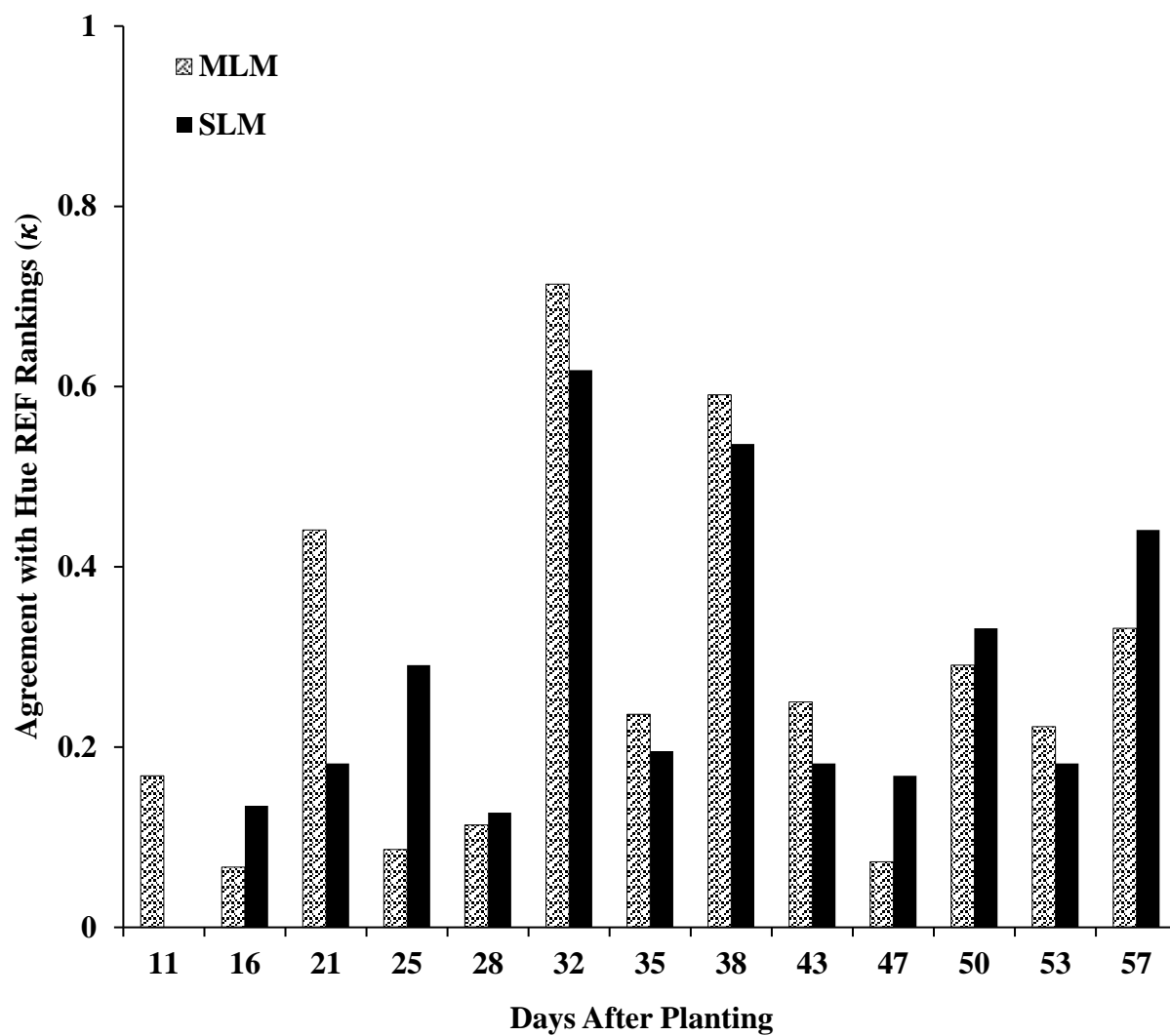


Figure 9. Agreement of rankings of hue for 21 test plots on 13 flight dates from Single Layer Mosaics (SLMs), Multilayer Mosaics (MLMs), and nadir-view ground reference images (REF) according to Cohen's Kappa statistic ( $\kappa$ ) with linear weighting (Watson & Petrie, 2010).

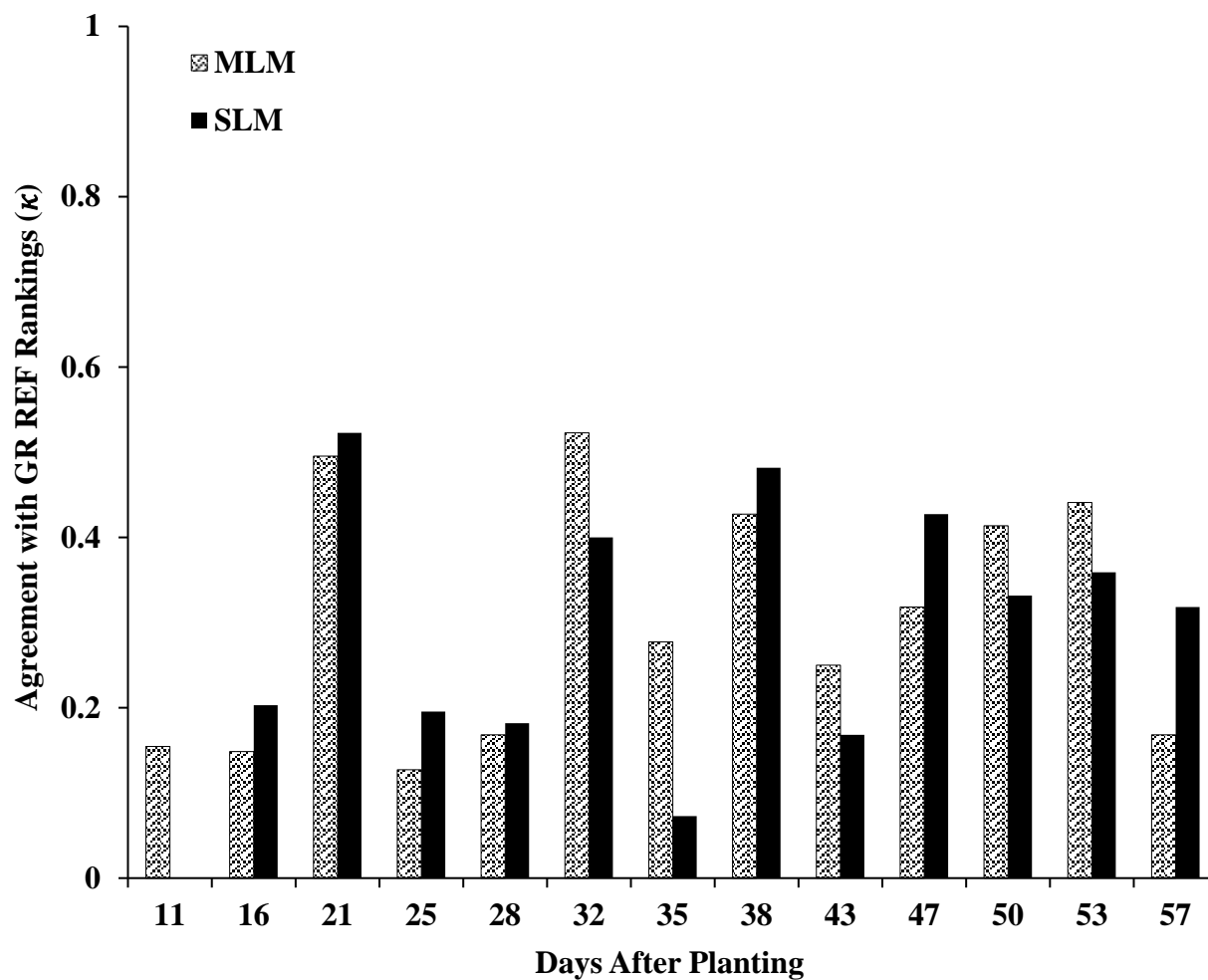


Figure 10. Agreement of rankings of green-to-red ratio (GR) for 21 test plots on 13 flight dates from Single Layer Mosaics (SLMs), Multilayer Mosaics (MLMs), and nadir-view ground reference images (REF) according to Cohen's Kappa statistic ( $\kappa$ ) with linear weighting (Watson & Petrie, 2010).

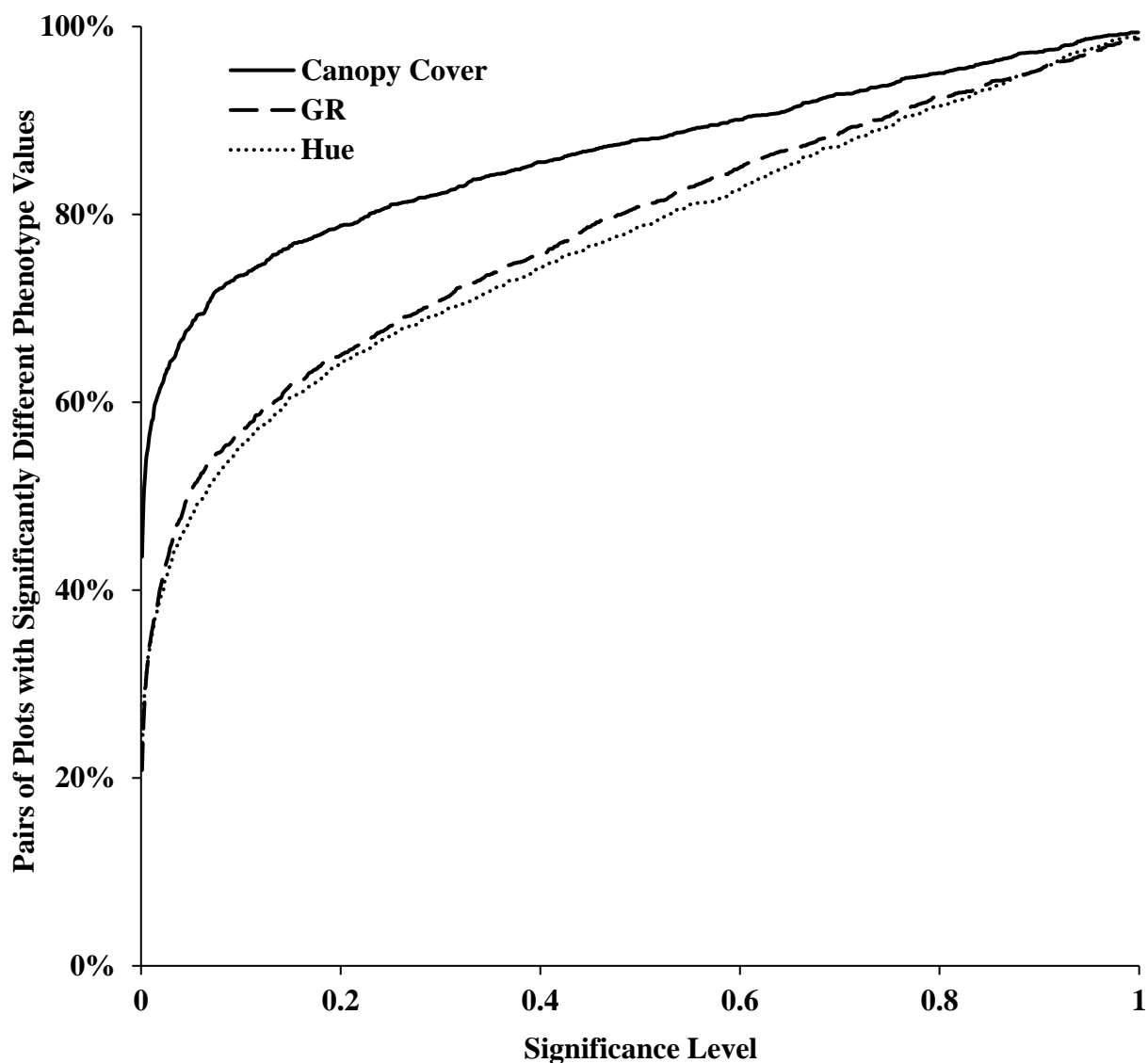


Figure 11. Fraction of 2730 unique pairs of 21 soybean test plots on 13 flight dates for which Wilcoxon Rank-Sum tests indicated significantly different median phenotype values as a function of the significance level of the two-sided hypothesis test. The plant phenotypes observed in this study were canopy cover, hue, and green-to-red ratio (GR). Replicate observations of plant phenotypes for each plot from multilayer mosaics were used for these pairwise plot comparisons.

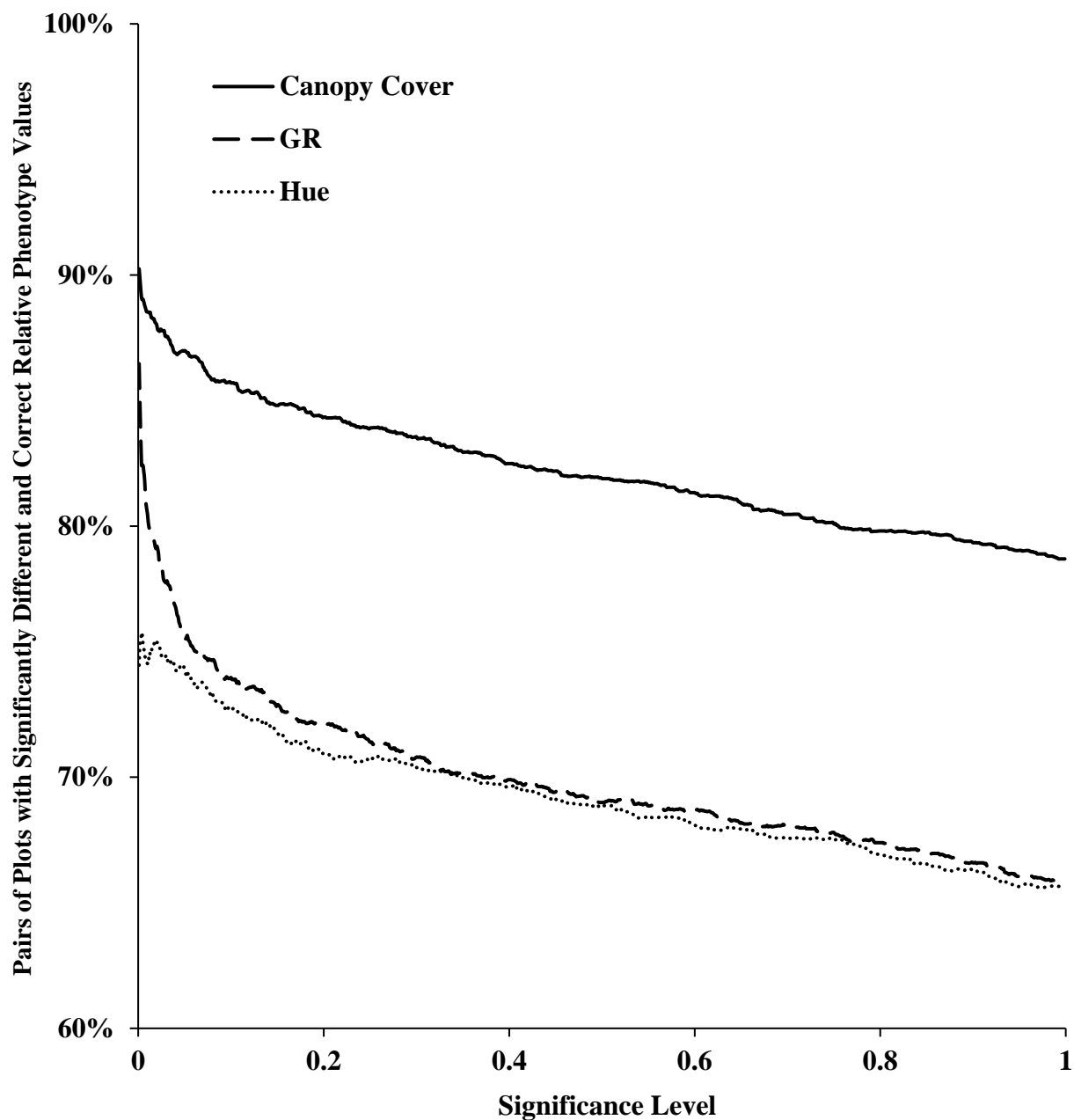


Figure 12. Fraction of unique pairs of 21 soybean test plots on 13 flight dates that had significantly different and correct relative phenotype values (e.g. plot A higher or lower phenotype value than plot B) according to nadir-view ground reference images as a function of the significance level of the two-sided hypothesis test. The plant phenotypes observed in this study were canopy cover, hue, and green-to-red ratio (GR). Wilcoxon Rank-Sum tests were used to compare replicate observations of plant phenotypes for pairs of plots from multilayer mosaics.

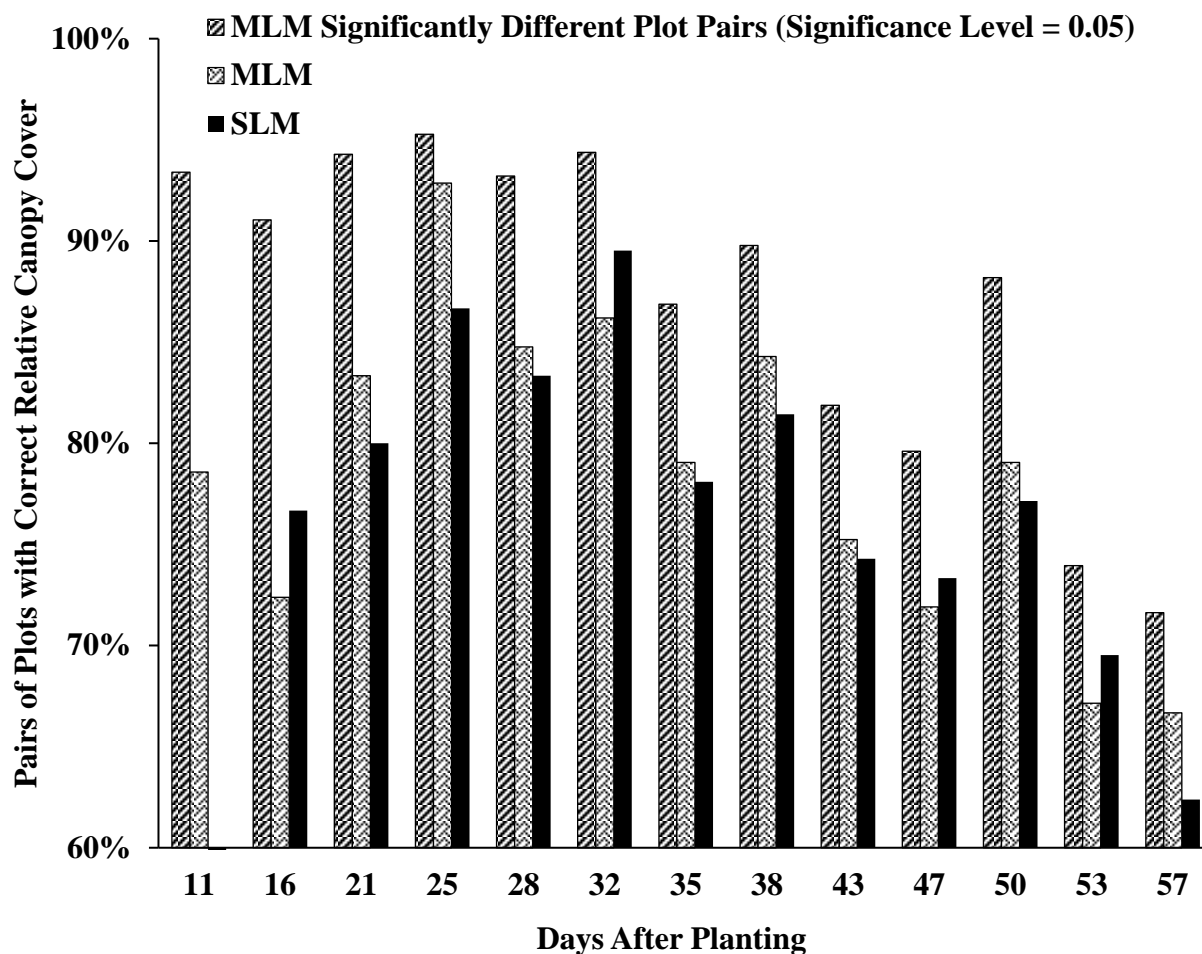


Figure 13. Fraction of 210 unique pairs of 21 test plots on each of 13 flight dates for which canopy cover observations from single layer mosaics (SLM) and multilayer mosaics (MLM) had the same relative values (e.g. plot A has a higher or lower phenotype value than plot B) as those from ground reference images (REF). Median values from MLMs and Wilcoxon Rank-Sum tests with a significance level of 0.05 were used for plot comparisons.

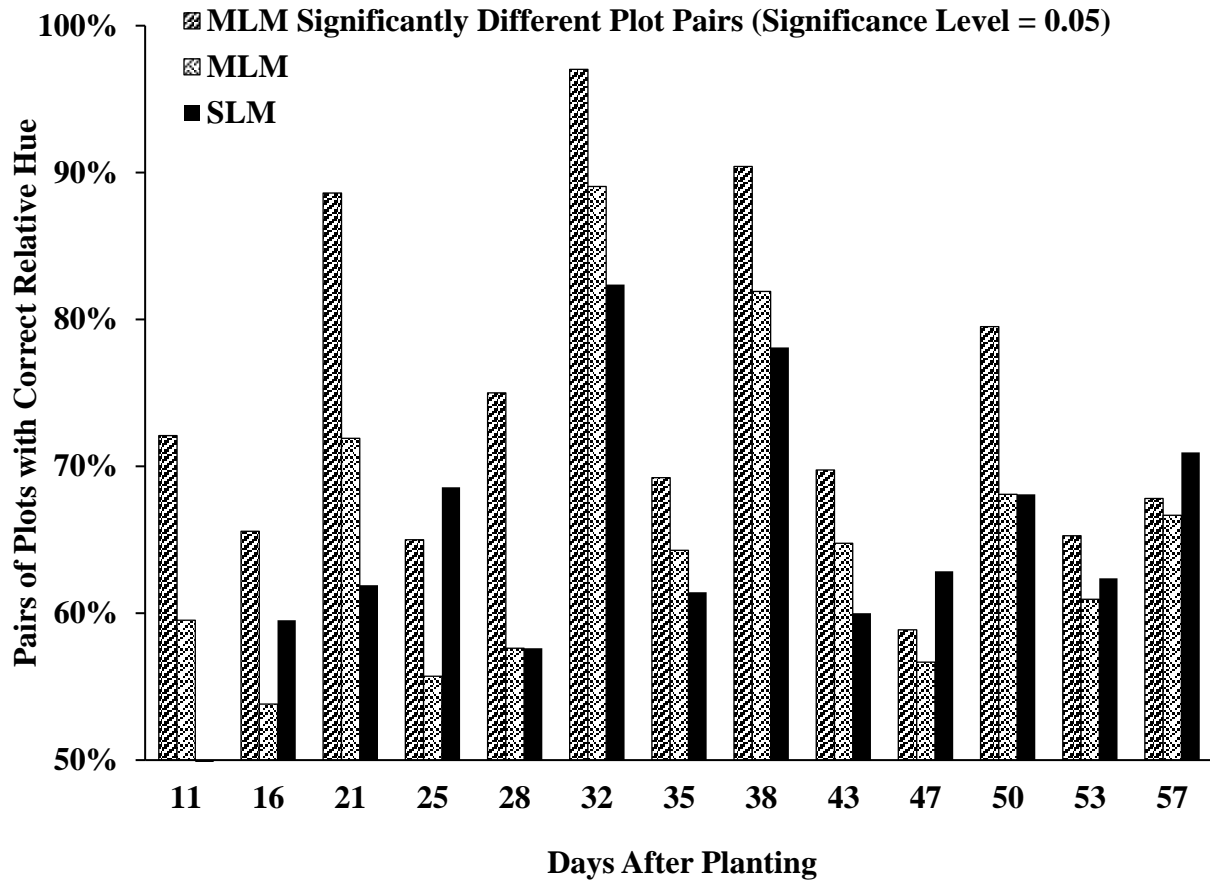


Figure 14. Fraction of 210 unique pairs of 21 test plots on each of 13 flight dates for which hue observations from single layer mosaics (SLM) and multilayer mosaics (MLM) had the same relative values (e.g. plot A has a higher or lower phenotype value than plot B as those from ground reference images (REF)). Median values from MLMs and Wilcoxon Rank-Sum tests with a significance level of 0.05 were used for plot comparisons.

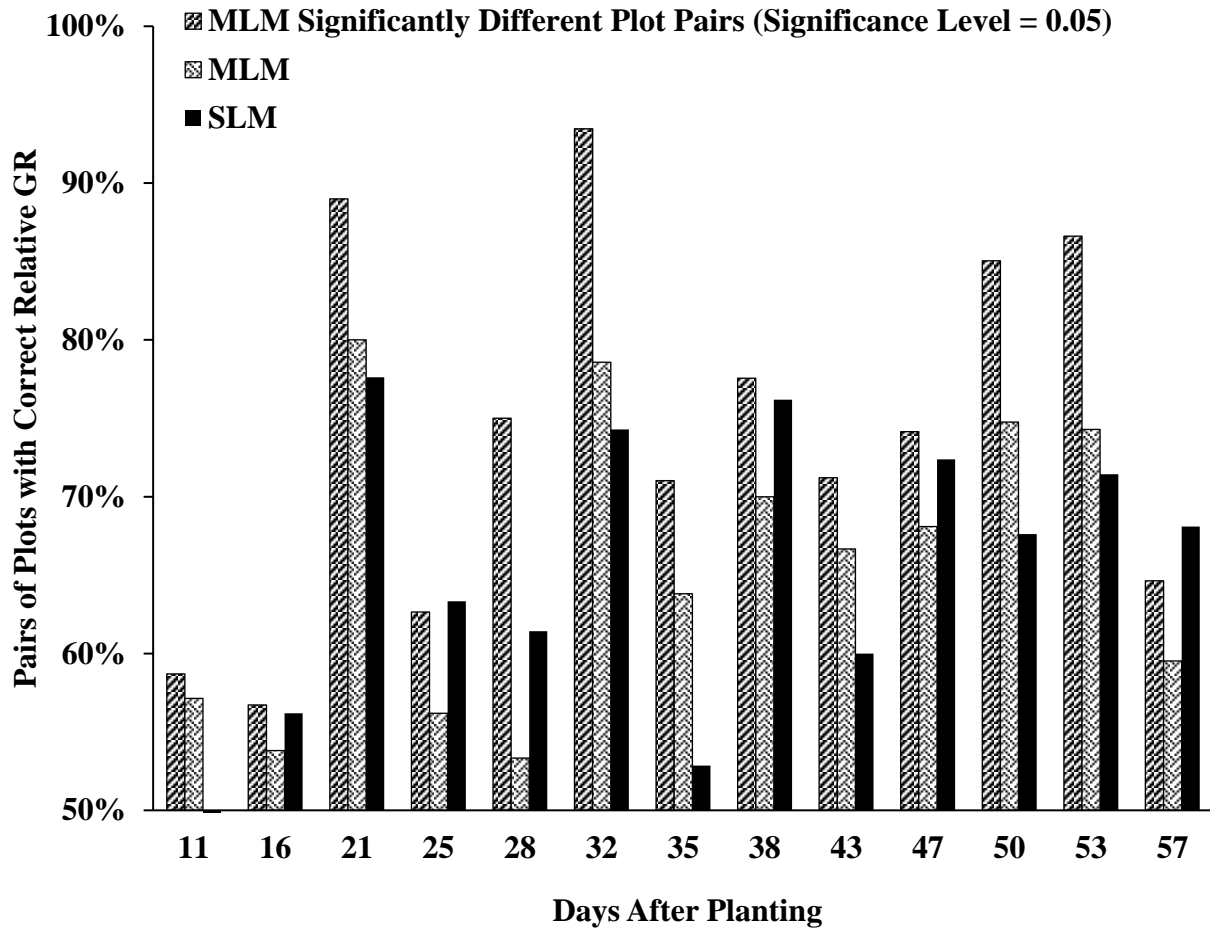


Figure 15. Fraction of 210 unique pairs of 21 test plots on each of 13 flight dates for which GR observations from single layer mosaics (SLM) and multilayer mosaics (MLM) had the same relative values (e.g. plot A has a higher or lower phenotype value than plot B) as those from ground reference images (REF). Median values from MLMs and Wilcoxon Rank-Sum tests with a significance level of 0.05 were used for plot comparisons.



Figure 16. Map of Purdue University Agronomy Center for Research and Education (ACRE) with fields 43 and 62 and the local weather station outlined in red. The area outlined in yellow is approximately 200 hectares.

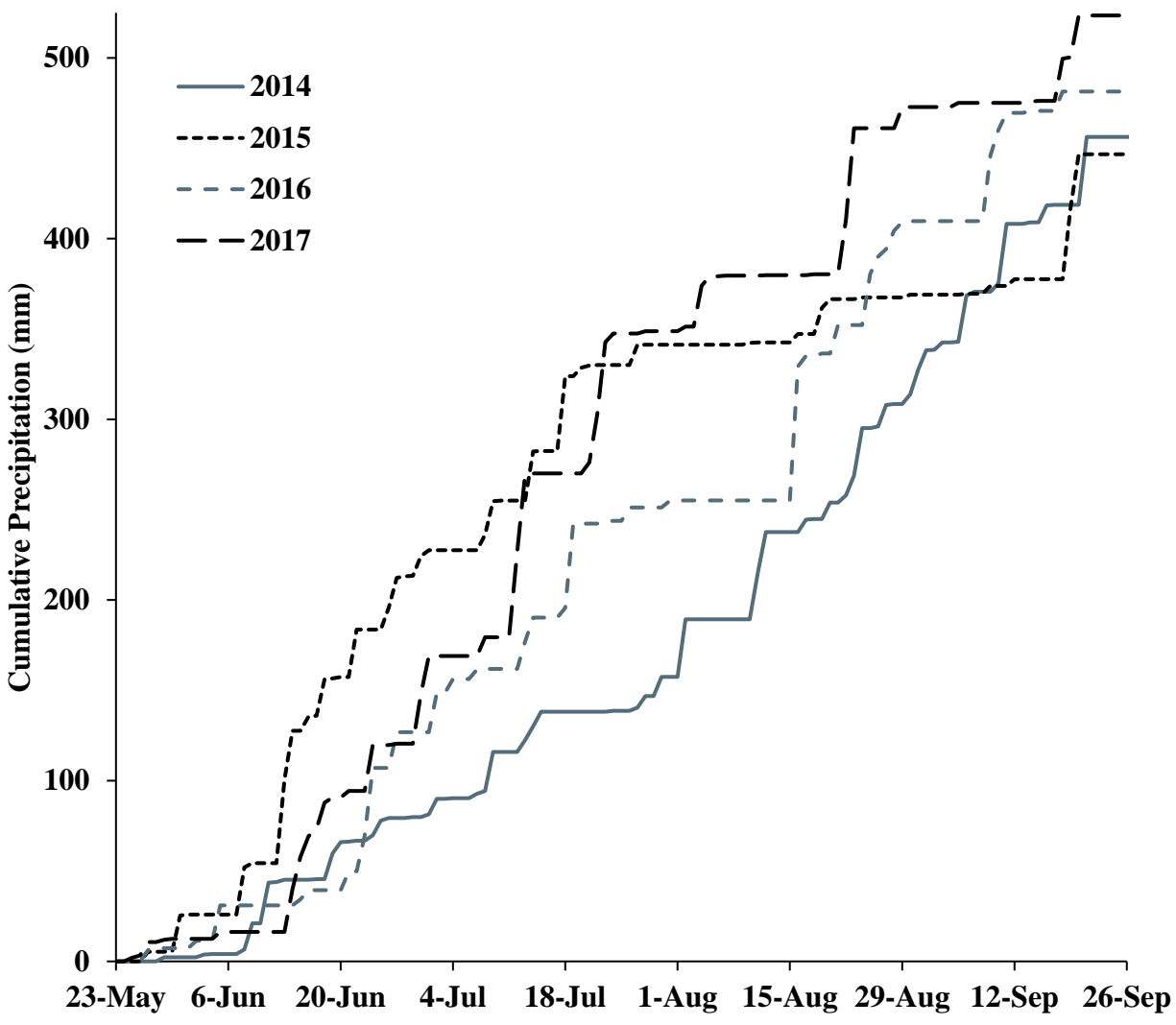


Figure 17. Cumulative precipitation in 2014, 2015, 2016, and 2017 measured at ACRE.

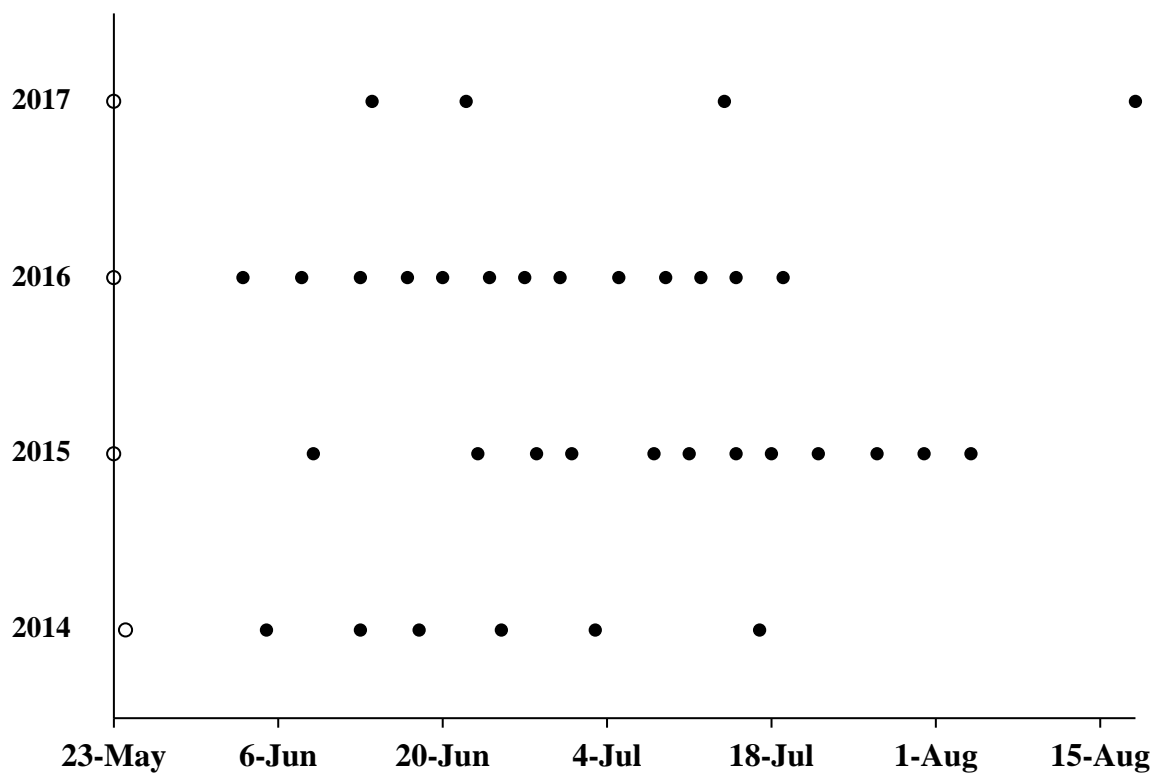


Figure 18. Timeline of planting and UAS flight dates in 2014, 2015, 2016, and 2017. Planting dates are indicated by unfilled points. The tick marks on the x-axis represent 2-week intervals.

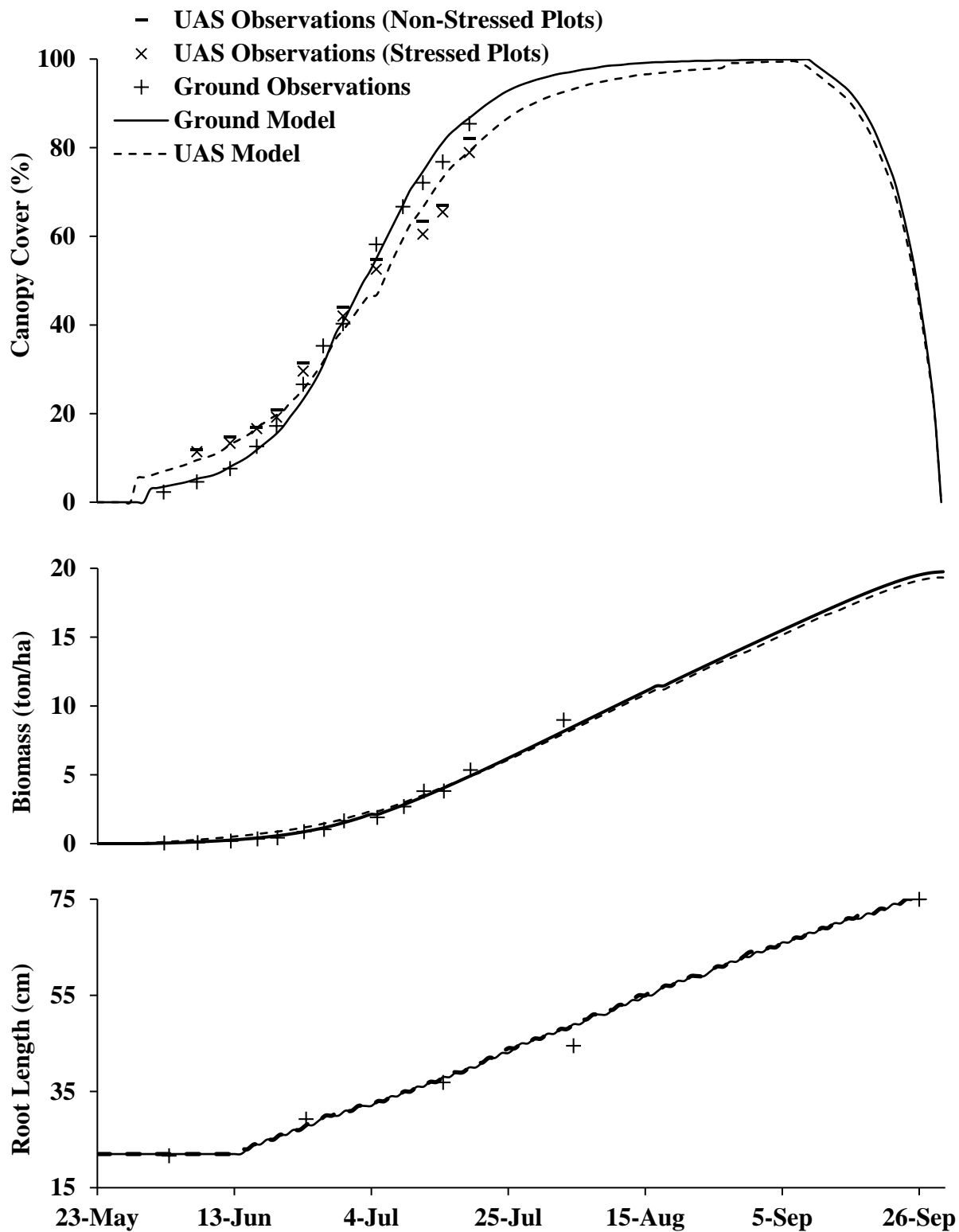


Figure 19. Observed and simulated soybean canopy cover, biomass, and root length using AquaCrop calibrated with UAS and ground-based observations from 2016 at ACRE.

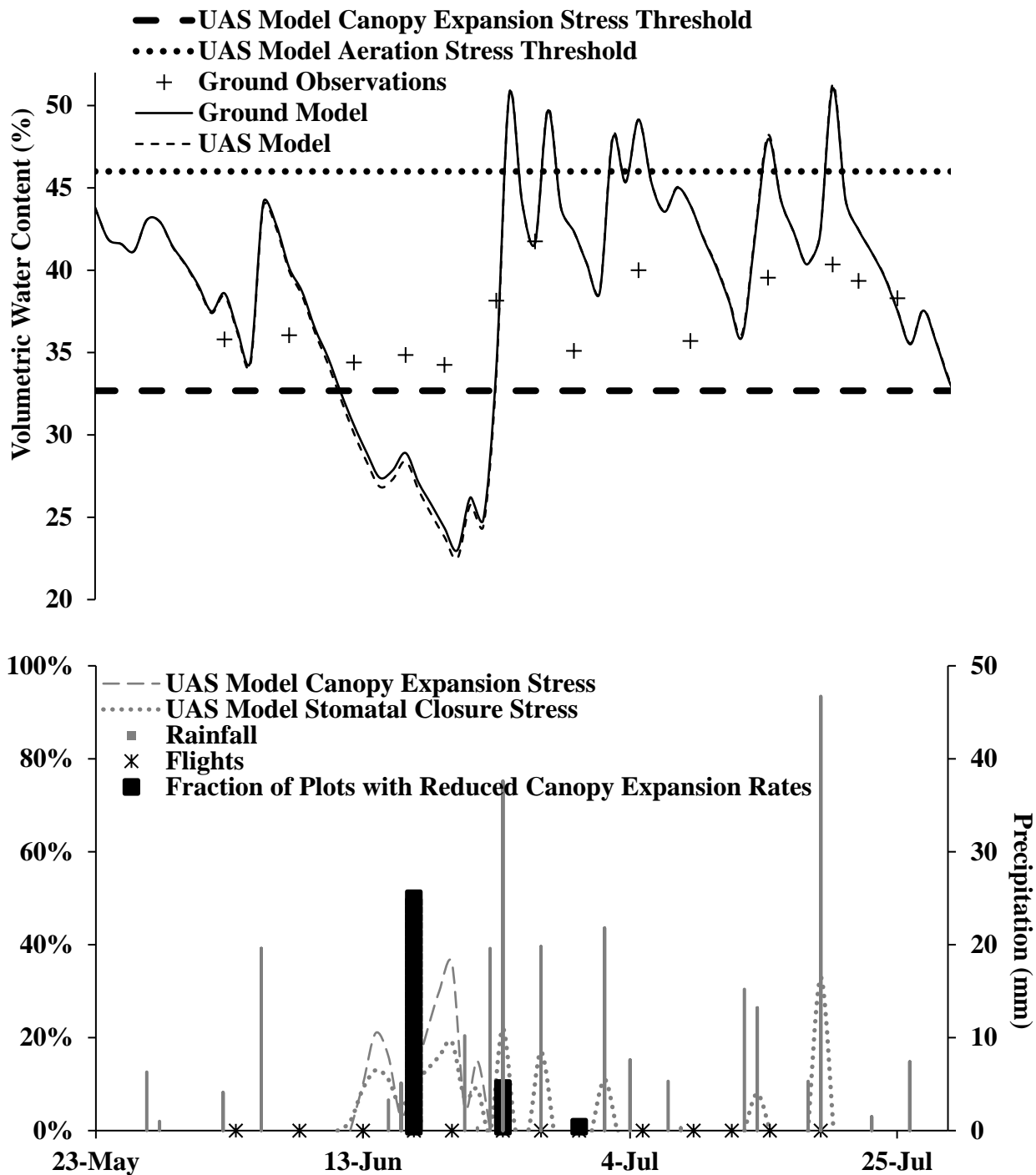


Figure 20. Rainfall and observed and simulated soil water content and moisture stress using AquaCrop calibrated with UAS and ground-based observations from 2016 at ACRE. Note that the ground-based model did not detect any moisture stress while the UAS-based model detected moisture stress consistently with dates when plots exhibited reduced canopy expansion rates.

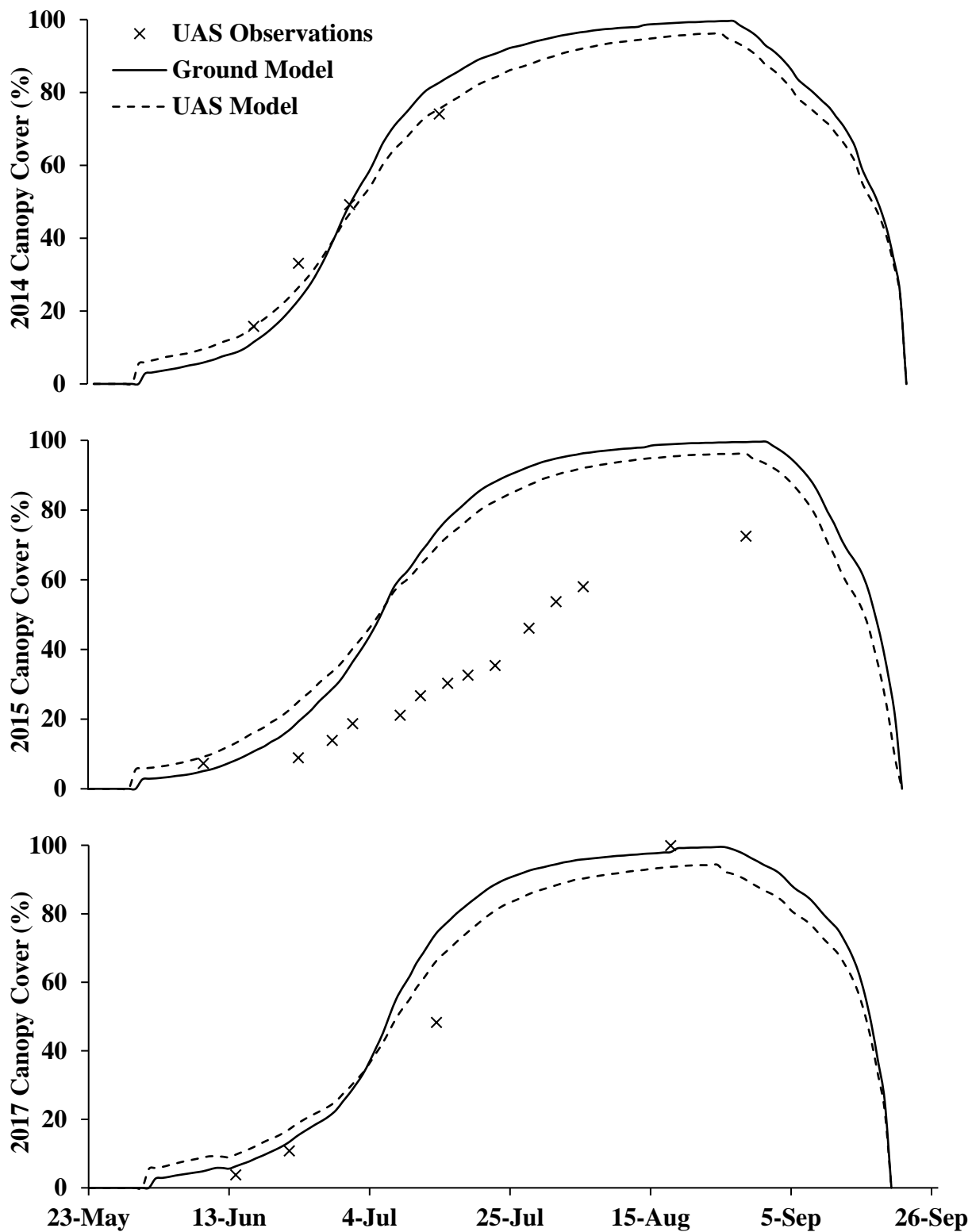


Figure 21. Observed and simulated soybean canopy cover in 2014, 2015, and 2017 at ACRE using AquaCrop calibrated with UAS and ground-based observations from 2016.

## TABLES

Table 1. Summary of the basic inputs needed to run AquaCrop.

<b>Input</b>	<b>Description</b>
Air Temperature	Daily air temperature.
Reference Evapotranspiration	Daily reference evapotranspiration calculated based on the Penman-Monteith equation.
Rainfall	Daily rainfall amounts.
Initial Soil Moisture Conditions	Volumetric water content of the soil at the start of the simulation period.
Soil drainage properties	Volumetric water content of the soil at saturation (1), field capacity (2), and permanent wilting point (3), as well as saturated hydraulic conductivity of the soil and corresponding drainage coefficient (4).
Growth Stages	The dates when flowering, seed-filling, and maturity occur.

Table 2. Summary of observations of outputs that may be used to calibrate AquaCrop.

<b>Observation</b>	<b>Description</b>
Canopy Cover	Periodic observations of canopy cover.
Biomass	Periodic observations of above-ground dry weight.
Soil Moisture	Periodic observations of volumetric water content in the root zone.
Root Length	Periodic observations of the length of the roots in the root zone.
Yield	Observations of crop yield.
Timing of the Onset of Moisture Stress	Observations of visible indicators of moisture stress (e.g. reductions in canopy expansion rate).

Table 3. Frequencies of row-offset errors (offset images/replicate images) for different plots on different flight dates based on visual inspection of replicate plot images from multilayer mosaics.

Plot	Days after Planting												
	11	16	21	25	28	32	35	38	43	47	50	53	57
A	0	0	0	0	0	0	0	0	0	0	0	0	0
B	0	0	0	0	0	0	0	0	0	0	0	0	0
C	0	0	0	0	0	0	0	0	0	0	0	0	0
D	0	0	0	0	0	0	0	0	0	1/18	1/7	0	0
E	0	0	0	0	0	0	0	0	0	0	0	0	0
F	0	0	0	0	0	0	0	0	0	0	0	0	0
G	0	0	0	0	0	0	0	0	0	0	0	0	0
H	0	0	0	0	0	0	0	0	0	0	0	0	0
I	0	0	0	0	0	4/21	0	0	0	0	0	0	0
J	0	0	0	0	0	3/25	0	0	0	0	0	0	0
K	0	0	0	0	0	1/19	0	0	0	0	0	0	0
L	0	0	0	0	0	0	0	0	0	0	0	0	0
M	0	0	0	0	0	0	0	0	0	0	0	0	0
N	0	0	0	0	0	0	0	0	0	0	0	0	0
O	0	0	0	0	0	0	0	0	0	0	0	0	1/13
P	0	0	0	0	0	0	0	0	0	0	0	0	0
Q	0	0	0	0	0	0	0	0	0	0	0	0	1/15
R	0	0	0	0	0	1/22	0	0	0	0	0	0	0
S	0	0	0	0	0	2/31	0	0	0	0	0	0	0
T	0	0	0	0	0	6/27	0	0	0	0	0	0	0
U	0	0	0	0	0	3/25	0	0	0	0	0	0	0

Table 4. Rankings of canopy cover for 21 test plots labelled ‘a’ through ‘u’ on 13 flight dates based on ground reference measurements (REF), single layer mosaics (SLM), and multilayer mosaics (MLM).

Plot	Days After Planting																																						
	11			16			21			25			28			32			35			38			43			47			50			53			57		
	REF	SLM	MLM	REF	SLM	MLM	REF	SLM	MLM	REF	SLM	MLM	REF	SLM	MLM	REF	SLM	MLM	REF	SLM	MLM	REF	SLM	MLM	REF	SLM	MLM	REF	SLM	MLM	REF	SLM	MLM	REF	SLM	MLM			
a	15	/	9	11	10	2	8	7	4	7	12	7	13	15	14	10	12	11	8	15	13	9	11	9	6	8	9	5	16	13	12	14	11	4	10	8	9	14	10
b	12	/	18	12	3	19	6	4	7	9	3	10	8	4	6	12	9	7	14	9	5	8	4	4	7	6	5	14	14	16	7	12	7	8	16	17	17	9	9
c	10	/	14	16	5	11	13	5	10	8	6	9	12	5	10	5	7	6	11	6	9	10	6	7	8	7	7	2	8	11	15	13	10	9	9	7	6	15	14
d	1	/	7	9	8	9	16	21	13	14	7	12	16	11	11	19	15	15	16	12	12	17	16	16	16	13	16	20	12	14	14	17	18	7	14	15	5	20	20
e	3	/	13	6	6	15	10	6	15	10	13	13	10	10	9	8	6	8	10	8	11	7	12	12	13	11	10	15	11	7	6	9	14	14	5	4	13	5	5
f	6	/	3	3	2	6	7	8	8	4	4	5	6	8	4	4	5	4	12	3	7	11	8	8	10	5	6	9	10	5	10	10	6	16	7	5	16	6	7
g	9	/	8	7	12	16	11	15	14	13	15	16	14	16	16	16	18	17	17	14	19	19	18	19	21	20	20	21	17	18	20	19	17	20	20	19	20	21	19
h	7	/	1	10	17	1	15	11	12	15	14	14	15	14	13	13	13	14	13	13	15	15	13	15	12	15	13	6	9	8	8	8	5	13	11	6	10	13	6
i	16	/	16	20	21	21	17	17	19	19	17	19	18	20	19	15	20	20	19	20	21	13	21	21	15	19	18	8	19	17	16	16	16	15	13	9	12	12	11
j	8	/	4	5	7	8	9	14	5	11	10	8	3	6	8	9	11	12	7	11	6	12	10	13	14	10	11	10	6	4	4	6	9	6	18	13	18	16	16
k	4	/	6	8	11	12	3	12	11	6	8	4	11	9	5	11	10	10	9	7	10	16	7	10	5	12	14	17	15	15	13	7	15	17	8	14	14	10	15
l	20	/	21	17	15	17	19	13	16	18	16	15	17	12	15	20	16	13	18	16	14	14	14	11	18	14	12	16	13	12	19	5	12	21	15	11	19	18	17
m	13	/	12	13	9	4	5	3	2	5	9	3	5	7	7	6	4	5	5	5	2	5	5	5	11	4	3	12	7	6	11	11	8	10	6	10	11	7	8
n	19	/	10	19	18	18	20	18	18	20	21	20	20	21	21	18	19	18	15	19	18	20	19	18	20	18	19	13	21	21	17	20	19	18	21	21	15	17	18
o	18	/	19	18	20	13	18	19	17	17	19	18	21	19	18	21	21	21	21	21	20	21	20	20	17	21	21	18	18	19	18	20	12	19	18	7	19	21	
p	21	/	20	21	19	20	21	20	21	21	20	21	19	18	20	17	17	19	20	18	17	18	17	17	19	17	17	19	20	20	21	21	21	19	17	20	21	8	12
q	14	/	15	14	16	14	14	16	20	16	18	17	9	17	17	14	14	16	4	17	16	6	15	14	3	16	15	4	5	10	1	15	13	11	12	16	8	11	13
r	17	/	17	15	13	7	12	9	9	12	11	11	7	13	12	7	8	9	6	10	8	4	9	6	2	9	8	11	4	9	5	4	4	2	2	12	4	3	4
s	5	/	5	2	1	5	1	1	1	1	1	1	1	1	1	2	1	2	3	2	3	3	2	2	4	3	4	3	1	1	2	1	2	3	1	3	1	1	2
t	11	/	11	4	14	10	4	10	6	3	5	6	4	3	3	3	3	1	2	4	4	2	3	3	9	2	2	7	3	3	9	3	3	1	3	1	3	2	1
u	2	/	2	1	4	3	2	2	3	2	2	2	2	2	2	1	2	3	1	1	1	1	1	1	1	1	1	1	2	2	3	2	1	5	4	2	2	4	3

Table 5. Rankings of hue for 21 test plots labelled ‘a’ through ‘u’ on 13 flight dates based on ground reference measurements (REF), single layer mosaics (SLM), and multilayer mosaics (MLM).

Plot	Days After Planting																																									
	11			16			21			25			28			32			35			38			43			47			50			53			57					
	REF	SLM	MLM	REF	SLM	MLM	REF	SLM	MLM	REF	SLM	MLM	REF	SLM	MLM	REF	SLM	MLM	REF	SLM	MLM	REF	SLM	MLM	REF	SLM	MLM	REF	SLM	MLM	REF	SLM	MLM	REF	SLM	MLM						
<b>a</b>	<b>8</b>	/	<b>18</b>	<b>13</b>	<b>13</b>	<b>9</b>	<b>1</b>	<b>8</b>	<b>4</b>	<b>8</b>	<b>8</b>	<b>12</b>	<b>6</b>	<b>18</b>	<b>11</b>	<b>11</b>	<b>7</b>	<b>9</b>	<b>11</b>	<b>10</b>	<b>11</b>	<b>6</b>	<b>10</b>	<b>10</b>	<b>10</b>	<b>11</b>	<b>13</b>	<b>8</b>	<b>3</b>	<b>8</b>	<b>6</b>	<b>4</b>	<b>12</b>	<b>7</b>	<b>3</b>	<b>6</b>	<b>9</b>	<b>5</b>	<b>7</b>			
<b>b</b>	<b>6</b>	/	<b>5</b>	<b>13</b>	<b>4</b>	<b>5</b>	<b>5</b>	<b>3</b>	<b>1</b>	<b>10</b>	<b>5</b>	<b>1</b>	<b>4</b>	<b>1</b>	<b>9</b>	<b>10</b>	<b>6</b>	<b>7</b>	<b>10</b>	<b>15</b>	<b>16</b>	<b>10</b>	<b>11</b>	<b>15</b>	<b>11</b>	<b>4</b>	<b>6</b>	<b>9</b>	<b>13</b>	<b>15</b>	<b>18</b>	<b>8</b>	<b>16</b>	<b>16</b>	<b>18</b>	<b>14</b>	<b>12</b>	<b>13</b>	<b>13</b>			
<b>c</b>	<b>1</b>	/	<b>2</b>	<b>16</b>	<b>2</b>	<b>1</b>	<b>12</b>	<b>5</b>	<b>3</b>	<b>11</b>	<b>1</b>	<b>3</b>	<b>2</b>	<b>2</b>	<b>17</b>	<b>5</b>	<b>4</b>	<b>4</b>	<b>8</b>	<b>5</b>	<b>9</b>	<b>5</b>	<b>6</b>	<b>6</b>	<b>9</b>	<b>5</b>	<b>4</b>	<b>15</b>	<b>11</b>	<b>11</b>	<b>4</b>	<b>12</b>	<b>6</b>	<b>6</b>	<b>14</b>	<b>13</b>	<b>13</b>	<b>14</b>	<b>14</b>			
<b>d</b>	<b>2</b>	/	<b>1</b>	<b>4</b>	<b>9</b>	<b>10</b>	<b>7</b>	<b>15</b>	<b>11</b>	<b>2</b>	<b>4</b>	<b>20</b>	<b>1</b>	<b>14</b>	<b>4</b>	<b>1</b>	<b>8</b>	<b>3</b>	<b>7</b>	<b>3</b>	<b>1</b>	<b>1</b>	<b>9</b>	<b>2</b>	<b>1</b>	<b>1</b>	<b>1</b>	<b>12</b>	<b>1</b>	<b>8</b>	<b>2</b>	<b>1</b>										
<b>e</b>	<b>16</b>	/	<b>8</b>	<b>17</b>	<b>7</b>	<b>8</b>	<b>15</b>	<b>19</b>	<b>16</b>	<b>17</b>	<b>6</b>	<b>2</b>	<b>7</b>	<b>15</b>	<b>16</b>	<b>14</b>	<b>11</b>	<b>12</b>	<b>4</b>	<b>14</b>	<b>14</b>	<b>8</b>	<b>16</b>	<b>13</b>	<b>5</b>	<b>13</b>	<b>8</b>	<b>14</b>	<b>17</b>	<b>14</b>	<b>7</b>	<b>11</b>	<b>5</b>	<b>3</b>	<b>8</b>	<b>8</b>	<b>21</b>	<b>18</b>	<b>12</b>			
<b>f</b>	<b>7</b>	/	<b>3</b>	<b>5</b>	<b>3</b>	<b>4</b>	<b>16</b>	<b>10</b>	<b>6</b>	<b>18</b>	<b>12</b>	<b>4</b>	<b>13</b>	<b>6</b>	<b>18</b>	<b>19</b>	<b>16</b>	<b>16</b>	<b>17</b>	<b>9</b>	<b>13</b>	<b>17</b>	<b>15</b>	<b>14</b>	<b>12</b>	<b>17</b>	<b>18</b>	<b>10</b>	<b>14</b>	<b>19</b>	<b>13</b>	<b>15</b>	<b>18</b>	<b>9</b>	<b>16</b>	<b>17</b>	<b>20</b>	<b>19</b>	<b>21</b>			
<b>g</b>	<b>17</b>	/	<b>16</b>	<b>19</b>	<b>17</b>	<b>3</b>	<b>18</b>	<b>12</b>	<b>15</b>	<b>20</b>	<b>17</b>	<b>13</b>	<b>17</b>	<b>13</b>	<b>15</b>	<b>20</b>	<b>19</b>	<b>20</b>	<b>16</b>	<b>17</b>	<b>20</b>	<b>20</b>	<b>20</b>	<b>20</b>	<b>14</b>	<b>21</b>	<b>21</b>	<b>7</b>	<b>21</b>	<b>21</b>	<b>19</b>	<b>21</b>	<b>21</b>	<b>17</b>	<b>21</b>	<b>19</b>	<b>17</b>	<b>21</b>	<b>19</b>			
<b>h</b>	<b>3</b>	/	<b>15</b>	<b>11</b>	<b>20</b>	<b>20</b>	<b>17</b>	<b>1</b>	<b>18</b>	<b>14</b>	<b>18</b>	<b>18</b>	<b>8</b>	<b>11</b>	<b>3</b>	<b>6</b>	<b>9</b>	<b>8</b>	<b>6</b>	<b>13</b>	<b>10</b>	<b>11</b>	<b>14</b>	<b>12</b>	<b>2</b>	<b>12</b>	<b>12</b>	<b>1</b>	<b>4</b>	<b>7</b>	<b>3</b>	<b>5</b>	<b>11</b>	<b>10</b>	<b>9</b>	<b>12</b>	<b>18</b>	<b>12</b>	<b>15</b>			
<b>i</b>	<b>14</b>	/	<b>9</b>	<b>14</b>	<b>14</b>	<b>18</b>	<b>14</b>	<b>16</b>	<b>12</b>	<b>4</b>	<b>14</b>	<b>8</b>	<b>12</b>	<b>9</b>	<b>10</b>	<b>13</b>	<b>20</b>	<b>18</b>	<b>2</b>	<b>18</b>	<b>18</b>	<b>14</b>	<b>18</b>	<b>17</b>	<b>7</b>	<b>18</b>	<b>19</b>	<b>16</b>	<b>19</b>	<b>20</b>	<b>11</b>	<b>20</b>	<b>20</b>	<b>5</b>	<b>20</b>	<b>21</b>	<b>19</b>	<b>20</b>	<b>17</b>			
<b>j</b>	<b>15</b>	/	<b>10</b>	<b>3</b>	<b>12</b>	<b>6</b>	<b>9</b>	<b>17</b>	<b>9</b>	<b>3</b>	<b>9</b>	<b>6</b>	<b>14</b>	<b>8</b>	<b>1</b>	<b>4</b>	<b>1</b>	<b>2</b>	<b>9</b>	<b>1</b>	<b>2</b>	<b>3</b>	<b>5</b>	<b>5</b>	<b>3</b>	<b>9</b>	<b>3</b>	<b>4</b>	<b>8</b>	<b>3</b>	<b>2</b>	<b>10</b>	<b>7</b>	<b>12</b>	<b>13</b>	<b>4</b>	<b>15</b>	<b>3</b>	<b>8</b>			
<b>k</b>	<b>4</b>	/	<b>12</b>	<b>1</b>	<b>11</b>	<b>13</b>	<b>6</b>	<b>11</b>	<b>19</b>	<b>7</b>	<b>3</b>	<b>5</b>	<b>18</b>	<b>5</b>	<b>8</b>	<b>7</b>	<b>5</b>	<b>6</b>	<b>14</b>	<b>12</b>	<b>6</b>	<b>9</b>	<b>8</b>	<b>9</b>	<b>8</b>	<b>7</b>	<b>10</b>	<b>3</b>	<b>12</b>	<b>13</b>	<b>5</b>	<b>9</b>	<b>13</b>	<b>2</b>	<b>12</b>	<b>9</b>	<b>4</b>	<b>17</b>	<b>16</b>			
<b>l</b>	<b>20</b>	/	<b>14</b>	<b>8</b>	<b>19</b>	<b>12</b>	<b>10</b>	<b>14</b>	<b>14</b>	<b>9</b>	<b>15</b>	<b>15</b>	<b>9</b>	<b>17</b>	<b>13</b>	<b>3</b>	<b>3</b>	<b>5</b>	<b>1</b>	<b>2</b>	<b>3</b>	<b>2</b>	<b>2</b>	<b>3</b>	<b>6</b>	<b>2</b>	<b>2</b>	<b>5</b>	<b>2</b>	<b>2</b>	<b>8</b>	<b>6</b>	<b>2</b>	<b>4</b>	<b>2</b>	<b>2</b>	<b>6</b>	<b>6</b>	<b>4</b>			
<b>m</b>	<b>5</b>	/	<b>20</b>	<b>10</b>	<b>5</b>	<b>11</b>	<b>2</b>	<b>2</b>	<b>5</b>	<b>5</b>	<b>2</b>	<b>10</b>	<b>15</b>	<b>16</b>	<b>7</b>	<b>9</b>	<b>13</b>	<b>14</b>	<b>3</b>	<b>7</b>	<b>7</b>	<b>4</b>	<b>4</b>	<b>7</b>	<b>4</b>	<b>6</b>	<b>9</b>	<b>11</b>	<b>7</b>	<b>4</b>	<b>16</b>	<b>13</b>	<b>10</b>	<b>19</b>	<b>7</b>	<b>5</b>	<b>10</b>	<b>10</b>	<b>9</b>			
<b>n</b>	<b>12</b>	/	<b>19</b>	<b>20</b>	<b>18</b>	<b>17</b>	<b>19</b>	<b>9</b>	<b>17</b>	<b>16</b>	<b>19</b>	<b>19</b>	<b>19</b>	<b>20</b>	<b>19</b>	<b>16</b>	<b>17</b>	<b>17</b>	<b>15</b>	<b>19</b>	<b>17</b>	<b>15</b>	<b>17</b>	<b>18</b>	<b>15</b>	<b>16</b>	<b>14</b>	<b>18</b>	<b>10</b>	<b>6</b>	<b>15</b>	<b>14</b>	<b>9</b>	<b>11</b>	<b>4</b>	<b>7</b>	<b>1</b>	<b>4</b>	<b>2</b>			
<b>o</b>	<b>19</b>	/	<b>17</b>	<b>21</b>	<b>21</b>	<b>19</b>	<b>20</b>	<b>18</b>	<b>20</b>	<b>19</b>	<b>20</b>	<b>14</b>	<b>10</b>	<b>19</b>	<b>20</b>	<b>18</b>	<b>18</b>	<b>19</b>	<b>20</b>	<b>20</b>	<b>19</b>	<b>18</b>	<b>19</b>	<b>19</b>	<b>17</b>	<b>19</b>	<b>17</b>	<b>21</b>	<b>15</b>	<b>12</b>	<b>12</b>	<b>17</b>	<b>14</b>	<b>20</b>	<b>15</b>	<b>10</b>	<b>5</b>	<b>7</b>	<b>6</b>			
<b>p</b>	<b>18</b>	/	<b>21</b>	<b>9</b>	<b>10</b>	<b>21</b>	<b>13</b>	<b>20</b>	<b>20</b>	<b>6</b>	<b>20</b>	<b>18</b>	<b>14</b>	<b>19</b>	<b>19</b>	<b>14</b>	<b>19</b>	<b>20</b>	<b>3</b>	<b>16</b>	<b>20</b>																					
<b>q</b>	<b>9</b>	/	<b>11</b>	<b>15</b>	<b>6</b>	<b>16</b>	<b>13</b>	<b>6</b>	<b>7</b>	<b>6</b>	<b>16</b>	<b>17</b>	<b>5</b>	<b>10</b>	<b>12</b>	<b>8</b>	<b>14</b>	<b>11</b>	<b>13</b>	<b>6</b>	<b>5</b>	<b>16</b>	<b>12</b>	<b>16</b>	<b>16</b>	<b>10</b>	<b>7</b>	<b>2</b>	<b>5</b>	<b>9</b>	<b>17</b>	<b>3</b>	<b>3</b>	<b>18</b>	<b>5</b>	<b>15</b>	<b>2</b>	<b>1</b>	<b>11</b>			
<b>r</b>	<b>10</b>	/	<b>13</b>	<b>7</b>	<b>15</b>	<b>15</b>	<b>3</b>	<b>13</b>	<b>13</b>	<b>1</b>	<b>11</b>	<b>9</b>	<b>3</b>	<b>7</b>	<b>5</b>	<b>2</b>	<b>2</b>	<b>1</b>	<b>12</b>	<b>4</b>	<b>4</b>	<b>7</b>	<b>1</b>	<b>1</b>	<b>19</b>	<b>3</b>	<b>5</b>	<b>13</b>	<b>6</b>	<b>10</b>	<b>10</b>	<b>7</b>	<b>4</b>	<b>13</b>	<b>6</b>	<b>3</b>	<b>7</b>	<b>9</b>	<b>3</b>			
<b>s</b>	<b>11</b>	/	<b>7</b>	<b>2</b>	<b>1</b>	<b>2</b>	<b>4</b>	<b>4</b>	<b>2</b>	<b>13</b>	<b>10</b>	<b>7</b>	<b>11</b>	<b>4</b>	<b>6</b>	<b>12</b>	<b>12</b>	<b>10</b>	<b>19</b>	<b>8</b>	<b>8</b>	<b>12</b>	<b>7</b>	<b>4</b>	<b>20</b>	<b>8</b>	<b>11</b>	<b>17</b>	<b>9</b>	<b>5</b>	<b>9</b>	<b>2</b>	<b>8</b>	<b>8</b>	<b>11</b>	<b>11</b>	<b>16</b>	<b>8</b>	<b>5</b>			
<b>t</b>	<b>13</b>	/	<b>4</b>	<b>6</b>	<b>16</b>	<b>14</b>	<b>8</b>	<b>20</b>	<b>10</b>	<b>15</b>	<b>13</b>	<b>16</b>	<b>16</b>	<b>12</b>	<b>14</b>	<b>15</b>	<b>15</b>	<b>15</b>	<b>18</b>	<b>11</b>	<b>15</b>	<b>13</b>	<b>3</b>	<b>8</b>	<b>21</b>	<b>14</b>	<b>16</b>	<b>20</b>	<b>18</b>	<b>16</b>	<b>20</b>	<b>16</b>	<b>15</b>	<b>21</b>	<b>17</b>	<b>18</b>	<b>11</b>	<b>11</b>	<b>10</b>			
<b>u</b>	<b>21</b>	/	<b>6</b>	<b>18</b>	<b>8</b>	<b>7</b>	<b>11</b>	<b>7</b>	<b>8</b>	<b>12</b>	<b>7</b>	<b>11</b>	<b>20</b>	<b>3</b>	<b>2</b>	<b>17</b>	<b>10</b>	<b>13</b>	<b>5</b>	<b>16</b>	<b>12</b>	<b>19</b>	<b>13</b>	<b>11</b>	<b>18</b>	<b>15</b>	<b>15</b>	<b>19</b>	<b>16</b>	<b>17</b>	<b>21</b>	<b>18</b>	<b>17</b>	<b>15</b>	<b>10</b>	<b>16</b>	<b>14</b>	<b>15</b>	<b>18</b>			

Table 6. Rankings of green-to-red ratio (GR) for 21 test plots labelled ‘a’ through ‘u’ on 13 flight dates based on ground reference measurements (REF), single layer mosaics (SLM), and multilayer mosaics (MLM).

Plot	Days After Planting																																								
	11			16			21			25			28			32			35			38			43			47			50			53			57				
	REF	SLM	MLM	REF	SLM	MLM	REF	SLM	MLM	REF	SLM	MLM	REF	SLM	MLM	REF	SLM	MLM	REF	SLM	MLM	REF	SLM	MLM	REF	SLM	MLM	REF	SLM	MLM	REF	SLM	MLM	REF	SLM	MLM					
a	6	/	13	13	13	9	1	8	4	7	8	10	11	18	11	15	7	10	13	8	17	12	12	11	8	16	15	8	5	14	12	8	14	11	4	19	2	7	18		
b	4	/	3	13	8	7	3	1	1	12	2	1	7	1	5	11	6	7	10	12	18	8	10	14	4	11	13	10	17	21	19	13	21	17	15	20	3	16	19		
c	1	/	1	20	3	1	10	5	5	11	1	4	2	4	17	6	4	8	7	1	3	7	7	7	7	8	4	12	10	11	13	20	17	10	6	11	7	13	15		
d	3	/	2	7	9	11	17	15	14	14	5	20	3	17	18	8	17	16	9	17	10	6	16	13	10	4	5	14	9	6	4	12	10	5	13	7	5	6	9		
e	10	/	5	16	4	8	15	18	12	16	4	3	10	14	12	14	10	17	6	13	14	13	15	12	15	15	10	16	19	19	9	17	12	8	11	10	20	21	17		
f	7	/	4	3	1	3	11	9	6	15	9	2	8	3	8	16	8	11	17	2	5	18	13	4	13	9	11	7	6	10	7	7	6	7	7	3	14	12	12		
g	12	/	17	15	17	4	6	10	11	18	13	7	16	9	6	18	15	15	12	5	12	15	18	17	6	18	16	5	15	15	18	14	19	14	20	15	9	20	16		
h	2	/	19	2	20	20	9	2	15	6	15	14	1	8	10	3	11	3	4	11	8	3	11	5	2	5	1	3	1	2	5	1	1	3	1	2	4	3	2		
i	11	/	12	4	5	18	4	17	13	8	14	8	12	13	14	17	19	18	2	18	15	14	17	18	11	17	19	17	16	16	8	9	18	6	16	14	16	11	8		
j	16	/	10	1	11	6	14	13	9	1	10	9	5	7	1	1	5	5	8	4	4	1	4	6	1	13	7	1	7	4	1	6	4	12	8	4	8	2	7		
k	8	/	9	5	12	13	8	11	17	3	7	11	14	6	13	4	3	2	14	14	9	5	3	16	5	3	6	6	8	7	2	5	7	1	10	8	19	9	14		
l	19	/	14	8	19	12	18	9	18	17	9	16	15	2	1	6	1	6	2	2	6	3	3	1	2	4	2	1	3	4	2	2	5	1	6	4	3				
m	5	/	15	11	10	10	2	3	7	2	6	13	13	15	7	9	13	14	3	15	16	9	8	9	9	10	14	11	12	9	16	15	8	19	14	9	12	17	10		
n	9	/	21	17	18	17	19	12	19	19	19	19	18	19	19	19	18	19	19	19	19	19	19	19	19	19	19	19	19	19	19	19	19	19	19	19	19	19	19	19	
o	13	/	20	21	21	19	20	19	20	20	20	18	19	20	20	20	20	20	20	20	20	20	20	20	20	20	20	20	20	20	20	20	20	20	20	20	20	20	20	20	20
p	20	/	18	18	16	21	21	21	21	21	21	21	21	21	21	21	21	21	21	21	21	21	21	21	21	21	21	21	21	21	21	21	21	21	21	21	21	21	21	21	21
q	14	/	16	19	6	16	12	7	8	4	17	16	6	12	16	5	12	12	11	9	7	11	14	15	14	6	8	2	3	5	14	2	5	9	2	6	1	1	4		
r	15	/	11	9	15	15	16	16	16	13	16	12	4	10	4	10	14	9	18	10	11	16	5	2	20	7	12	15	11	8	10	11	9	18	9	12	11	15	6		
s	17	/	7	6	2	2	7	4	2	10	11	6	15	2	3	7	9	1	15	3	1	4	2	1	16	2	3	13	4	3	6	3	3	4	3	5	13	5	1		
t	18	/	8	14	14	14	13	14	10	17	12	15	17	11	9	12	16	13	16	7	13	10	1	10	21	12	18	18	18	17	20	16	16	16	17	13	18	14	5		
u	21	/	6	10	7	5	5	6	3	5	3	5	20	5	2	13	2	4	5	16	6	17	9	8	17	14	9	19	13	20	21	10	15	13	19	18	15	19	21		

Table 7. List of planting and flight dates during the 2014, 2015, 2016, and 2017 growing seasons.

Month	Year			
	2014	2015	2016	2017
May	24 <sup>th</sup> *	23 <sup>rd</sup> *	23 <sup>rd</sup> *	23 <sup>rd</sup> *
June	5 <sup>th</sup> , 13 <sup>th</sup> , 18 <sup>th</sup> , 25 <sup>th</sup>	9 <sup>th</sup> , 23 <sup>rd</sup> , 28 <sup>th</sup>	3 <sup>rd</sup> , 8 <sup>th</sup> , 13 <sup>th</sup> , 17 <sup>th</sup> , 20 <sup>th</sup> , 24 <sup>th</sup> , 27 <sup>th</sup> , 30 <sup>th</sup>	14 <sup>th</sup> , 22 <sup>nd</sup>
July	3 <sup>rd</sup> , 17 <sup>th</sup>	1 <sup>st</sup> , 8 <sup>th</sup> , 11 <sup>th</sup> , 15 <sup>th</sup> , 18 <sup>th</sup> , 22 <sup>nd</sup> , 27 <sup>th</sup> , 31 <sup>st</sup>	5 <sup>th</sup> , 9 <sup>th</sup> , 12 <sup>th</sup> , 15 <sup>th</sup> , 19 <sup>th</sup>	14 <sup>th</sup>
August	None	4 <sup>th</sup>	None	18 <sup>th</sup>

\*Planting dates

Table 8. AquaCrop parameters for non-stressed growth and how they were constrained using ground-based observations from 2016.

<b>Category</b>	<b>Parameters to be Calibrated</b>	<b>Constraining Observation</b>
<b>Soil Drainage</b>	Volumetric water content at saturation ( $\theta_{sat}$ )	Field-Scale Volumetric Water Content
	Volumetric water content at field capacity ( $\theta_{FC}$ )	
	Volumetric water content at the permanent wilting point ( $\theta_{PWP}$ )	
	Soil drainage coefficient ( $\tau$ )	
<b>Canopy Expansion</b>	Initial canopy cover ( $CC_0$ )	Field-Scale Canopy Cover
	Maximum canopy cover ( $CC_x$ )	
	Canopy growth coefficient ( $CGC$ )	
	Canopy decline coefficient ( $CDC$ )	
<b>Root Extension</b>	Planting depth ( $Z_{ini}$ )	Field-Scale Root Length
	Maximum root length ( $Z_x$ )	
	Time from planting until crop is autotrophic ( $t_0$ )	
	Time from planting until $Z_x$ is reached ( $t_x$ )	
	Shape factor for root extension ( $n$ )	
<b>Biomass</b>	Biomass Water Productivity ( $WP$ )	Field-Scale Above-Ground Biomass
<b>Yield</b>	Harvest Index ( $HI$ )	Field-Scale Yield

Table 9. AquaCrop model parameters for stressed growth and how they were constrained using ground-based observations from 2016.

Category	Parameters to be Calibrated	Constraining Observation
PAW Thresholds for Moisture Stress Coefficients	Upper PAW threshold for reduced canopy expansion ( $a_{exp}$ )	Field-Scale Canopy Cover
	Lower PAW threshold for reduced canopy expansion ( $b_{exp}$ )	
	Upper PAW threshold for stomatal closure ( $a_{sto}$ )	
	Upper PAW threshold for accelerated senescence ( $a_{sen}$ )	
	Upper PAW threshold for aeration stress ( $a_{aer}$ )	
Shape Parameters for Stress Coefficients	Shape factor for stress coefficient for canopy expansion ( $f_{exp}$ )	
	Shape factor for stress coefficient for stomatal closure ( $f_{sto}$ )	
	Shape factor for stress coefficient for accelerated senescence ( $f_{sen}$ )	

Table 10. AquaCrop parameters for non-stressed growth and how they were constrained using UAS-based observations from 2016.

Category	Parameters to be Calibrated	Constraining Observation
Soil Drainage	Volumetric water content at saturation ( $\theta_{sat}$ )	Field-Scale Volumetric Water Content
	Volumetric water content at field capacity ( $\theta_{FC}$ )	
	Volumetric water content at the permanent wilting point ( $\theta_{PWP}$ )	
	Soil drainage coefficient ( $\tau$ )	
Canopy Expansion	Initial canopy cover ( $CC_0$ )	Field-Scale Canopy Cover Based on Non-Stressed Plots
	Maximum canopy cover ( $CC_x$ )	
	Canopy growth coefficient ( $CGC$ )	
	Canopy decline coefficient ( $CDC$ )	
Root Extension	Planting depth ( $Z_{ini}$ )	Field-Scale Root Length
	Maximum root length ( $Z_x$ )	
	Time from planting until crop is autotrophic ( $t_0$ )	
	Time from planting until $Z_x$ is reached ( $t_x$ )	
	Shape factor for root extension ( $n$ )	
Biomass	Biomass Water Productivity ( $WP$ )	Field-Scale Above-Ground Biomass
Yield	Harvest Index ( $HI$ )	Field-Scale Yield

Table 11. AquaCrop parameters for stressed growth and how they were constrained using UAS-based observations from 2016.

Category	Parameters to be Calibrated	Constraining Observation
PAW Thresholds for Moisture Stress	Upper PAW threshold for reduced canopy expansion ( $a_{exp}$ )	Field-Scale Canopy Cover and Dates of Reductions in Canopy Expansion Rates Based on Stressed Plots
	Lower PAW threshold for reduced canopy expansion ( $b_{exp}$ )	
	Upper PAW threshold for stomatal closure ( $a_{sto}$ )	
	Upper PAW threshold for accelerated senescence ( $a_{sen}$ )	
	Upper PAW threshold for aeration stress ( $a_{aer}$ )	
Shape Parameters for Stress Coefficients	Shape factor for stress coefficient for canopy expansion ( $f_{exp}$ )	
	Shape factor for stress coefficient for stomatal closure ( $f_{sto}$ )	
	Shape factor for stress coefficient for accelerated senescence ( $f_{sen}$ )	

Table 12. Selected AquaCrop model parameter values from ground and UAS-based calibrations with default values for reference.

Model	Soil Drainage				Canopy Expansion				Root Extension					Biomass	Yield
	$\theta_{sat}$	$\theta_{FC}$	$\theta_{PWP}$	$\tau$	$CC_0$	$CC_x$	$CGC$	$CDC$	$Z_{ini}$	$Z_x$	$t_0$	$t_x$	$n$	$WP$	$HI$
<b>Default</b>	52%	44%	20%	0.5	1.75%	98%	10.4 %/d	2.9 %/d	30 cm	2 m	7 d	92 d	1.5	15 g/m <sup>2</sup>	40%
<b>Ground</b>	52%	46%	10%	1.0	2.63%	100%	9.2 %/d	14.5 %/d	22 cm	75 cm	22 d	125 d	1.0	20 g/m <sup>2</sup>	32%
<b>UAS</b>	52%	46%	10%	1.0	5.25%	100%	6.9 %/d	13.8 %/d	22 cm	75 cm	22 d	125 d	1.0	20 g/m <sup>2</sup>	32%
	<b>Moisture Stress</b>														
	$a_{exp}$		$b_{exp}$		$a_{sto}$		$a_{sen}$		$a_{aer}$		$f_{exp}$	$f_{sto}$	$f_{sen}$		
<b>Default</b>	0.85 PAW		0.35 PAW		0.40 PAW		0.30 PAW		1.13 PAW		3.0	3.0	3.0		
<b>Ground</b>	0.53 PAW		0.23 PAW		0.52 PAW		0.51 PAW		1.17 PAW		3.0	3.0	3.0		
<b>UAS</b>	0.63 PAW		0.33 PAW		0.62 PAW		0.51 PAW		1.00 PAW		3.0	3.0	3.0		

Table 13. Calibration metrics of agreement between observed and simulated UAS and ground-based AquaCrop outputs in 2016.

Metric	Canopy Cover (%)		Biomass (tons/ha)		Volumetric Water Content (%)	
	Ground	UAS	Ground	UAS	Ground	UAS
$r^2$	1.00	0.99	1.00	1.00	0.68	0.68
RMSE	2.8	4.0	0.3	0.4	6.5	6.6
Normalized RMSE	7.2	10.3	13.1	18.5	17.3	17.8
Nash-Sutcliffe Model Efficiency	0.99	0.97	0.99	0.97	-6.17	-6.57
Wilmott's Index of Agreement	1.00	0.99	1.00	0.99	0.58	0.58

Table 14. Validation metrics of agreement between observed and simulated UAS and ground-based AquaCrop model canopy cover for the 2014, 2015, and 2017 growing seasons.

Metric	Canopy Cover (%)					
	2014		2015		2017	
	Ground	UAS	Ground	UAS	Ground	UAS
<b>r<sup>2</sup></b>	0.99	0.99	0.89	0.91	0.96	0.98
<b>RMSE</b>	7.0	3.6	36.6	33.6	13.2	10.5
<b>Normalized RMSE</b>	16.2	8.4	111.9	102.6	32.5	25.7
<b>Nash-Sutcliffe Model Efficiency</b>	0.89	0.97	-2.63	-2.06	0.88	0.92
<b>Wilmott's Index of Agreement</b>	0.98	0.99	0.64	0.65	0.97	0.98

Table 15. Observed and simulated soybean yields and yield prediction errors using ground and UAS-based AquaCrop models.

Year	No. Plots	Average Observed Yield (tons/ha)	Simulated Yield (tons/ha)		Yield Prediction Error*		Observed Yield Standard Deviation (tons/ha)
			Ground	UAS	Ground	UAS	
2014	151	4.3	6.2	6.1	44%	42%	0.7
2015	47	4.3	5.6	5.3	30%	23%	0.9
2016	147	6.1	6.1	6.1	0%	0%	0.9
2017	11	5.0	5.6	5.4	12%	8%	0.7

\*Yield prediction errors were computed as:  $Error = (Simulated\ Value - Observed\ Value) / Observed\ Value$

## REFERENCES

- [1] Bradshaw, C. J. A., & Barry W. B. (2014) Human population reduction is not a quick fix for environmental problems. *Proceedings of the National Academy of Sciences of the United States of America*, 111(46): 16610-16615. doi: 10.1073/pnas.1410465111.
- [2] Cohen, J. E. (2003). Human population: the next half century. *Science*, 302(5648), 1172-1176.
- [3] FAO's director- general on how to feed the world in 2050. (2009). *Population and Development Review*, 35(4), 837-839.
- [4] Sinha, S. K., Rao, N. H., & Swaminathan, M. S. (1989). Food security in the changing global climate. *International Symposium on Climate Variability and Food Security in Developing Countries*, New Delhi (India).
- [5] Cherkauer, K. A., & Sinha, T. (2010). Hydrologic impacts of projected future climate change in the Lake Michigan region. *Journal of Great Lakes Research*, 36, 33-50. doi:10.1016/j.jglr.2009.11.012.
- [6] Fan, F. (2014). Climate change in the northeastern US: regional climate model validation and climate change projections. *Climate Dynamics*, 43(1/2), 145-162. doi:10.1007/s00382-014-2198-1.
- [7] Pryor, S. C. (2013). Climate change in the Midwest: impacts, risks, vulnerability, and adaptation. Bloomington: Indiana University Press.
- [8] Rosenzweig, C. (2002). Increased crop damage in the US from excess precipitation under climate change. *Global Environmental Change Part A: Human & Policy Dimensions*, 12(3), 197-203.
- [9] Boote, K. J., Jones, J. W., & Pickering, N. B. (1996). Potential uses and limitations of crop models. *Agronomy Journal*, 88(5), 704-716.
- [10] Widuri, L. I. I., Mei, M., Kartika, K., Erna, S., Benyamin, L., Mery, H., Erizal, S., and Andi, W. (2017) Relative leaf expansion rate and other leaf-related indicators for detection of drought stress in chili pepper (*Capsicum Annuum L.*)." *Australian journal of crop science*, 11(12): 1617-1625. doi: 10.21475/ajcs.17.11.12.pne800.

- [11] Jones, H. G. (2004). Irrigation scheduling: advantages and pitfalls of plant-based methods. *Journal of Experimental Botany*, 55(407), 2427.
- [12] Steduto, P., Hsiao, T., Raes, D., & Fereres, E. (2009a). AquaCrop - the FAO crop model to simulate yield response to water: I. concepts and underlying principles. *Agronomy Journal*, 101(3), 426-437.
- [13] Xing, G., Liu, K., & Gai, J. (2017). A high-throughput phenotyping procedure for evaluation of antixenosis against common cutworm at early seedling stage in soybean. *Plant Methods*, 13(1), 1-13. doi: 10.1186/s13007-017-0215-1.
- [14] Araus, J. L., & Cairns, J. E. (2014). Field high-throughput phenotyping: The new crop breeding frontier. *Trends in Plant Science*, 19(1), 52-61.
- [15] Cabrera-Bosquet, L., Crossa, J., von Zitzewitz, J., Serret, M. D., & Luis Araus, J. (2012). High-throughput phenotyping and genomic selection: the frontiers of crop breeding converge. *Journal of Integrative Plant Biology*, 54(5), 312-320. doi:10.1111/j.1744-7909.2012.01116.x.
- [16] Eysn, L., Hollaus, M., Pfeifer, N., & Schadauer, K. (2012). Forest delineation based on airborne LIDAR data. *Remote Sensing*, 4(12), 762-783. doi: 10.3390/rs4030762.
- [17] Xavier, A., Hall, P. B., Hearst, A. A., Cherkauer, K. A., & Rainey, K. A. (2017). Genetic architecture of phenomic-enabled canopy coverage in glycine max. *Genetics*, 206(2), 1081-1089.
- [18] Steduto, P., Raes, D., Hsiao, T. C., Fereres, E., Heng, L. K., Howell, T. A., . . . Geerts, S. (2009b). Concepts and applications of AquaCrop: the FAO crop water productivity model. 175-191: Beijing: Berlin; New York: Tsinghua University Press; Springer.
- [19] Oikawa, S., Okada, M., & Hikosaka, K. (2013). Effects of elevated CO<sub>2</sub> on leaf area dynamics in nodulating and non-nodulating soybean stands. *Plant and Soil*, 373(1/2), 627-639.
- [20] Board, J. E. (1996). Growth dynamics during the vegetative period affects yield of narrow-row, late-planted soybean. *Agronomy Journal*, 88, 567-573.

- [21] Purcell, L. C., Montserrat, S., & Lanny, A. (2014). Soybean growth and development. Arkansas Soybean Production Handbook, 7-12, University of Arkansas Division of Agriculture Research.
- [22] Ahuja, L. (2008). Response of crops to limited water: understanding and modeling water stress effects on plant growth processes. Madison, WI: American Society of Agronomy.
- [23] Denmead, O., & Shaw, R. (1962). Availability of soil water to plants as affected by soil moisture content and meteorological conditions. *Agronomy Journal*, 54(5), 385.
- [24] Meyer, W., & Green, G. (1981). Plant indicators of wheat and soybean crop water stress. *Irrigation Science*, 2(3), 167-176. doi:10.1007/BF00257978.
- [25] Sadras, V. O., & Milroy, S. P. (1996). Soil-water thresholds for the responses of leaf expansion and gas exchange: A review. *Field Crops Research*, 47(2), 253-266. doi:10.1016/0378-4290(96)00014-7.
- [26] Ritchie, J. T. (1981). Water dynamics in the soil-plant-atmosphere system. *Plant Soil*, 58(1), 81-96. doi:10.1007/BF02180050.
- [27] Rhine, M., Stevens, G., Shannon, G., Wrather, A., & Sleper, D. (2010). Yield and nutritional responses to waterlogging of soybean cultivars. *Irrigation Science*, 28(2), 135-142. doi:10.1007/s00271-009-0168-x.
- [28] Pezeshki, S., & DeLaune, R. (2012). Soil oxidation-reduction in wetlands and its impact on plant functioning. *Biology*, 1(2), 196-221. doi: 10.3390/biology1020196.
- [29] Troedson, R. J., Lawn, R. J., Byth, D. E., & Wilson, G. L. (1989). Response of field-grown soybean to saturated soil culture 1. patterns of biomass and nitrogen accumulation. *Field Crops Research*, 21(3), 171-187. doi:10.1016/0378-4290(89)90001-4.
- [30] Sullivan, M., Vantoai, T., Fausey, N., & Beuerlein, J. (2001). Evaluating on-farm flooding impacts on soybean. *Crop Science*, 41(1), 93-100.
- [31] De Souza, P. I. (1997). Water stress during seed filling and leaf senescence in soybean. *Agronomy Journal*, 89, 807-813.

- [32] Pathan, S. M. (2014). Two soybean plant introductions display slow leaf wilting and reduced yield loss under drought. *Journal of Agronomy & Crop Science*, 200(3), 231-237. doi:10.1111/jac.12053.
- [33] Sloane, R. J., Patterson, R. P., & Carter, T. E., Jr. (1990). Field drought tolerance of a soybean plant introduction. *Crop science*, 30(1), 118-123.
- [34] Purcell, L. C., Vories, E. D., Counce, P. A., & King, C. A. (1997). Soybean growth and yield response to saturated soil culture in a temperate environment. *Field Crops Research*, 49(2), 205-213. doi:10.1016/S0378-4290(96)01004-0.
- [35] Linkemer, G. (1998). Waterlogging effects on growth and yield components in late-planted soybean. *Crop Science*, 38(6), 1576.
- [36] Reyna, N., Cornelious, B., Shannon, J., & Sneller, C. (2003). Evaluation of a QTL for waterlogging tolerance in southern soybean germplasm. *Crop Science*, 43(6), 2077-2082.
- [37] Henshaw, T. L. (2007). Soya bean (*glycine max l. merr.*) genotype response to early-season flooding: II. aboveground growth and biomass. *Journal of Agronomy & Crop Science*, 193(3), 189-198. doi:10.1111/j.1439-037X.2007.00258.x.
- [38] Sivakumar, M. V. K., & Shaw, R. H. (1978). Relative evaluation of water stress indicators for soybeans. *Agronomy Journal*, 70(4), 619-623.
- [39] Boyer, J. S. (1970). Leaf enlargement and metabolic rates in corn, soybean, and sunflower at various leaf water potentials. *Plant Physiology*, 46(2), 233.
- [40] Liu, F., Jensen, C. R., & Andersen, M. N. (2003). Hydraulic and chemical signals in the control of leaf expansion and stomatal conductance in soybean exposed to drought stress. *Functional Plant Biology*, 30(1), 65-73. doi:10.1071/FP02170.
- [41] King, C. A. (2009). Differential wilting among soybean genotypes in response to water deficit. *Crop Science*, 49(1), 290-299. doi:10.2135/cropsci2008.04.0219.
- [42] Oosterhuis, D. M., Walker, S., & Eastham, J. (1985). Soybean leaflet movements as an indicator of crop water stress. *Crop science*, 25(6), 1101-1106.
- [43] Wright, A., & Berliner, P. (1986). The use of soybean leaflet angle data for irrigation scheduling. *Irrigation Science*, 7(4), 245-248. doi:10.1007/BF00270434.

- [44] Carter, G. A., & Miller, R. L. (1994). Early detection of plant stress by digital imaging within narrow stress-sensitive wavebands. *Remote Sensing of Environment*, 50(3), 295-302. doi:10.1016/0034-4257(94)90079-5.
- [45] Marquez-Garcia, B. (2015). Redox markers for drought-induced nodule senescence, a process occurring after drought-induced senescence of the lowest leaves in soybean (*Glycine max*). *Annals of Botany*, 116(4), 497. doi:10.1093/aob/mcv030.
- [46] Kramer, P. J. (1951). Causes of injury to plants resulting from flooding of the soil. *Plant Physiology*, 26(4), 722-736.
- [47] Mozafar, A., Gämperle, R., & Loch, J. (1992). Root aeration inhibits the recovery of soybean from flooding-induced chlorosis under non-calcareous conditions. *Journal of Plant Nutrition*, 15(10), 1927-1937. doi:10.1080/01904169209364448.
- [48] Nathanson, K., Lawn, R. J., De Jabrun, P. L. M., & Byth, D. E. (1984). Growth, nodulation and nitrogen accumulation by soybean in saturated soil culture. *Field Crops Research*, 8, 73-92. doi:10.1016/0378-4290(84)90053-4.
- [49] Govender, M., Dye, P., Weiersbye, I., Witkowski, E., & Ahmed, F. (2009). Review of commonly used remote sensing and ground-based technologies to measure plant water stress. *Water SA*, 35, 741-752. Gezina: Water Research Commission.
- [50] Zhou, J., Khot, L. R., Bahlol, H. Y., Boydston, R., & Miklas, P. N. (2016). Evaluation of ground, proximal and aerial remote sensing technologies for crop stress monitoring. *IFAC Papers On Line*, 49(16), 22-26. doi: 10.1016/j.ifacol.2016.10.005.
- [51] van Ittersum, M. K., Leffelaar, P. A., van Keulen, H., Kropff, M. J., Bastiaans, L., & Goudriaan, J. (2003). On approaches and applications of the Wageningen crop models. *European Journal of Agronomy*, 18(3), 201-234. doi:10.1016/S1161-0301(02)00106-5.
- [52] Hammer, G. L., Kropff, M. J., Sinclair, T. R., & Porter, J. R. (2002). Future contributions of crop modeling - from heuristics and supporting decision making to understanding genetic regulation and aiding crop improvement. *European Journal of Agronomy*, 18(1), 15-31. doi:10.1016/S1161-0301(02)00093-X.

- [53] Stöckle, C. O., Donatelli, M., & Nelson, R. (2003). CropSyst, a cropping systems simulation model. *European Journal of Agronomy*, 18(3), 289-307. doi:10.1016/S1161-0301(02)00109-0.
- [54] Wang, F., Fraisse, C. W., Kitchen, N. R., & Sudduth, K. A. (2003). Site-specific evaluation of the CROPGRO-soybean model on Missouri claypan soils. *Agricultural Systems*, 76(3), 985-1005. doi:10.1016/S0308-521X(02)00029-X.
- [55] Keating, B. A. (2003). An overview of APSIM, a model designed for farming systems simulation. *European Journal of Agronomy*, 18(3/4), 267-289.
- [56] Gassman, P. W., Reyes, M. R., Green, C. H., & Arnold, J. G. (2007). The soil and water assessment tool: historical development, applications, and future research directions: *Transactions of the ASABE*, 50(4), 1211-1250.
- [57] McMaster, G. S., & Wilhelm, W. W. (1997). Growing degree-days: one equation, two interpretations. *Agricultural and Forest Meteorology*, 87(4), 291-300. doi:10.1016/S0168-1923(97)00027-0.
- [58] Bindi, M., Sinclair, T. R., & Harrison, J. (1999). Analysis of seed growth by linear increase in harvest index. *Crop science*, 39(2), 486-493.
- [59] Steduto, P., Hsiao, T., & Fereres, E. (2007). On the conservative behavior of biomass water productivity. *Irrigation Science*, 25(3), 189-207. doi:10.1007/s00271-007-0064-1.
- [60] Warmink, J. J. (2010). Identification and classification of uncertainties in the application of environmental models. *Environmental Modeling & Software*, 25(12), 1518-1528. doi:10.1016/j.envsoft.2010.04.011.
- [61] Saxton, K. E., & Rawls, W. J. (2006). Soil water characteristic estimates by texture and organic matter for hydrologic solutions. *Soil Science Society of America Journal*, 70(5), 1569-1578.
- [62] Wang, R., Bowling, L. C., & Cherkauer, K. A. (2016). Estimation of the effects of climate variability on crop yield in the Midwest USA. *Agricultural and Forest Meteorology*, 216, 141-156.

- [63] Willmott, C. J. (1982). Some comments on the evaluation of model performance. *American Meteorological Society*, 63(11), 1309-1313.
- [64] Gaile, G. L., & Willmott, C. J. (1984). On the evaluation of model performance in physical geography. *Spatial Statistics and Models*, 443-460. Boston: MA, D. Reidel Pub. Co.
- [65] Legates, D. R., & McCabe, G. J. (1999). Evaluating the use of “goodness- of- fit” measures in hydrologic and hydroclimatic model validation. *Water Resources Research*, 35(1), 233-241. doi:10.1029/1998WR900018.
- [66] Beven, K. (2006). A manifesto for the equifinality thesis. *Journal of Hydrology*, 320(1), 18-36. doi:10.1016/j.jhydrol.2005.07.007.
- [67] Rajib, M. A., Merwade, V., & Yu, Z. (2016). Multi-objective calibration of a hydrologic model using spatially distributed remotely sensed/in-situ soil moisture. *Journal of Hydrology*, 536, 192-207. doi:10.1016/j.jhydrol.2016.02.037.
- [68] Bhatia, V. S. (2008). Analysis of potential yields and yield gaps of rainfed soybean in India using CROPGRO-soybean model. *Agricultural & Forest Meteorology*, 148(8/9), 1252-1266. doi:10.1016/j.agrformet.2008.03.004.
- [69] Holzworth, D. P. (2014). APSIM - evolution towards a new generation of agricultural systems simulation. *Environmental Modeling & Software*, 62, 327-351. doi:10.1016/j.envsoft.2014.07.009.
- [70] Geerts, S. (2008). Could deficit irrigation be a sustainable practice for quinoa (chenopodium quinoa willd.) in the southern Bolivian altiplano? *Agricultural Water Management*, 95(8), 909-918. doi:10.1016/j.agwat.2008.02.012.
- [71] Lorite, I. J. (2013). AquaData and AquaGIS: two computer utilities for temporal and spatial simulations of water-limited yield with AquaCrop. *Computers & Electronics in Agriculture*, 96, 227-238. doi:10.1016/j.compag.2013.05.010.
- [72] Raes, D., Steduto, P., Hsiao, T., & Fereres, E. (2009). AquaCrop - the FAO crop model to simulate yield response to water: II. main algorithms and software description. *Agronomy Journal*, 101(3), 438-447.

- [73] Vanuytrecht, E. (2014). Global sensitivity analysis of yield output from the water productivity model. *Environmental Modeling & Software*, 51, 323-333. doi:10.1016/j.envsoft.2013.10.017.
- [74] Refsgaard, J. C. (2007). Uncertainty in the environmental modeling process - a framework and guidance. *Environmental Modeling & Software*, 22(11), 1543-1557. doi:10.1016/j.envsoft.2007.02.004.
- [75] Adeboye, O., Schultz, B., Adekalu, K., & Prasad, K. (2017). Modelling of response of the growth and yield of soybean to full and deficit irrigation by using aquacrop. *Irrigation and Drainage*, 66(2), 192-205. doi: 10.1002/ird.2073.
- [76] Da Silva, V. P. R., Silva, R. A., Maciel, G. F., Braga, C. C., Da Silva, J. L. C., De Souza, E. P., . . . De Holanda, R. M. (2018). Calibration and validation of the AquaCrop model for the soybean crop grown under different levels of irrigation in the Motopiba region, Brazil. *Ciencia Rural*, 48(1). doi: 10.1590/0103-8478cr20161118.
- [77] Saab, M. T. A., Marie T., Albrizio, R., Nangia, V., Karam, F., & Roupheal, Y. (2014). Developing scenarios to assess sunflower and soybean yield under different sowing dates and water regimes in the Bekaa valley (Lebanon): simulations with Aquacrop. *International Journal of Plant Production*, 8(4), 457-482.
- [78] Heng, L., Hsiao, T., Evett, S., Howell, T., & Steduto, P. (2009a). Validating the FAO AquaCrop model for irrigated and water deficient field maize. *Agronomy Journal*, 101(3), 488-498. doi:10.2134/agronj2008.0029xs.
- [79] Hsiao, T., Heng, L., Steduto, P., Rojas-Lara, B., Raes, D., & Fereres, E. (2009b). AquaCrop- the FAO crop model to simulate yield response to water: III. parameterization and testing for maize. *Agronomy Journal*, 101(3), 448-459.
- [80] Mebane, V. J., Day, R. L., Watson, J. E., Hamlett, J. M., & Roth, G. W. (2013). Validating the FAO AquaCrop model for rainfed maize in Pennsylvania. *Agronomy Journal*, 105(2), 419-427. doi:10.2134/agronj2012.0337.

- [81] Jin, X. L., Feng, H. K., Zhu, X. K., Li, Z. H., Song, S. N., Song, X. Y., . . . Guo, W. S. (2014). Assessment of the AquaCrop model for use in simulation of irrigated winter wheat canopy cover, biomass, and grain yield in the north China plain. *PLoS One*, 9(1). doi:10.1371/journal.pone.0086938.
- [82] Raes, D., Steduto, P., Hsiao, C. T., & Fereres, E. (2012). AquaCrop reference manual.
- [83] Monteith, J. L. (1965). Evaporation and environment. *Symposia of the Society for Experimental Biology*, 19, 205-234.
- [84] Hjelmfelt, A. (1991). Investigation of curve number procedure. *Journal of Hydraulic Engineering*, 117(6), 725-737.
- [85] Hawkins, R. H. (2014). Curve number method: time to think anew? *Journal of Hydrologic Engineering*, 19(6), 1059-1060.
- [86] Philip, J. R. (1957). Evaporation, and moisture and heat fields in the soil. *Journal of Meteorology*, 14(4), 354-366.
- [87] Ritchie, J. T. (1972). Model for predicting evaporation from a row crop with incomplete cover. *Water Resources Research*, 8(5), 1204-1213. doi:10.1029/WR008i005p01204.
- [88] Allen, R. G., Pereira, L. S., Raes, D., & Smith, M. (1998). Crop evapotranspiration - guidelines for computing crop water requirements. *FAO Irrigation and Drainage Paper*, (56).
- [89] Adams, J., Arkin, G., & Ritchie, J. (1976). Influence of row spacing and straw mulch on first stage drying. *Soil Science Society of America Journal*, 40(3), 436-442.
- [90] Villalobos, F. J. (1990). Evaporation measurements beneath corn, cotton, and sunflower canopies. *Agronomy Journal*, 82, 1153-1160.
- [91] Belmans, C., Wesseling, J. G., & Feddes, R. A. (1983). Simulation model of the water balance of a cropped soil: SWATRE. *Journal of Hydrology*, 63(3), 271-286. doi:10.1016/0022-1694(83)90045-8.
- [92] Feddes, R. A. (1978). *Simulation of field water use and crop yield*. New York: Wiley.
- [93] Brocca, L. (2010). Spatial-temporal variability of soil moisture and its estimation across scales. *Water Resources Research*, 46(2). doi <https://doi.org/10.1029/2009WR008016>.

- [94] De Lannoy, G. J. M. (2006). Spatial and temporal characteristics of soil moisture in an intensively monitored agricultural field (OPE). *Journal of Hydrology*, 331(3/4), 719-731. doi:10.1016/j.jhydrol.2006.06.016.
- [95] Jacobs, J. M. (2004). SMEX02: field scale variability, time stability and similarity of soil moisture. *Remote Sensing of Environment*, 92(4), 436-447. doi:10.1016/j.rse.2004.02.017.
- [96] Reynolds, S. G. (1974). A note on the relationship between size of area and soil moisture variability. *Journal of Hydrology*, 22(1), 71-76. doi:10.1016/0022-1694(74)90096-1.
- [97] Vereecken, H., Huisman, J. A., Pachepsky, Y., Montzka, C., van der Kruk, J., Bogaen, H., . . . Vanderborght, J. (2014). On the spatio-temporal dynamics of soil moisture at the field scale. *Journal of Hydrology*, 516, 76-96. doi:10.1016/j.jhydrol.2013.11.061.
- [98] Wang, C. (2008). Estimating the necessary sampling size of surface soil moisture at different scales using a random combination method. *Journal of Hydrology*, 352(3/4), 309-322. doi:10.1016/j.jhydrol.2008.01.011.
- [99] Meyer, G. E. (2008). Verification of color vegetation indices for automated crop imaging applications. *Computers & Electronics in Agriculture*, 63(2), 282-294. doi:10.1016/j.compag.2008.03.009.
- [100] Otsu, N. (1979). A threshold selection method from gray-level histograms. *Systems, Man and Cybernetics, IEEE Transactions*, 9(1), 62-66. doi:10.1109/TSMC.1979.4310076.
- [101] Hearst, A. A. & Cherkauer, K. A. (2015). Extraction of small spatial plots from geo-registered UAS imagery of crop fields. *Environmental Practice*, 17(3), 178-188. doi:10.1017/S1466046615000162.
- [102] Pix4D. Processed with Pix4Dmapper by Pix4D. Lausanne, Switzerland.
- [103] Mikhail, E. M. (1974). An introduction to photogrammetry. *Coherent Optics in Mapping*. doi:10.1117/12.953952.
- [104] Haghgattalab, A., Pérez, L. A., Mondal, S., et al. (2016). Application of unmanned aerial systems for high throughput phenotyping of large wheat breeding nurseries. *Plant Methods*. 12(1). doi:10.1186/s13007-016-0134-6.

- [105] Shi, Y., Thomasson, J. A., Murray, S. C., et al. (2016). Unmanned aerial vehicles for high-throughput phenotyping and agronomic research. *PLoS ONE*, 11(17). doi:10.1371/journal.pone.0159781.
- [106] Tao, D., Bangyou, Z., Wei, C., Seishi, N., et al. (2017). Comparison of ground cover estimates from experiment plots in cotton, sorghum and sugarcane based on images and ortho-mosaics captured by UAV. *Functional Plant Biology*, 44(1), 169-183. doi: <https://doi.org/10.1071/FP16123>.
- [107] Woebbecke, D. M., Meyer, G. E., Von Bargen, K., et al. (1995). Color indices for weed identification under various soil, residue, and lighting conditions. *Transactions of the ASAE*. 38. 259-269.
- [108] Normanly J. (2012). High-throughput phenotyping in plants: methods and protocols. New York: Humana Press.
- [109] Hall, B. P. (2015). Quantitative characterization of canopy coverage in the genetically diverse soynam population. ProQuest Dissertations & Theses Global. <https://search.proquest.com/docview/1776609221?accountid=13360>.
- [110] Hatfield, J. L., Prueger, J. H. (2010). Value of using different vegetative indices to quantify agricultural crop characteristics at different growth stages under varying management practices. *Remote Sensing*, 2(2). 562-578. doi:10.3390/rs2020562.
- [111] Viña, A. (2004). Monitoring maize (*Zea mays* L.) phenology with remote sensing. *Agronomy*. 96. 1139-1148.
- [112] Xue, J., & Su, B. (2017). Significant remote sensing vegetation indices: a review of developments and applications. *Journal of Sensors*, 2017, 1-17. doi: 10.1155/2017/1353691.
- [113] Torres-Sánchez, J., Peña, J. M., de Castro A. I., et al. (2014). Multi-temporal mapping of the vegetation fraction in early-season wheat fields using images from UAV. *Computers and Electronics in Agriculture*. 103. 104-113. doi:10.1016/j.compag.2014.02.009.
- [114] Majer, P. (2010). Leaf hue measurements offer a fast, high-throughput initial screening of photosynthesis in leaves. *Journal Of Plant Physiology*, 167(1), 74. doi:10.1016/j.jplph.2009.06.015.

- [115] Adamsen, F. J., Pinter, P. J., Jr., Barnes, E. M., LaMorte, R. L., Wall, G. W., Leavitt, S. W., & Kimball, B. A. (1999). Measuring wheat senescence with a digital camera. *Crop science*, 39(3), 719-724.
- [116] Marchant, J. A. (2004). Dealing with color changes caused by natural illumination in outdoor machine vision. *Cybernetics & Systems*, 35(1), 19-34.
- [117] Campbell, J. B., & Wynne, R. H. (2011). *Introduction to Remote Sensing* (5 ed.). New York: The Guilford Press.
- [118] Watson, P. F., & Petrie, A. (2010). Method agreement analysis: a review of correct methodology. *Theriogenology Journal*, 73(9), 1167-1179. doi:10.1016/j.theriogenology.2010.01.003.
- [119] Paredes, P. (2015). Performance assessment of the FAO AquaCrop model for soil water, soil evaporation, biomass and yield of soybeans in North China Plain. *Agricultural Water Management*, 152, 57-72. doi:10.1016/j.agwat.2014.12.007.
- [120] Meyer, G. E. (2008). Verification of color vegetation indices for automated crop imaging applications. *Computers & Electronics in Agriculture*, 63(2), 282-294. doi:10.1016/j.compag.2008.03.009.